Dynamics of an Organic Rankine Cycle for OTEC

Performance analysis of the transient regions

J.J.K. van Senden

Technische Universiteit Delft

TU Delft

Dynamics of an Organic Rankine Cycle for OTEC

Performance analysis of the transient regions

by

J.J.K. van Senden

in partial fulfillment of the requirements for the degree of

Master of Science
in Mechanical Engineering

at the Delft University of Technology,
to be defended publicly on 28 April 2020 at 10:00 AM.

Student number:	4300793	
Thesis committee:	Dr. ir. C. A. Infante Ferreira,	TU Delft, supervisor
	Dr. O. Moulthos,	TU Delft
	Prof. dr. ir. B. J. Boersma,	TU Delft
	Ir. J. V. Groot,	Allseas, supervisor

This thesis is confidential and cannot be made public until 28 April 2022.

TU Delft

Abstract

The global energy demand is growing, while climate change is demanding a sustainable way of generating this energy. Ocean Thermal Energy Conversion (OTEC) can be a part of the solution for this problem. OTEC generates electricity by using the temperature difference between the surface water of the ocean and the water at 1000 meters depth as a driving force. As this temperature difference is present all year round, there is no need for energy storage, which is the case for wind- and solar energy.
An OTEC system utilizes an Organic Rankine Cycle (ORC), which uses ammonia as a working fluid. A lot of research is conducted on this cycle, all assuming steady-state. However, as the system is constantly changing its state, either by a changing temperature difference or by variations in the operating conditions of components, more research is required to investigate the impact of these changes. Therefore, a dynamic model has been developed. In order to cope with these changes and to ensure the optimal power output at all times, a control strategy is developed and implemented on the model.

As the system has been developed with the use of a control system as a boundary condition, a model is adapted which prioritises computational time over accuracy, but, according to literature, is still accurate enough for the small transients. This model has been implemented for the OTEC cycle and improved from normal dynamic models by including pressure drops and storage tanks.
Allseas, in cooperation with the TU Delft, has built an experimental set-up of an OTEC cycle. Experiments conducted on this set-up were used to compare the model with reality, both steady-state and dynamically. It has been proven that the steady-state values matched the experiments within 1%, and the dynamics matched the experiments almost perfectly.

As a next step, the system has been scaled to match the desired 3 MW output. With this scaled model, realistic scenarios were simulated to check the response on larger transients. The scenarios consists of a start-up and shutdown of the system, a changing inlet temperature, pumps being shut off and a number of heat exchangers that are decoupled from the system, for example when a number of heat exchangers need maintenance.

The outcome proved that, from a dynamic perspective, the influence of a seawater temperature change was negligible. As the temperature changes per second are very small, the net output scales linearly with the temperature difference. A start-up and shutdown of the system was successfully simulated, which is the largest possible transient in the system. The influence of pumps that are stopped and heat exchangers being turned off for maintenance have been simulated, which showed just a slight decrease in net output. It also showed that the system, when running at the nominal conditions of the pump and turbine curve, was not running at an optimum. Therefore, a control strategy was developed by conducting a sensitivity analysis and, after using an optimisation to find the optimum point, the resulting control strategy was implemented. This new strategy resulted in an increase of 15% in the net output, compared to the nominal conditions. This proves that an OTEC cycle could greatly benefit from using a dynamic model to predict its dynamic performance and the implementation of a control system.

Acknowledgements

I would like to thank my supervisor Dr. Ir. Carlos Infante Ferreira for his guidance during the writing of this thesis. The regular meetings kept me on track, gave me different insights of the problem and helped me stay confident during the process. I would also like to thank Jeffrey Groot for his supervision. By showing me a different way of looking at problems, the process became a lot simpler.
Many thanks also goes out to Joost Kirkenier, for giving me the chance to conduct my research at Allseas and helping me with all my technological questions. You were never shy for a good discussion about the subject at hand. I would also like to thank all the colleagues at Allseas.
Also many thanks to my family, for their endless support and positiveness during the time spend on this thesis.

J.J.K. van Senden
Delft, April 2020

Contents

Nomenclature

Roman Symbols

A	Area	$\left(m^2\right)$
Bo	Boiling number	(-)
C	Coefficient	(-)
c_p	Specific Heat Capacity	$\left(\frac{kJ}{kgK}\right)$
Co	Convection number	(-)
d	Diameter	(mm)
$\vec{f}$	Body force vector	(N)
f	Factor (friction/VTG)	(-)
Fr	Froude number	(-)
G	Mass flux	$\left(\frac{kg}{m^2 s}\right)$
g	Gravity	$\left(\frac{m}{s^2}\right)$
h	Enthalpy	$\left(\frac{kJ}{kg}\right)$
K	Stodola/Minor loss coefficient	(-)
L	Length	(m)
$\dot{m}$	Mass Flow	$\left(\frac{kg}{s}\right)$
n	Rotational speed	$\left(\frac{1}{s}\right)$
Nu	Nusselt number	(-)
p	Pressure	(bar)
Pr	Prandtl number	(-)
$\dot{Q}$	Heat flow	(W)
q	Heat flux	$\left(\frac{W}{m^2}\right)$
Re	Reynolds number	(-)
S	Slip ratio	(-)
s	Specific Entropy	$\left(\frac{kJ}{kgK}\right)$
T	Temperature	$(°C)$
t	Time	(s)
$\vec{u}$	Velocity vector	$\left(\frac{m}{s}\right)$
U	Overall Heat Transfer Coefficient	$\left(\frac{W}{m^2 K}\right)$
u	Internal energy	$\left(\frac{kJ}{kg}\right)$
$\dot{V}$	Volume flow	$\left(\frac{m^3}{s}\right)$
V	Volume	$\left(m^3\right)$
v	Velocity	$\left(\frac{m}{s}\right)$
$\dot{W}$	Power	(kW)
We	Weber number	(-)
$\mathbf{x}$	State space vector	
x	Quality	(-)
$\dot{\mathbf{x}}$	Time derivative of state space vector	
y	Output vector	
z	Axial coordinate	(m)

Greek Symbols

α	Heat transfer coefficient	$\left(\frac{W}{m^2 K}\right)$

β	Corrugation angle	(°)
Δ	Difference	
ϵ	Surface roughness	(m)
η	Efficiency	(%)
γ	Void fraction	(-)
$\overline{\gamma}$	Mean Void Fraction	(-)
λ	Thermal conductivity	$\left(\frac{W}{mK}\right)$
μ	Dynamic Viscosity	$\left(\frac{kg}{m*s}\right)$
π	Pi Number	(-)
ρ	Density	$\left(\frac{kg}{m^3}\right)$
σ	Stress tensor	(MPa)

Subscripts

0	Initial condition
1	Single-phase region of evaporator
2	Two-phase region of evaporator
bt	Buffer Tank
c	Cold
cc	Convective condensation
cond	Condenser
corr	Corrected
crit	Critical
cs	Cross section
cw	Cooling water
D	Darcy
d	Discharge
des	Design
eq	Equivalent
evap	Evaporator
g	Saturated vapor
gc	Gravity controlled condensation
gen	Generator
h	Hot
hyd	Hydrostatic
i,in	Inlet
is	Isentropic
l	Saturated liquid
m	Mean
maj	Major
min	Minor
o,out	Outlet
ref	Reference value
sat	Saturated
sep	Separator
sp	Single phase
sw	Sea Water
tp	Two-phase
turb	Turbine
vap	Vaporization
w	Wall
wf	Working Fluid

Acronyms

BT	Buffer Tank
FV	Finite Volume
HEX	Heat Exchanger
LMTD	Logarithmic Mean Temperature Difference
MB	Moving Boundary
NOP	Nominal Operating Point
ODE	Ordinary Differential Equation
ORC	Organic Rankine Cycle
OTEC	Ocean Thermal Energy Conversion
P&ID	Process & Instrumentation Diagram
PDE	Partial Differential Equation
PFD	Process Flow Diagram
PL	Partial load
SMB	Switching Moving Boundary
VTG	Variable Turbine Geometry

1 Introduction

1.1. Background

The global energy demand is growing, while climate change is demanding a sustainable way of generating electricity. In 2050, electricity has to be generated for 3.6 billion more people, up to 9.6 billion people in total [18]. A lot of research has been conducted on solar, wind and hydro energy, and biomass and nuclear power have been around for several decades already. However, there are some downsides with these types of electricity generation. Biomass takes up a lot of land to grow crops, nuclear plants are expensive, hydro energy is limited to certain places where the height difference is large enough and solar and wind have the problem of being discontinuous sources of energy [18].

The main problem with renewable sources such as wind and solar is the discontinuity. This discontinuity can be averted when using a form of storage. The natural storage location of solar energy is the ocean. Almost 70% of the planet consists of water, which is heated up by the sun. All this stored energy can be harnessed by using a power cycle that requires a small temperature difference, and is called Ocean Thermal Energy Conversion. It uses the temperature difference between the ocean surface and the water at 1000 meter depth. It works properly when the temperature difference is at least 20 °C. This is the case in most equatorial regions, where most islands generate electricity using large diesel generators and are dependent on the import of fossil fuels. As such, OTEC can have a big impact on the sustainability of the energy supply and economics of these regions. The regions where the implementation of OTEC is possible, can be found in Figure 1.1.

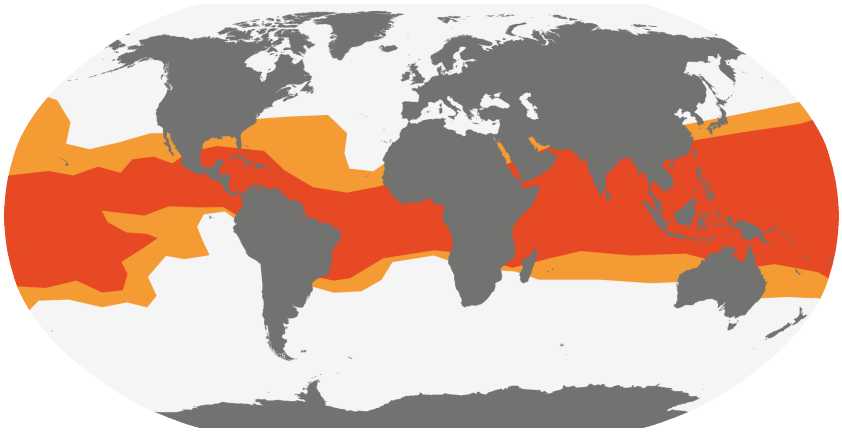

Figure 1.1: Sea surface temperature around the globe. Light orange indicates a temperature difference of at least 20 °C, while darker orange indicates a temperature difference of at least 24 °C [52]

1.2. OTEC

OTEC generates electricity from the temperature difference between the surface of the ocean and at a 1000 meters depth. It works using an Organic Rankine Cycle, or ORC. This is the same as a standard Rankine cycle, but uses a different working fluid than water, which allows it to operate at lower temperatures. The closed cycle can be seen in Figure 1.2. In this cycle, the warm water of the ocean is fed to the evaporator (step 2-3). There, the heat is transferred to the working fluid, which then evaporates. This vapor is expanded in the turbine (step 3-4) where the electricity is generated. The working fluid is condensed in the condenser (step 4-1) using the coldness of the deep sea water. A pump increases the pressure of the working fluid (step 1-2), which returns the working fluid back to its original state and the cycle continues.

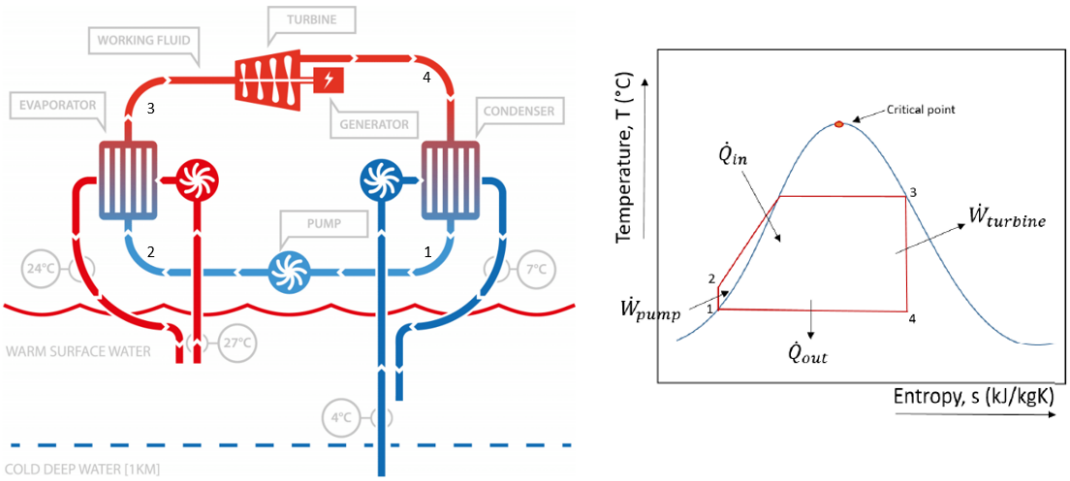

Figure 1.2: Schematic of an OTEC cycle, including *T-s* diagram [52]

The *T-s* diagram in Figure 1.2 shows the thermodynamics of an ideal OTEC cycle. The evaporator and condenser are isobaric, while the pump and turbine are isentropic. This ideal situation is not representative for real OTEC cycles, but gives a good impression on how the cycle operates.

When looking at the heat exchangers, something interesting can be found in the evaporator. Djordjevic and Kabelac [12] show that the heat transfer coefficient of the evaporation of ammonia changes with the vapor quality. It can be seen in Figure 1.3 that for a vapor quality greater than 0.7, the heat transfer coefficient drops. Therefore, a maximum output quality of 0.7 is assumed as a design value. This is also done by Stelwagen [52] and Kirkenier [30] in their optimisation models of an OTEC cycle. It can also be seen from Figure 1.3, that the heat transfer coefficient is high between 0.4 and 0.7. Therefore, the heat exchanger is designed to operate in this region.
To ensure no liquid enters the turbine, a separator needs to be installed between the evaporator and the turbine. This separator splits the vapor fraction and the liquid fraction that exit the evaporator. This is needed due to turbine failure when a liquid fraction enters the turbine.

The liquid that is separated will be re-circulated, back into the cycle after the working fluid pump. This can be seen in Figure 1.4. The mass flow of the evaporator and the re-circulation rate are dependent. With increasing mass flow, the vapor quality decreases due to overfeeding of the evaporator. With a decreasing vapor quality comes an increasing re-circulation rate. This results in a lower power generation as the mass flow to the turbine decreases.
The temperature of the ocean is almost constant at 5 °C at a 1000 meter depth, while the temperature at the surface fluctuates. In tropical regions, the surface temperature can vary between 25 and 29 °C. Therefore, an OTEC system requires a working fluid which has a boiling point between 5 °C and 25 °C in addition to a high thermal conductivity and latent heat. The choice of the working fluid is based on Ganic and Wu [17], who state that ammonia seems to be the best working fluid, despite its toxic nature. Its high thermal conductivity and latent heat are more important, as less heat transfer area is needed. Therefore, ammonia was used in this

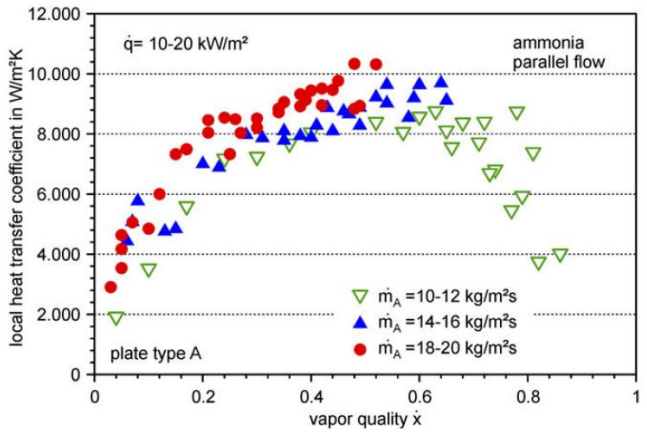

Figure 1.3: Heat transfer coefficient of evaporating ammonia with varying vapor quality and mass flux [12]

research.

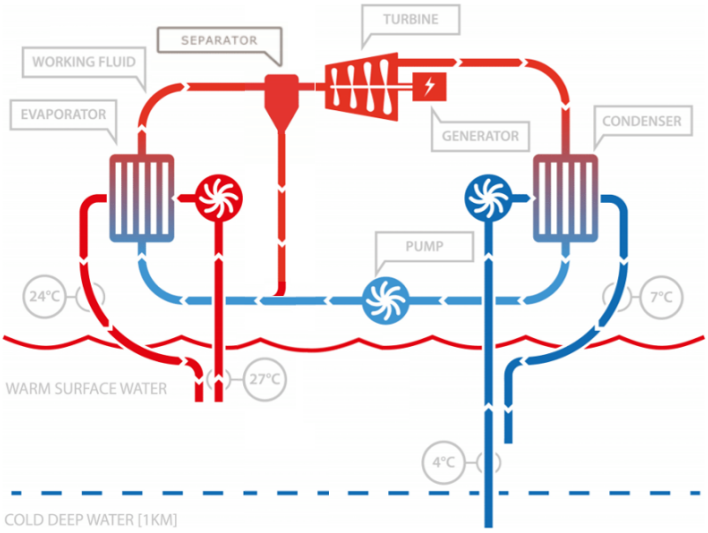

Figure 1.4: Schematic of the new ORC with a separator and re-circulation [52]

1.3. Relevance

The optimisation research conducted by Kirkenier [30], Stelwagen [52] and van Strijp [59] helped to understand the OTEC cycle and to find the optimum parameters for an OTEC cycle. A lot of research has been done on OTEC systems, but these are almost all conducted with steady-state models. But in reality, the parameters are continuously changing, e.g. the temperature of the ocean. This can be seen in Figure 1.5, which represents the temperature difference of the sea water in Curaçao. The figure shows that the temperature is fluctuating. The steady-state models are useful for design conditions and the optimisation of a process, but they fail to represent reality. Therefore, dynamic modeling is more appropriate for the fluctuating real-life cycles an OTEC cycle operates in.

To be able to run the plant at optimal conditions at all times, the power cycle has to be regulated using a control system. Some parts of the cycle can be controlled using feedback loops and sensors, to ensure optimal outlet conditions. For example, the mass flow can be regulated using the rotational speed of the pump. The dynamic input of the cycle will be used to control the cycle, using feedback loops. For instance, when the working fluid mass flow in the evaporator is too high, which results in a low outlet quality, the pump can be

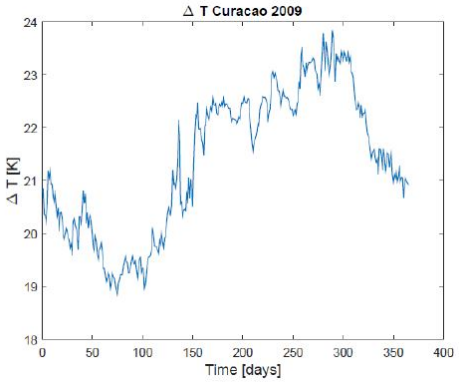

Figure 1.5: Temperature difference of Curacao during the year. As can be seen, the temperature difference fluctuates between 19 and 23 degrees in a year [59]

regulated to decrease the mass flow.

1.4. Objective

The main objective of this thesis is to investigate the impact of the transient region and propose a control strategy to optimise the cycle. A dynamic model is developed to research the impact of the transient region. The results of Kirkenier [30], Stelwagen [52] and van Strijp [59] are used as input, as these optimisation models give the best steady-state performance. With this dynamic model, the transient behaviour can be investigated, which can be used for further optimisation. For example, whether to lower the mass flow using the pumps at higher temperatures to reduce the energy consumption of the pumps instead of increasing the electricity generation of the turbine. Therefore, the following research question is defined:

"What is the impact of the transient region on the performance of an OTEC power cycle, and how can this be optimised using control?"

Accompanying sub-questions regarding this are:

- What are the controllable variables in an OTEC power cycle?
- What is the influence of the time-dependent temperature of the surface water?
- How does the system react to varying mass flows?
- How does the system react to start-up and shut-down procedures?
- How fast does the system react to failure of certain components?
- What is the optimal control strategy for an OTEC power plant?

1.5. Methodology

To develop the dynamic model, a literature study was conducted to find out which type of models are best applicable for each component of this research. After a model was selected for each component, this model was implemented as a modular model. This means that every component is modeled as a stand-alone component, so it can later be adjusted in case of changing geometry or configuration [6]. The model was built in Matlab & Simulink [38]. The thermodynamic properties of the ammonia were calculated using Fluidprop [5] with REFPROP [32] as database. REFPROP is a database containing many fluids and mixtures. As it does not contain the properties of sea water, a different program is used for the thermodynamic properties of the sea water. This is done using CoolProp [2].
After the model was built, it was validated with experimental data of the OTEC demo, residing at the TU Delft. After validation it was used to conduct simulations of the OTEC cycle in transient regions. Also, the optimisation using control was researched. Finally, the total impact of the transient region as well as the influence of control was determined through a comparison with existing steady-state models.

1.6. Thesis Outline

- Chapter 2 contains a literature review, describing the choice for the modelling method
- Chapter 3 contains the information about how the model is built, alongside the related calculations
- Chapter 4 shows the validation of the dynamic model
- Chapter 5 shows an overview of the results of the simulations
- Chapter 6 describes the optimisation using control in an OTEC power cycle
- Chapter 7 presents the conclusions and recommendations of this study

2

Model Selection

In this chapter, the different types of dynamic models will be explained and the decisions on how to model each component are elaborated.

2.1. Introduction

There are three types of dynamic modeling: white-box, grey-box and black-box. White-box modeling uses physical equations, such as the conservation equations, to describe the transient behaviour. These conservation equations consist of three equations: conservation of mass, conservation of energy and conservation of momentum. Black-box modeling uses experimental data and empirical relations to describe the transient behaviour. Grey-box modeling is a combination of black- and white-box modeling and consists of both physical equations and empirical relations. Grey-box modeling is mostly used in engineering practice, as most problems can be solved using the physics equations but some unknowns have to be solved through empirical results, such as efficiency maps and/or experimental data [58].

As the dynamics of pumps and turbines are much faster than the dynamics in heat exchangers, the influence of their dynamics is negligible. Therefore, the pumps and turbines can be modeled as static components [63]. The dynamics in the heat exchangers and tanks are leading in the model developed in this thesis. Therefore, they are modeled dynamically. An overview of the components and their modelling approach can be found in the next sections.

2.2. Heat Exchangers

In heat exchangers, there are three thermodynamic phases: liquid, liquid-vapor and vapor. There are two major distinctive methods to model a heat exchanger: using Finite Volumes (FV) and using a Moving Boundary (MB). These will be explained in Sections 2.2.1 and 2.2.2.

2.2.1. Finite Volume

The finite volume method is a method which subdivides the heat exchanger into several control volumes of equal volume across the heat exchanger. An example of a finite volume model can be seen in Figure 2.1. According to Desideri et al. [10], the conservation equations are derived from the one-dimensional conservation laws at constant volume. These laws are applicable for each control volume, and the output of the first volume will be used as input for the next volume. This can provide a very high level of detail, especially for the two-phase region. This is done by either assuming average or lumped parameters, or by directly discretizing the conservation equations. The larger the number of volumes is, the higher the level of detail is, but this comes at the cost of computational time.

According to Weerstra [62], one of the main problems with FV models is the conservation of momentum, as this results in long computation times. He states three solutions to implement the momentum equation: with an assumed pressure gradient, with static pressure drops between each volume or an accumulated pressure drop from all the volumes at the end. With this last solution, the pressure drop can be neglected as well, as

done by Bendapudi et al. [3] and Bamgbopa and Uzgoren [1]. The influence of the momentum equation is investigated by Zhang et al. [69] and Qiao et al. [44]. They both conclude that neglecting the pressure drop still is within the margin of error for large transients on a system level.

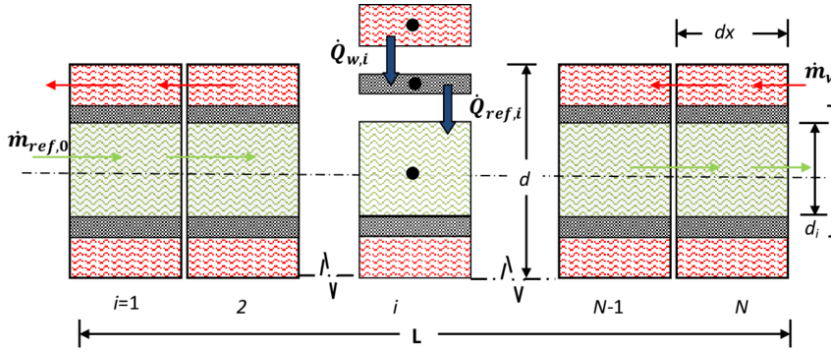

Figure 2.1: Finite Volume model. The gaps show the different control volumes. Seawater (red) flows through the boundaries, where the ammonia (green) flows through the center, only separated by a wall (grey) [1]

According to Desideri [10], the minimum number of 20 volumes is needed to avoid numerical inconsistency when using plate heat exchangers. Bendapudi [3] states that an FV model of 20 volumes is 20% slower than real-time. This makes an FV model not eligible for control, as at least real-time outputs are required to influence the cycle at the moment a change is needed.

2.2.2. Moving Boundary

The moving boundary method is a method which consists of a maximum of three volumes: one for each phase in the heat exchanger. There are three phases in the heat exchangers: liquid, liquid-vapor and vapor. The boundaries are time-dependent and can shift, depending on where the phase shift will take place.
Where the FV method captures great levels of detail due to the many volumes, the MB model tries to capture the dynamics by making use of lumped parameters. According to Wei et al. [63], a MB model is accurate enough to capture the leading dynamics behavior but simple enough to be used for real-time simulations and control. Because of the small number of volumes, the computational time will be low. These volumes are illustrated in Figure 2.2.

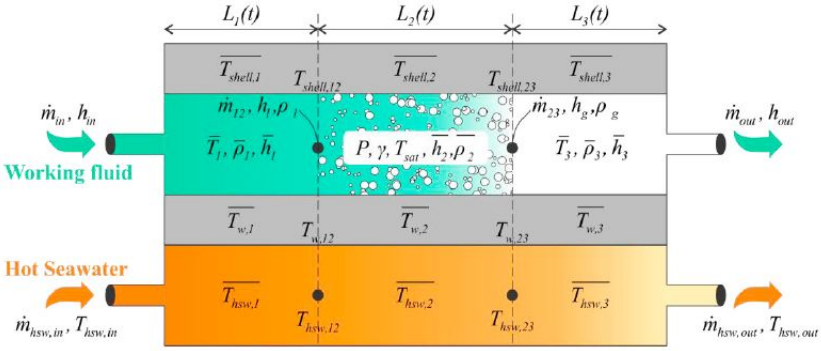

Figure 2.2: Moving boundary model. The dashed line indicates the boundary of a thermodynamic state. The hot seawater (orange) flows at the boundary, where the ammonia (cyan) flows through the center, only separated by a wall (grey) [11]

The MB method uses lumped parameters to model the volume. This means that the parameters are averaged per zone. To enable this in the two-phase region, Wedekind et al. [61] proposed a new variable, the mean void fraction. The mean void fraction assumption is almost universally applied by all researchers developing moving boundary models [48]. The void fraction is the ratio between the vapor volume and the total volume. The void fraction is given by Equation (2.1) [66].

$$\gamma(x) = \frac{x}{x + (1-x)\left(\frac{\rho_g}{\rho_l}\right)S} \tag{2.1}$$

where S = 1 for homogenous flow and S = $\left(\frac{\rho_l}{\rho_g}\right)^{\frac{1}{3}}$ when using the Zivi-correlation [70]. According to Wilson [66], the Zivi correlation is extremely accurate for void fractions above 0.8. As stated in Section 1.2, the vapor quality has to be between 0.4 and 0.7 to ensure the highest heat transfer coefficient. As shown by Wilson [66], the void fraction is around 0.8 for an average quality of 0.2-0.35, which corresponds to an outlet quality of 0.4 - 0.7. As this is within the range of this research, the Zivi correlation is applicable in this research.

Rasmussen and Shenoy [49] show that when a phase is not included in the model anymore, e.g. when the evaporator does not fully evaporates the fluid, the standard MB model gets a numerical failure. To be able to cope with this problem, another model was developed called the switching moving boundary, or SMB. This model is able to switch between certain modes, when a certain error margin is reached. This is shown by Fasl [16]. Fasl has improved the model of Li and Alleyne [33].

2.2.3. Comparison

The moving boundary and finite volume methods have been compared by several researchers, such as Desideri [10] and Bendapudi [3]. Desideri uses a small ORC of 11 kW and validates it with a test rig. From his research it appears that the accuracy of both the FV and MB method are almost the same, while the computational time of MB is 10 times faster. It should be noted that Desideri's research was only conducted for small changes. Large transient regions, such as start-up and shut-down procedures have not been investigated. Bendapudi [3] compares the FV and MB methods in a 300 kW centrifugal system. In this study he states that the FV and MB methods are almost the same in accuracy, but the moving boundary method used three times less computational time. However, he notes that the MB model was unable to handle the start-up transient. Pangborn [42] compares a FV with an SMB model, using data from an earlier report from Rasmussen [48]. His conclusion was that the SMB and the FV method with 200 volumes have a similar accuracy, but the SMB computes almost 85 times faster than the 200 FV method. This is in line with Bendapudi [3] and Desideri [10]. He does state another difference. An SMB uses the principal of mean void fraction, and is therefore dependent on the type and geometry of heat exchangers. This makes it less flexible than the FV method.

As stated in Section 1.3, the model will be used for control, so it requires at least real-time as computational time. It will contain heat exchangers in parallel, which requires even more computational time. With a fast computer, it is possible to receive real-time results for a single heat exchanger with the finite-volume method. But when using heat exchangers in parallel, also including the dynamics in the separator and buffer tank, the computational time will be too long to be able to use real-time control. Therefore, a moving boundary model will be used in this report as the model for the heat exchangers.

2.3. Pump & Turbine

The dynamics of the pump and the turbine are much faster than the dynamics of the heat exchangers. They are expected to reach a new steady-state almost instantaneously. Therefore, the pump and turbine are modeled as a steady-state component. This is also done by Wei et al. [63] and Quoilin et al. [47]. Semi-empirical relations are needed. They are dependent on the geometry of the component and therefore not easily scalable. The empirical relation can be found using the characteristic curves from the manufacturer. With regression analysis, performance and efficiency maps can be developed [36].

According to Tummescheit [57], there are two ways to compute these maps:

- Data-intensive approximation using interpolation. When data is available, this is the best way to go, as this can give the most accurate results
- Non-dimensionalized parameters which can be used to scale the parameters up to the real size

For the pump, a centrifugal pump is used. This is for both the seawater pumps as the working fluid pumps. This is also done in previous research into OTEC cycles, conducted by Stelwagen [52] and Kirkenier [30]. Wei et al. [63] use a regression analysis of the performance data presented by the manufacturer. The model depends on the pressure, the rotational speed and the volume flow, normalized over the design conditions. Zhang [68] uses a relation between the mass flow and the rotational speed. Ziviani [71] developed a correlation which relates the volumetric flow rate to both the pressure difference and the frequency. These correlations all depend on a specific pump, which makes it difficult to change the model and to scale the model.

Colonna and van Putten [7] developed a correlation that depends on certain parameters like the optimum point and the zeroes, in order to create a performance map. As this model is interchangeable and scales better, this correlation will be used.

According to van Strijp [59], the best type of turbine for an OTEC cycle is a single stage axial turbine. A single stage is best as the temperature difference is very low. The choice between a radial or axial turbine is made using the categorization done by Walsh [60]. According to Walsh, only axial turbines are applicable in the design conditions of OTEC.

For the modeling of the turbine, the well-known Stodola equation [53] will be used. This equation can be found in Equation (2.2).

$$\dot{m} = K\sqrt{\rho_i p_i \left(1 - \left(\frac{p_o}{p_i}\right)^2\right)} \tag{2.2}$$

This is also done by Tummescheit [57]. He states that the standard Stodola equation is only valid for multi-stage turbines or low-detailed models. This is due to an error that the equation gives, when calculating the mass flow around choking conditions. Choking conditions are the conditions when the flow becomes compressible, which is around a Mach number of one for homogeneous fluids. Dankerlui [8] concludes that for all working conditions for OTEC, the maximum Mach number is around 0.7. Therefore, it can be concluded that the flow will always be subsonic and the Stodola equation can be used without an extra factor.

Colonna and van Putten [7] also use the Stodola equation for calculating a mass flow. For calculating the outlet enthalpy, they use the thermodynamic states and the isentropic efficiency. They also include the heat transferred to the metal parts in the energy equation. The isentropic efficiency in their paper is dependent on the velocity of the working fluid and the blade, as well as the angle of the blades. Van Strijp [59] compares different correlations for the isentropic efficiency. Both the correlation of Jüdes & Tsatsaronis [27] and the correlation of Keeley [28] are checked. His conclusion is that the correlation of Jüdes is more reliable, as this is based on experimental data. As the study of van Strijp focuses on an OTEC cycle, the correlation of Jüdes & Tsatsaronis will be used in this report.

2.4. Piping

In literature, the piping is excluded from the model. This is done because the influence is relatively small, while it increases the computational time. Usually, the output of a pipe model is a pressure drop over the pipe. As most systems have a large pressure difference, the pressure drop due to the piping is negligible. But in an OTEC cycle, the pressure difference is small and the volume flow is high. This means that all the pressure drop, no matter how small, has an influence on the total energy production. Therefore, the choice was made to include the piping. The pipes are modeled as a steady-state component to keep the increase of computational time as low as possible, while still including the pressure drop in the model.

3

Model

In this chapter, all the different components of the model will be discussed. It includes both the dynamic and static models. As all outputs from components are the input for other components, an input-output scheme or a causality diagram is used to visualize the dependencies.

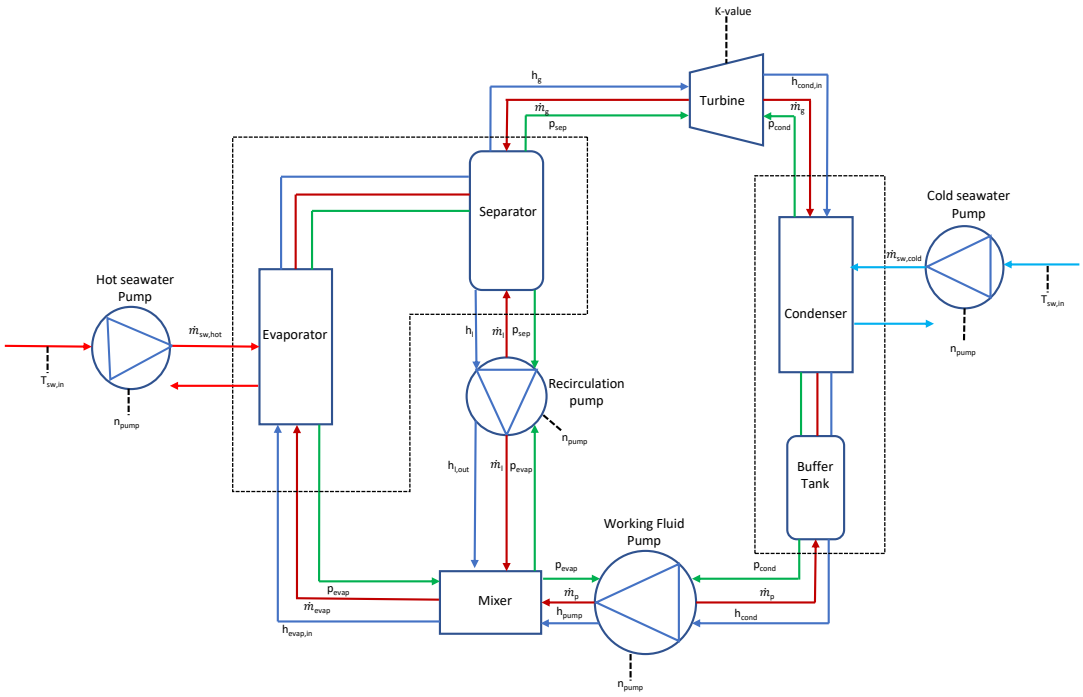

Figure 3.1: Causality diagram. The arrows show which component generates a parameter and feeds this to another component. For example, enthalpy (blue) and pressure (green) flow out of the separator, and the mass flow (red) goes into the separator. The dashed blocks have combined equations but a modular structure. The dashed lines represent the input for the model.

This diagram can be seen in Figure 3.1. A dashed block represents a combined model. This applies for the evaporator with the separator and the condenser with the buffer tank. See Sections 3.2.1 and 3.2.2 for more details. From this scheme, it can be seen that the mass flows are derived from the pump and turbine models, while the pressure levels are determined by the heat exchanger blocks.

3.1. Heat Exchangers

An OTEC power cycle makes use of heat exchangers: an evaporator and a condenser. In Section 2, the modeling choice for the heat exchanger has been explained. This method will be further elaborated in this section.

It uses inlet parameters from the cycle conditions (mixing point of re-circulation- and working fluid pump for the evaporator and the turbine outlet for the condenser) and the sea water pumps. These inputs (u) will, in combination with physical parameters and the state vector (x), give a time derivative of the state vector ($\dot{x}$). By integrating this time derivative, the solution of the new time step can be found. This requires initial conditions (x_0) to be set. The model outputs (y) depend on the other system components. They are derived using another function of the state vector.

Certain assumptions are made for the model:

- The heat exchanger is in a single pass arrangement.
- The working fluid flow is one-dimensional, compressible and unsteady.
- The cross-section area of the heat exchanger is assumed constant over the heat exchanger length.
- Axial heat conduction is neglected in the fluid element.
- The wall cross-section has a uniform temperature.

The governing equations are the conservation equations, namely conservation of mass and conservation of energy. The generic form can be found in Equations (3.1) and (3.2). Here, $\vec{u}$ is the fluid velocity vector, $\vec{f}$ is the body force vector and σ is the stress tensor. By applying the above mentioned assumptions, they can be simplified to Equations (3.3) and (3.4). This derivation is done by Grald & MacArthur [35]. They also give an equation for the conservation of the wall energy of the heat exchanger. This is given in Equation (3.5).

$$\frac{\partial \rho}{\partial t} + \nabla \cdot (\rho \vec{u}) = 0 \tag{3.1}$$

$$\frac{\partial (\rho \vec{u})}{\partial t} + \nabla \cdot (\rho \vec{u} \vec{u}) = \rho \vec{f} + \nabla \cdot \sigma \tag{3.2}$$

$$\frac{\partial (\rho A_{cs})}{\partial t} + \frac{\partial \dot{m}}{\partial z} = 0 \tag{3.3}$$

$$\frac{\partial (\rho A_{cs} h - p)}{\partial t} + \frac{\partial (\dot{m} h)}{\partial z} + \alpha_{wf} A (T_{wf} - T_w) = 0 \tag{3.4}$$

$$(c_p \rho A)_w \frac{\partial T_w}{\partial t} = \alpha_{wf} A (T_{wf} - T_w) + \alpha_{sw} A (T_{sw} - T_w) \tag{3.5}$$

A heat exchanger can be divided in three regions: a sub-cooled region, where the fluid is pure liquid, a two-phase region, where the fluid is both liquid and vapor, and a superheated region, where the fluid is pure vapor. The conservation equations given in Equations (3.3), (3.4) and (3.5) are applied on all three regions individually.
To be able to model the dynamics correctly, Partial Differential Equations (PDE) give difficulties. Therefore, these PDE's have to be rewritten to Ordinary Differential Equations (ODE). This can be done using the Leibniz integration rule, which can be found in Equation (3.6). Here, the equation is dependent on z, so it depends on the length of each region.

$$\int_{z_1(t)}^{z_2(t)} \frac{\partial f(z,t)}{\partial t} = \frac{d}{dt} \left(\int_{z_1(t)}^{z_2(t)} f(z,t) dz \right) + f\big(z_1(t),t\big) \frac{d(z_1(t))}{dt} - f\big(z_2(t),t\big) \frac{d(z_2(t))}{dt} \tag{3.6}$$

3.1.1. Evaporator

As stated in Section 1.2, the evaporator will only partially evaporate the working fluid. Therefore, there is no superheated model needed for the evaporator. The only phases which will be discussed are the sub-cooled region and the two-phase region. The governing equations are obtained by integrating Equations (3.3), (3.4) and (3.5) along the length of the heat exchanger, considering lumped parameters for each zone.

Mean void fraction

To be able to use lumped parameters in the two-phase region, a new parameter has been introduced: the mean void fraction. The void fraction is the ratio between the vapor volume and the total volume. A generalised form of the void fraction can be found in Equation (3.7). In this equation, S is defined as the slip factor. When the flow is homogeneous, S=1, which will provide the upper bound. The lower bound will be provided by the Zivi-correlation, which is $S = \left(\frac{\rho_l}{\rho_g}\right)^{\frac{1}{3}}$ [70]. As stated in Section 2.2.2, this is a valid assumption considering the evaporating conditions. Equation (3.7) will be integrated and averaged in Equation (3.8). The final form of the mean void fraction is given by Equation (3.9), with quantity μ_s given in Equation (3.10) [45].

$$\gamma(x) = \frac{x}{x + (1-x)\mu_s} \tag{3.7}$$

$$\overline{\gamma} = \frac{1}{x_o - x_i} \int_{x_i}^{x_o} \gamma(x)\, dx \tag{3.8}$$

$$\overline{\gamma} = \frac{1}{x_o - x_i} \left[\frac{\mu_s}{(\mu_s - 1)^2} \ln\left(\frac{x_i(\mu_s - 1) - \mu_s}{x_o(\mu_s - 1) - \mu_s} \right) \right] - \frac{1}{\mu_s - 1} \tag{3.9}$$

$$\mu_s = \left(\frac{\rho_g}{\rho_l}\right) S \tag{3.10}$$

The lumped variables in the two-phase region can be described as follows: $h_2 = h_l(1-\overline{\gamma}) + h_g(\overline{\gamma})$. This is applicable for all state variables. It is stated by Wedekind [61] that a mean void fraction that is invariant of time is valid for small system transients. This could be a problem in start-up and shut-down procedures. But as the output of the evaporator will be two-phase, the outlet quality will be determined using the mean void fraction. Therefore, the mean void fraction will be variant with time.

Governing equations

The governing equations for the conservation of mass and energy of the sub-cooled region are given in Equations (3.11) and (3.12). The governing equations for the two-phase region can be found in Equations (3.13) and (3.14). A full derivation can be found in Appendix A.

$$\left(\left(\left.\frac{\partial \rho_1}{\partial p}\right|_{h_1} + \frac{1}{2}\frac{\partial \rho_1}{\partial h_1}\left|_p \frac{\partial h_l}{\partial p} \right.\right) \frac{dp}{dt} + \frac{1}{2}\left.\frac{\partial \rho_1}{\partial h_1}\right|_p \frac{dh_{in}}{dt} \right) L_1 A_{cs} + (\rho_1 - \rho_l)\frac{dL_1}{dt} A_{cs} + \dot{m}_{12} - \dot{m}_{in} = 0 \tag{3.11}$$

$$\begin{aligned} &\left(\left.\frac{\partial \rho_1}{\partial h_1}\right|_p h_1 + \rho_1 \right) L_1 A_{cs} \frac{1}{2}\frac{dh_{in}}{dt} + \left(\frac{1}{2}\left(\left.\frac{\partial \rho_1}{\partial h_1}\right|_p \frac{\partial h_l}{\partial p} h_1 + \rho_1 \frac{\partial h_l}{\partial p} \right) + \left.\frac{\partial \rho_1}{\partial p}\right|_{h_1} h_1 - 1 \right) L_1 A_{cs} \frac{dp}{dt} \\ &\quad + (\rho_1 h_1 - \rho_l h_l) A_{cs} \frac{dL_1}{dt} + \dot{m}_{12} h_l - \dot{m}_{in} h_{in} = \alpha_{1wf} A_{wf} \frac{L_1}{L} \left(T_{1w} - T_{1wf} \right) \end{aligned} \tag{3.12}$$

$$\left(\frac{\partial \rho_l}{\partial p}(1-\overline{\gamma}) + \frac{\partial \rho_g}{\partial p}\overline{\gamma} \right) A_{cs} L_2 \frac{dp}{dt} + \left(\rho_g - \rho_l\right) A_{cs} L_2 \frac{d\overline{\gamma}}{dt} + \left(\rho_l - \rho_g\right)\overline{\gamma} A_{cs} \frac{dL_1}{dt} + \dot{m}_o - \dot{m}_{12} = 0 \tag{3.13}$$

$$\begin{aligned} &\left(\frac{\partial(\rho_g h_g)}{\partial p}\overline{\gamma} + (1-\overline{\gamma})\frac{\partial(\rho_l h_l)}{\partial p} - 1 \right) A_{cs} L_2 \frac{dp}{dt} + (\rho_l h_l - \rho_g h_g) A_{cs} \overline{\gamma} \frac{dL_1}{dt} + (\rho_g h_g - \rho_l h_l) A_{cs} L_2 \frac{d\overline{\gamma}}{dt} \\ &= \dot{m}_{12} h_l - \dot{m}_o h_o + \alpha_2 A_{wf} \frac{L_2}{L} (T_{2w} - T_{2wf}) \end{aligned} \tag{3.14}$$

The energy conservation of the wall zones is given in Equations (3.15) and (3.16).

$$(c_p \rho V)_w \left(\frac{dT_{1w}}{dt} - \left(\frac{T_{1w} - T_{2w}}{L_1} \right) \frac{dL_1}{dt} \right) = \alpha_1 A_{wf} (T_{1wf} - T_{1w}) + \alpha_{sw} A_{sw} (T_{1sw} - T_{1w}) \tag{3.15}$$

$$(c_p \rho V)_w \frac{dT_{2w}}{dt} = \alpha_2 A_{wf} (T_{2wf} - T_{2w}) + \alpha_{sw} A_{sw} (T_{2sw} - T_{2w}) \tag{3.16}$$

The six equations only contain five explicit time derivatives: $\frac{dL_1}{dt}$, $\frac{dp}{dt}$, $\frac{d\overline{\gamma}}{dt}$, $\frac{dT_{1w}}{dt}$ and $\frac{dT_{2w}}{dt}$. The time derivative $\frac{dh_{in}}{dt}$ is neglected as this is sufficiently small [15]. By rearranging the six equations, $\dot{m}_{12}$ can be eliminated. This derivation is done in Appendix A. These time derivatives are the state-space time derivatives, stated as $\dot{\mathbf{x}}$.

The equations can be rearranged in the descriptor form $Z(u,x)\dot{\mathbf{x}} = f(x,u)$. The new equations can be found in Equation (3.17). The values for Z(u,x) can be found in Table 3.1.

$$\begin{bmatrix} z_{11} & z_{12} & 0 & 0 & 0 \\ z_{21} & z_{22} & z_{23} & 0 & 0 \\ z_{31} & z_{32} & z_{33} & 0 & 0 \\ z_{41} & 0 & 0 & z_{44} & 0 \\ 0 & 0 & 0 & 0 & z_{55} \end{bmatrix} \begin{bmatrix} \frac{dL_1}{dt} \\ \frac{dp}{dt} \\ \frac{d\overline{\gamma}}{dt} \\ \frac{dT_{1w}}{dt} \\ \frac{dT_{2w}}{dt} \end{bmatrix} = \begin{bmatrix} \dot{m}_i(h_i - h_l) + \alpha_1 A_{wf} \frac{L_1}{L}(T_{1w} - T_{1wf}) \\ \dot{m}_o(h_l - h_o) + \alpha_2 A_{wf} \frac{L_2}{L}(T_{2w} - T_{2wf}) \\ \dot{m}_i - \dot{m}_o \\ \alpha_1 A_{wf}(T_{1wf} - T_{1w}) + \alpha_{sw} A_{sw}(T_{1sw} - T_{1w}) \\ \alpha_2 A_{wf}(T_{2wf} - T_{2w}) + \alpha_{sw} A_{sw}(T_{2sw} - T_{2w}) \end{bmatrix} \tag{3.17}$$

Table 3.1: Matrix elements of Z(x,u) for the evaporator

z_{11}	$(\rho_1 (h_1 - h_l) A_{cs}$
z_{12}	$\left[\left(\frac{\partial \rho_1}{\partial p} + \frac{1}{2}\frac{\partial \rho_1}{\partial h_1}\frac{dh_l}{dp}\right)(h_1 - h_l) + \left(\frac{1}{2}\frac{dh_l}{dp}\right)\rho_1 - 1\right] A_{cs} L_1$
z_{21}	$[\rho_g (h_l - h_g)] A_{cs} \overline{\gamma}$
z_{22}	$\left[\left(\frac{\partial (\rho_g h_g)}{\partial p} - \frac{\partial \rho_g}{\partial p} h_l\right)\overline{\gamma} + (1 - \overline{\gamma})\frac{\partial h_l}{\partial p}\rho_l - 1\right] A_{cs} L_2$
z_{23}	$\rho_g (h_g - h_l) A_{cs} L_2$
z_{31}	$[(\rho_1 - \rho_l) + (\rho_l - \rho_g)(\overline{\gamma} - 1)] A_{cs}$
z_{32}	$\left[\left(\frac{\partial \rho_1}{\partial p} + \frac{1}{2}\frac{\partial \rho_1}{\partial h_1}\frac{dh_l}{dp}\right) L_1 + \left(\frac{d\rho_l}{dp}(1 - \overline{\gamma}) + \frac{d\rho_g}{dp}\overline{\gamma}\right) L_2\right] A_{cs}$
z_{33}	$(\rho_g - \rho_l) A_{cs} L_2$
z_{41}	$(c_p \rho V)_w \left(\frac{T_{1w} - T_{2w}}{L_1}\right)$
z_{44}	$(c_p \rho V)_w$
z_{55}	$(c_p \rho V)_w$

As the mean void fraction is a state variable, this can be used to calculate the new outlet quality, on which all new working fluid properties depend. Rasmussen [48] shows a simplification for the calculation of the outlet quality. When saturated vapor exits the evaporator, $x_o = 1$. For small deviations, we can set $x_o = 1$ inside the natural log. This can be solved for x_o. According to Eldredge [15], this is valid when the outlet quality is between 0.8 and 1. As the outlet quality of this research is set to be around 0.7, this is not deemed valid. Therefore, the full solution is calculated. This can be found in Equation (3.18), where W is the product log function, or the Lambert W function.

$$x_o = \frac{\mu_s \left(W\left(\frac{(\mu_s x_i - x_i - \mu_s) e^{\left(\mu_s \overline{\gamma} x_i + \frac{\overline{\gamma} x_i}{\mu_s} - 2\overline{\gamma} x_i - \frac{x_i}{\mu_s} + x_i + \frac{\mu_s \left(\mu_s \overline{\gamma} + \frac{\overline{\gamma}}{\mu_s} - 2\overline{\gamma} - \frac{1}{\mu_s} + 1 \right)}{1 - \mu_s} \right)(\mu_s \overline{\gamma} - \overline{\gamma} + 1)}}{\mu_s} \right) \right) + \mu_s \overline{\gamma} - \overline{\gamma} + 1}{(\mu_s - 1)(\mu_s \overline{\gamma} - \overline{\gamma} + 1)} \tag{3.18}$$

3.1.2. Condenser

For the condenser, the working fluid inlet will always be either saturated vapor, or two-phase. Because saturated vapor enters the turbine, small liquid parts will exit the turbine after expanding. Therefore, only two regions have to be modeled, namely the two-phase region and the sub-cooling region. The condenser model is derived the same way and uses the same assumptions as the evaporator, but it also uses one extra assumption. From steady-state experiments conducted by Bluerise B.V., it can be seen that the sub-cooling heat transfer consist of less than 0.05% of the total heat transfer. Rasmussen [48] and Eldredge [15] state that for

a situation like this, pseudoquality can be introduced. Pseudoquality means that the quality can be negative in the calculations. This makes it possible to model only the two-phase region while still capturing the sub-cooling region. This will be further elaborated in this section.

Governing equations

The governing equations are derived the same way as for the evaporator, by integrating Equations (3.1), (3.2) and (3.5). They can be found in Equations (3.19), (3.20) and (3.21). The full derivation can be found in Appendix A.

$$\left(\frac{\partial \rho_l}{\partial p}(1-\overline{\gamma})+\frac{\partial \rho_g}{\partial p}\overline{\gamma}\right)V_{wf}\frac{dp}{dt}+(\rho_g-\rho_l)V_{wf}\frac{d\overline{\gamma}}{dt}=\dot{m}_i-\dot{m}_o \tag{3.19}$$

$$\left(\frac{\partial(\rho_f h_f)}{\partial p}(1-\overline{\gamma})+\frac{\partial(\rho_g h_g)}{\partial p}\overline{\gamma}-1\right)V_{wf}\frac{dp}{dt}+(\rho_g h_g-\rho_l h_l)V_{wf}\frac{d\overline{\gamma}}{dt}=\dot{m}_i h_i-\dot{m}_o h_o+\alpha_{wf}A_{wf}(T_w-T_{wf}) \tag{3.20}$$

$$(c_p\rho V)_w\frac{dT_w}{dt}=\alpha_{wf}A_{wf}(T_{wf}-T_w)+\alpha_{sw}A_{sw}(T_{sw}-T_w) \tag{3.21}$$

The resulting three equations contain three explicit time derivatives: $\frac{dp}{dt}$, $\frac{d\overline{\gamma}}{dt}$ and $\frac{dT_w}{dt}$. They can be rearranged in the descriptor form $Z(u,x)\dot{\mathbf{x}}=f(x,u)$. This form can be found in Equation (3.22). The values for Z(u,x) can be found in Table 3.2.

$$\begin{bmatrix} z_{11} & z_{12} & 0 \\ z_{21} & z_{22} & 0 \\ 0 & 0 & z_{33} \end{bmatrix}\begin{bmatrix} \frac{dp}{dt} \\ \frac{d\overline{\gamma}}{dt} \\ \frac{dT_w}{dt} \end{bmatrix}=\begin{bmatrix} \dot{m}_i-\dot{m}_o \\ \dot{m}_i h_i-\dot{m}_o h_o+\alpha_{wf}A_{wf}(T_w-T_{wf}) \\ \alpha_{wf}A_{wf}(T_{wf}-T_w)+\alpha_{sw}A_{sw}(T_{sw}-T_w) \end{bmatrix} \tag{3.22}$$

Table 3.2: Matrix elements of Z(x,u) for the condenser

z_{11}	$\left(\frac{\partial \rho_l}{\partial p}(1-\overline{\gamma})+\frac{\partial \rho_g}{\partial p}\overline{\gamma}\right)V_{wf}$
z_{12}	$(\rho_g-\rho_l)V_{wf}$
z_{21}	$\left(\frac{\partial(\rho_f h_f)}{\partial p}(1-\overline{\gamma})+\frac{\partial(\rho_g h_g)}{\partial p}\overline{\gamma}-1\right)V_{wf}$
z_{22}	$(\rho_g h_g-\rho_l h_l)V_{wf}$
z_{33}	$(c_p\rho V)_w$

As stated at the beginning of this section, the condenser model will make use of pseudoquality. This means that the outlet quality can become negative. The inlet quality is in the range of 0.95-1, according to the steady-state models made by Bluerise B.V. The equation to calculate the outlet quality of the condenser can be found in Equation (3.18). To use the pseudoquality, the properties should not be calculated using REFPROP, but by making use of the two-phase formula $h=h_l(1-x)+h_g(x)$. This also works for negative x. According to Eldredge [15], this allows the models to capture the sub-cooling outlet conditions without the need to switch modes.

3.1.3. Sea Water Temperature

To capture the average sea water temperature in the heat exchanger, an energy balance is made for a counter-current heat exchanger, based on the theory of Shah [50]. A visualization of the energy balance can be found in Figure 3.2a.

The energy balance over a small and arbitrary length dz becomes Equation (3.23).

$$\dot{m}_{sw}c_{p,sw}\left(T_{sw,z}-T_{sw,z+dz}\right)=\alpha_{sw}A_{sw}\frac{dz}{L}\left(T_{sw,z}-T_w\right) \tag{3.23}$$

By rewriting and integrating Equation (3.23), the temperatures at the boundaries can be calculated. The equations for the evaporator can be found in Equations (3.24) and (3.25). The outlet temperature of the condenser can be found in Equation (3.28). A full derivation can be found in Appendix A. The average temperature for

the evaporator for each region can be found in Equations (3.26) and (3.27). A visualization of the evaporator can be found in Figure 3.2b.

$$T_{sw,12} = T_{w,2} + \left(T_{sw,in} - T_{w,2}\right) e^{\frac{-\alpha_{sw} A_{sw} L_2}{m_{sw} c_{p,sw} L}} \tag{3.24}$$

$$T_{sw,out} = T_{w,1} + \left(T_{sw,12} - T_{w,1}\right) e^{\frac{-\alpha_{sw} A_{sw} L_1}{m_{sw} c_{p,sw} L}} \tag{3.25}$$

$$\overline{T}_{sw,1} = T_{w,1} + \left(T_{sw,12} - T_{w,1}\right)\left(\frac{m_{sw} c_{p,sw} L}{\alpha_{sw} A_{sw} L_1}\right)\left(1 - e^{\frac{-\alpha_{sw} A_{sw} L_1}{m_{sw} c_{p,sw} L}}\right) \tag{3.26}$$

$$\overline{T}_{sw,2} = T_{w,2} + \left(T_{sw,in} - T_{w,2}\right)\left(\frac{m_{sw} c_{p,sw} L}{\alpha_{sw} A_{sw} L_2}\right)\left(1 - e^{\frac{-\alpha_{sw} A_{sw} L_2}{m_{sw} c_{p,sw} L}}\right) \tag{3.27}$$

For the condenser, the equation for the average temperature can be found in Equation (3.29).

$$T_{sw,out} = T_w + \left(T_{sw,in} - T_w\right) e^{\frac{-\alpha_{sw} A_{sw}}{m_{sw} c_{p,sw}}} \tag{3.28}$$

$$\overline{T}_{sw} = T_w + \left(T_{sw,in} - T_w\right)\left(\frac{m_{sw} c_{p,sw}}{\alpha_{sw} A_{sw}}\right)\left(1 - e^{\frac{-\alpha_{sw} A_{sw}}{m_{sw} c_{p,sw}}}\right) \tag{3.29}$$

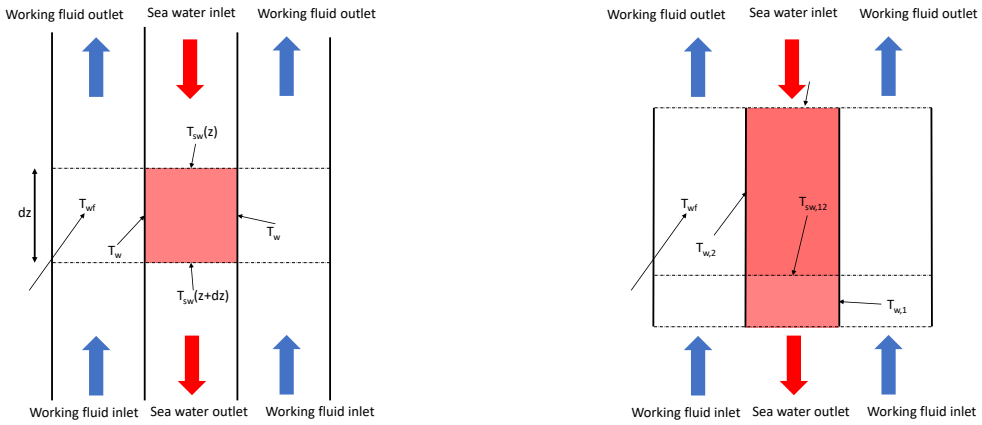

(a) Arbitrary length

(b) Evaporator of model

Figure 3.2: Visualisation of counter-current heat exchangers

3.1.4. Heat Transfer Correlations

Stelwagen [52] conducted research on the heat transfer correlations in an OTEC configuration for both single-phase and two-phase of the evaporator. He concludes that the best heat transfer correlations are Goudriaan & Kuikhoven [19] for the sea water, Donowski & Kandlikar [13] for the single-phase ammonia and Khan et al. [29] for the two-phase evaporating ammonia. Therefore, these correlations will be used in this research. They can be found in Table 3.3.

For the condenser, Tao et al. [56] have performed experiments for the best correlation of two-phase condensation. They conclude that the correlation of Kuo [31] has the best fit for calculating the heat transfer coefficient, but it was not tested for ammonia. They tested the correlations again and found that at low mass flux, the surface tension becomes more dominant. Therefore, they introduced a new correlation, where the heat transfer coefficient is dependent on both the convective condensation and the gravity controlled condensation. They state that the transition between gravity controlled condensation and convective condensation is at a Weber number of 0.12. The Weber number can be found in Appendix B. The heat transfer coefficient depends on the ratio between the liquid Weber number and the transition Weber number. The correlation can be found in Table 3.3. The equations can be found in Equations (3.30), (3.31), (3.32), based on the correlation for single phase by Martin et al. [37], (3.33), (3.34), (3.35) and (3.36), based on the film condensation equation made by Nusselt [41].

$$\xi_0 = \begin{cases} \frac{64}{Re_{eq}} & Re_{eq} < 2000 \\ \frac{1}{(1.8\log Re_{eq} - 1.5)^2} & Re_{eq} \geq 2000 \end{cases} \tag{3.30}$$

$$\xi_1 = \begin{cases} \frac{597}{Re_{eq}} + 3.85 & Re_{eq} < 2000 \\ Re_{eq}^{-0.289} & Re_{eq} \geq 2000 \end{cases} \tag{3.31}$$

$$f_D = \left(\frac{\cos\beta}{\sqrt{0.18\tan\beta + 0.36\sin\beta + \frac{\xi_0}{\cos\beta}}} + \frac{1-\cos\beta}{\sqrt{3.8\xi_1}} \right)^{-2} \tag{3.32}$$

$$\alpha_{lo} = 0.122\left(f_D \sin\beta\right)^{0.374} Re_{eq}^{0.748} Pr_l^{0.333} \left(\frac{\mu}{\mu_w}\right)^{0.167} \frac{\lambda_i}{d_h} \tag{3.33}$$

$$\alpha_{cc} = \alpha_{lo}\left(0.2275 Co^{-0.95} Fr_l^{-0.1905} + (1-x)^{0.748}\right) \tag{3.34}$$

$$\Theta = \frac{We_l}{We_{lt}} \tag{3.35}$$

$$\alpha_{gc} = 0.36(Co + 0.008)^{-0.32} \left(\frac{g\rho_l(\rho_l - \rho_g)h_{vap}\lambda_l^3}{\mu_l(T_{wf} - T_w)d_h} \right)^{0.25} \tag{3.36}$$

Table 3.3: Heat transfer correlations used in the system

Evaporator		
Author	**Fluid**	**Single-phase correlation**
Goudriaan & Kuikhoven [19]	Sea Water	$\alpha_{sw} = \frac{\lambda_i}{d_e} 0.291 Re_i^{0.72} Pr_i^{0.33}$
Donowski & Kandlikar [13]	Ammonia	$\alpha_{wf} = \frac{\lambda_i}{d_e} 0.2875 Re_i^{0.78} Pr_i^{\frac{1}{3}}$
Author	**Fluid**	**Two-phase correlation**
Khan et al. [29]	Ammonia	$Nu_{tp} = (-173.52\frac{\beta}{60} + 257.12)$ $* (Bo_e Re_e)^{-0.09\frac{\beta}{60}+0.0005} \left(\frac{p}{p_{crit}}\right)^{-0.624\frac{\beta}{60}+0.822}$

Condenser		
Author	**Fluid**	**Two-phase correlation**
Tao et al.[55]	Ammonia	$\alpha_{wf} = \Theta\alpha_{cc} + (1-\Theta)\alpha_{gc}$
Author	**Fluid**	**Single-phase correlation**
Goudriaan & Kuikhoven [19]	Sea Water	$\alpha_{sw} = \frac{\lambda_i}{d_e} 0.291 Re_i^{0.72} Pr_i^{0.33}$

By including pseudoquality in the condenser to create the sub-cooled region, the heat transfer coefficient changes. According to Shah [50], a steady-state heat balance will suffice due to the short moment of sub-cooling. By using the liquid heat transfer coefficient, the length of the sub-cooled region can be calculated using Equation (3.37). The new equation for the heat transfer coefficient can be found in Equation (3.38). This formula is only applicable when the outlet enthalpy h_o is smaller than the saturated liquid enthalpy h_l.

$$L_{sc} = \frac{\dot{m}_o(h_l - h_o)}{\alpha_l\left(T_w - T_{wf}\right)d_e} \tag{3.37}$$

$$\overline{\alpha} = \frac{\alpha_{tp}(L - L_{sc}) + \alpha_{sp}L_{sc}}{L} \tag{3.38}$$

3.1.5. Pressure drop

In almost all moving boundary models, the pressure drop in the heat exchanger is neglected as the computational time increases significantly when including the dynamic momentum equation, while the impact is small. This is done by Zhang et al. [68], Tummescheit [57], Shah et al. [50], Eldredge et al. [15], Rasmussen et al. [48], Pangborn et al. [42], Huster et al. [24] and Horst et al. [23]. But, as stated by Qiao and Laughman [44], in some applications the pressure drop cannot be neglected. In an OTEC cycle, all small pressure differences influence the outcome significantly, especially for the sea water side. Therefore, it was decided to include the pressure drop in the heat exchangers. Qiao and Laughman [44] compare five different methods of including the momentum equation. Their conclusion is that the friction-only method is the best choice when considering the trade-off between computational time and accuracy. Therefore, this method will be used in the model.

Qiao et al. [45] give two options for the pressure drop: A general pressure drop at the end of the heat exchanger and a linear changing pressure over the heat exchanger. The choice is made to use the first approach. This is done because Qiao uses the outlet pressure as a boundary, where the model uses the outlet mass flow as a boundary. The accuracy between a general pressure drop and a linear changing pressure drop is minimal, but an extra equation would be needed when using the linear changing pressure approach in comparison with the general pressure drop. Therefore, a general pressure drop is used.

This general pressure drop is calculated using a correlation. Different correlations for the pressure drop in the heat exchanger have been implemented in the model. According to Stelwagen [52], the best correlation for the single phase pressure drop is the correlation proposed by Martin [37]. This correlation can be found in Equations (3.30), (3.31) and (3.32), with the change that it is specifically for a liquid or vapor Reynolds number instead of the equivalent Reynolds number. The correlation is tested over a wide range of experimental data, and therefore deemed valid. This correlation will be used in the model for both the sea water and the single phase working fluid.

Stelwagen also conducted a research for the best correlation in the two-phase evaporating region. He concludes that the best correlation is made by Yan & Lin [67]. Therefore, this correlation will be used in the evaporator. The correlation can be found in Equation (3.39). The pressure drop is calculated using Equations (3.40) and (3.41)

$$f_{D,tp} = 4 * \frac{6.947 * 10^5 * Re_{eq}^{-1.109}}{Re_l^{0.5}} \tag{3.39}$$

$$\Delta P_{sp} = f_{D,sp} \frac{G^2 L_1}{2 d_h \rho_i} \tag{3.40}$$

$$\Delta P_{tp} = f_{D,tp} \frac{G^2 L_2}{2 d_h \rho_m} \tag{3.41}$$

Tao & Infante Ferreira conducted research for the condenser. They came up with a modified version of the Lockhart-Martinelli method [34]. This new correlation has been validated with ammonia. Therefore, this new correlation will be used in the condenser. All equations can be found in Equations (3.42), (3.43) and (3.44), where $f_{D,l}$ and $f_{D,g}$ are the Darcy friction factors for single phase liquid and single phase vapor.

$$\Delta P_l = f_{D,l} \frac{G^2 (1 - x_m)^2 L}{2 \rho_l d_h} \tag{3.42}$$

$$\Delta P_g = f_{D,g} \frac{G^2 x_m^2 L}{2 \rho_g d_h} \tag{3.43}$$

$$\Delta P_{tp} = \Delta P_l + 2 \sqrt{\Delta P_l \Delta P_g} + x_m \Delta P_g \tag{3.44}$$

All correlations can be found in Table 3.4.

Table 3.4: Pressure drop correlations used in the system

Author	Heat exchanger	Single-phase correlation
Martin [37]	Evaporator/Condenser	$f_{D,sp} = \left(\frac{\cos\beta}{\sqrt{0.18\tan\beta + 0.36\sin\beta + \frac{f_0}{\cos\beta}}} + \frac{1-\cos\beta}{\sqrt{3.8 f_1}} \right)^{-0.5}$
Author	**Heat exchanger**	**Two-phase correlation**
Yan and Lin [67]	Evaporator	$f_{D,tp} = 4 * \frac{6.947 * 10^5 * Re_e^{-1.109}}{Re^{0.5}}$
Tao et al.	Condenser	$\Delta P_{tp} = \Delta P_l + 2\sqrt{\Delta P_l \Delta P_g} + x_m \Delta P_g$

3.2. Working Fluid

To ensure a level of working fluid in the system, tanks are installed to store excess working fluid. These buffers are placed after the heat exchangers and are modeled in the same way, for the exception that the separator has more than one purpose: separating the two-phase ammonia exiting the evaporator.

3.2.1. Buffer Tank

The condenser outlet can be two-phase, as stated in Section 3.1.2. When small vapor parts enter the pump, they can implode at high pressure, resulting in cavitation. This can be prevented by sub-cooling inside the condenser, but all sub-cooling has to be re-heated in the evaporator. Therefore, a small sub-cooling is wanted in the design case. To ensure pure liquid flow into the pumps and to keep a consistent mass flow in the system, buffer tanks are installed between the condenser and the working fluid pump. These buffer tanks work as a receiver. There are a few assumptions done for the buffer tank, as done by Qiao [46] and Eldredge [15]:

- The outlet is saturated liquid
- The vapor and liquid are in phase equilibrium
- The pressure in the buffer tank is the same as in the condenser
- The buffer tank is adiabatic

The buffer tanks receive either pure liquid or two-phase flow from the condenser and only pure liquid flows out. When the outlet quality of the condenser is larger than 0 (i.e. two-phase flow), the pressure in the buffer tank will rise due to the increase of vapor in the tank. This increase will continue until the outlet enthalpy is equal to the enthalpy of saturated liquid. The opposite occurs when subcooled liquid exits the condenser. Due to the cooling in the buffer tank, the pressure will decrease until the outlet enthalpy equals the saturated liquid enthalpy.
To ensure this coupling between the condenser and the buffer tank, the buffer tank model is integrated in the condenser model, with the same pressure.
According to Sohel [51], the heat capacity in the structure is negligible when the Biot number is lower than 0.1. The Biot number can be found in Appendix B. As the Biot number is smaller than 0.1 for heat transfer coefficient of air, a heat conductivity coefficient of stainless steel and a length of more than 1 m, the heat accumulation in the structure is assumed negligible and will not be included in the calculation.

To model the buffer tank, a mass- and energy balance are made. It uses the pressure and enthalpy as state variables. The governing equations can be found in Equations (3.45) and (3.46). A full derivation can be found in Appendix A.

$$\frac{dm_{bt}}{dt} = \dot{m}_{in} - \dot{m}_{out} \tag{3.45}$$

$$\begin{aligned} &\left[\left(\frac{d\rho_g}{dp} V_g u_g + \frac{d\rho_l}{dp} V_l u_l + \frac{du_g}{dp} V_g \rho_g + \frac{du_l}{dp} V_l \rho_l \right) - \left(\frac{\rho_g u_g - \rho_l u_l}{\rho_g - \rho_l} \right) \left(\frac{d\rho_g}{dp} V_g + \frac{d\rho_l}{dp} V_l \right) \right] \frac{dp}{dt} \\ &+ \left(\frac{\rho_g u_g - \rho_l u_l}{\rho_g - \rho_l} \right) \frac{dm_{bt}}{dt} = \dot{m}_i h_i - m_o h_l \end{aligned} \tag{3.46}$$

V_l and V_g can be calculated using the following relations: Refrigerant mass in the buffer tank is $m_{bt} = m_g + m_l$, refrigerant energy is $m_{bt}u_{bt} = m_g u_g + m_l u_l$, receiver volume is $V_{bt} = V_g + V_l$ and mass of the vapor and

liquid part is m = ρV. From this, it follows:

$$V_l = \frac{\rho_g V_{bt} - m_{bt}}{\rho_g - \rho_l} \tag{3.47}$$

$$V_g = \frac{\rho_l V_{bt} - m_{bt}}{\rho_l - \rho_g} \tag{3.48}$$

As $\dot{m}_i$ for the receiver is $\dot{m}_o$ of the condenser, the governing equations of the condenser can be rewritten. The new governing equations, written in descriptor form, can be found in Equation (3.49). The values for Z can be found in Table 3.5

$$\begin{bmatrix} z_{11} & z_{12} & z_{13} & 0 \\ z_{21} & z_{22} & z_{23} & 0 \\ z_{31} & z_{32} & 0 & 0 \\ 0 & 0 & 0 & z_{44} \end{bmatrix} \begin{bmatrix} \frac{dp}{dt} \\ \frac{m_{rec}}{dt} \\ \frac{d\overline{\gamma}}{dt} \\ \frac{dT_w}{dt} \end{bmatrix} = \begin{bmatrix} \dot{m}_i - \dot{m}_o \\ \dot{m}_i h_i - \dot{m}_o h_l + \alpha_{wf} A_{wf} (T_w - T_{wf}) \\ \dot{m}_o (h_{cond,o} - h_l) \\ \alpha_{wf} A_{wf} (T_{wf} - T_w) + \alpha_{sw} A_{sw} (T_{sw} - T_w) \end{bmatrix} \tag{3.49}$$

Table 3.5: Matrix elements of Z(x,u) for the condenser, including buffer tank

z_{11}	$\left(\frac{\partial \rho_l}{\partial p}(1-\overline{\gamma}) + \frac{\partial \rho_g}{\partial p}\overline{\gamma}\right) V_{wf}$
z_{12}	1
z_{13}	$(\rho_g - \rho_l) V_{wf}$
z_{21}	$\left(\frac{\partial (\rho_l h_l)}{\partial p}(1-\overline{\gamma}) + \frac{\partial (\rho_g h_g)}{\partial p}\overline{\gamma} - 1\right) V_{wf}$
z_{22}	$h_{cond,o}$
z_{23}	$(\rho_g h_g - \rho_l h_l) V_{wf}$
z_{31}	$\left(\frac{d\rho_g}{dp} V_g u_g + \frac{d\rho_l}{dp} V_l u_l + \frac{du_g}{dp} V_g \rho_g + \frac{du_l}{dp} V_l \rho_l\right) - \left(\frac{\rho_g u_g - \rho_l u_l}{\rho_g - \rho_l}\right)\left(\frac{d\rho_g}{dp} V_g + \frac{d\rho_l}{dp} V_l\right)$
z_{32}	$\left(\frac{\rho_g u_g - \rho_l u_l}{\rho_g - \rho_l} - h_{cond,o}\right)$
z_{44}	$(c_p \rho V)_w$

To measure the level of liquid in the buffer tank, as well as in the separator, the density inside the tank is calculated. The density inside the tank is calculated using Equation (3.50). The liquid level in the tank is calculated using Equation (3.51).

$$\rho_{bt} = \frac{m_{bt}}{V_{bt}} \tag{3.50}$$

$$H_{bt,l} = \frac{\rho_{bt} - \rho_g}{\rho_l - \rho_g} H_{bt} \tag{3.51}$$

3.2.2. Separator

The separator splits the two-phase working fluid exiting the evaporator into saturated liquid and saturated vapor. It is modeled as an extra control volume of the evaporator with one inlet and two outlets. A few assumptions are made, as done by Qiao [46] and Eldredge [15]:

- The outlets are saturated conditions
- The vapor and liquid are in phase equilibrium
- The pressure in the separator is the same as in the evaporator
- The separator is adiabatic

It can be coupled with the evaporator by modeling the separator as an accumulator, or receiver. By changing the outlet of the receiver from only saturated liquid to both saturated liquid and saturated vapor, a separator can be modeled. Coupling the evaporator and the separator makes it possible to eliminate the outlet mass flow of the evaporator. Therefore, the choice is made to combine the equations of these two components. This results in one pressure for both components. The assumption of an adiabatic separator is deemed valid,

as the Biot number is smaller than 0.1. The separator is modeled in the same way as the buffer tank. The outlet of the evaporator is two-phase and the outlet of the separator is both saturated liquid and saturated vapor. The governing equations can be found in Equations (3.52) and (3.53). A full derivation can be found in Appendix A.

$$\frac{dm_{sep}}{dt} = \dot{m}_{in} - \dot{m}_{turb} - \dot{m}_{gear} \tag{3.52}$$

$$\begin{aligned}&\left[\left(\frac{d\rho_g}{dp}V_g u_g + \frac{d\rho_l}{dp}V_l u_l + \frac{du_g}{dp}V_g\rho_g + \frac{du_l}{dp}V_l\rho_l\right) - \left(\frac{\rho_g u_g - \rho_l u_l}{\rho_g - \rho_l}\right)\left(\frac{d\rho_g}{dp}V_g + \frac{d\rho_l}{dp}V_l\right)\right]\frac{dp}{dt} \\ &+\left(\frac{\rho_g u_g - \rho_l u_l}{\rho_g - \rho_l}\right)\frac{dm_{sep}}{dt} = \dot{m}_i h_i - m_{turb}h_g - m_{gear}h_l\end{aligned} \tag{3.53}$$

V_l and V_g can be calculated using the following relations: Refrigerant mass in the buffer tank is $m_{sep} = m_g + m_l$, refrigerant energy is $m_{sep}u_{sep} = m_g u_g + m_l u_l$, receiver volume is $V_{sep} = V_g + V_l$ and mass of the vapor and liquid part is $m = \rho V$. From this, it follows:

$$V_l = \frac{\rho_g V_{sep} - m_{sep}}{\rho_g - \rho_l} \tag{3.54}$$

$$V_g = \frac{\rho_l V_{sep} - m_{sep}}{\rho_l - \rho_g} \tag{3.55}$$

As $\dot{m}_i$ for the separator is $\dot{m}_o$ for the evaporator, the governing equations of the evaporator can be rewritten. The new governing equations, written in the descriptor form, can be found in Equation (3.56). The values for Z can be found in Table 3.6.

$$\begin{bmatrix} z_{11} & z_{12} & 0 & 0 & 0 & 0 \\ z_{21} & z_{22} & z_{23} & z_{24} & 0 & 0 \\ z_{31} & z_{32} & z_{33} & z_{34} & 0 & 0 \\ 0 & z_{42} & 0 & z_{44} & 0 & 0 \\ z_{51} & 0 & 0 & 0 & z_{55} & 0 \\ 0 & 0 & 0 & 0 & 0 & z_{66} \end{bmatrix} \begin{bmatrix} \frac{dL_1}{dt} \\ \frac{dp}{dt} \\ \frac{d\overline{\gamma}}{dt} \\ \frac{d\dot{m}_{sep}}{dt} \\ \frac{dT_{1w}}{dt} \\ \frac{dT_{2w}}{dt} \end{bmatrix} = \begin{bmatrix} \dot{m}_i(h_i - h_l) + \alpha_1 A_{wf}\frac{L_1}{L}(T_{1w} - T_{1wf}) \\ \left(\dot{m}_{gear} + \dot{m}_{turb}\right)(h_l - h_{evap,o}) + \alpha_2 A_{wf}\frac{L_2}{L}(T_{2w} - T_{2wf}) \\ \dot{m}_i - \dot{m}_{gear} - \dot{m}_{turb} \\ \dot{m}_{gear}(h_{evap,o} - h_l) + \dot{m}_{turb}(h_{evap,o} - h_g) \\ \alpha_1 A_{wf}(T_{1wf} - T_{1w}) + \alpha_{sw}A_{sw}(T_{1sw} - T_{1w}) \\ \alpha_2 A_{wf}(T_{2wf} - T_{2w}) + \alpha_{sw}A_{sw}(T_{2sw} - T_{2w}) \end{bmatrix} \tag{3.56}$$

3.2.3. Mixer

The working fluid gets separated by the separator, but is also combined again after the gear pump and the working fluid pump have increased the pressure again. As this is a simple junction, the mass- and energy balance are steady-state balances. From the mixer model, the inlet conditions of the evaporator can be found. The mass- and energy balance can be found in Equations (3.57) and (3.58). The junction has a small pressure drop. This pressure drop is modeled as a constant pressure drop of 0.05 bar, based on a calculation using Equation (3.79). More on this in Section 3.5.2.

$$\dot{m}_{evap,i} = \dot{m}_{gear} + \dot{m}_{pump} \tag{3.57}$$

$$\dot{m}_{evap,i}h_{evap,i} = \dot{m}_{gear}h_{gear,o} + \dot{m}_{pump}h_{pump,o} \tag{3.58}$$

3.3. Turbine

As stated in Section 2.3, the pump and turbine will be modeled as steady-state. The turbine will use the well-known Stodola equation [53]. This equation can be found in Equation (3.59). This equation can be used to calculate the mass flow at every pressure drop.

$$\dot{m} = K\sqrt{\rho_i p_i\left(1 - \left(\frac{p_o}{p_i}\right)^2\right)} \tag{3.59}$$

Table 3.6: Matrix elements of Z(x,u) for the evaporator, including the separator

z_{11}	$(\rho_1 (h_1 - h_l) A_{cs}$
z_{12}	$\left[\left(\frac{\partial \rho_1}{\partial p} + \frac{1}{2}\frac{\partial \rho_1}{\partial h_1}\frac{dh_l}{dp}\right)(h_1 - h_l) + \left(\frac{1}{2}\frac{dh_l}{dp}\right)\rho_1 - 1\right] A_{cs} L_1$
z_{21}	$[\rho_g (h_l - h_g)] A_{cs} \overline{\gamma}$
z_{22}	$\left[\left(\frac{\partial (\rho_g h_g)}{\partial p} - \frac{\partial \rho_g}{\partial p} h_l\right)\overline{\gamma} + (1-\overline{\gamma})\frac{\partial h_l}{\partial p}\rho_l - 1\right] A_{cs} L_2$
z_{23}	$\rho_g (h_g - h_l) A_{cs} L_2$
z_{24}	$h_o - h_l$
z_{31}	$[(\rho_1 - \rho_l) + (\rho_l - \rho_g)(\overline{\gamma} - 1)] A_{cs}$
z_{32}	$\left[\left(\frac{\partial \rho_1}{\partial p} + \frac{1}{2}\frac{\partial \rho_1}{\partial h_1}\frac{dh_l}{dp}\right) L_1 + \left(\frac{d\rho_l}{dp}(1-\overline{\gamma}) + \frac{d\rho_g}{dp}\overline{\gamma}\right) L_2\right] A_{cs}$
z_{33}	$(\rho_g - \rho_l) A_{cs} L_2$
z_{34}	1
z_{42}	$\left(\frac{d\rho_g}{dp} V_g u_g + \frac{d\rho_l}{dp} V_l u_l + \frac{du_g}{dp} V_g \rho_g + \frac{du_l}{dp} V_l \rho_l\right) - \left(\frac{\rho_g u_g - \rho_l u_l}{\rho_g - \rho_l}\right)\left(\frac{d\rho_g}{dp} V_g + \frac{d\rho_l}{dp} V_l\right)$
z_{44}	$\left(\frac{\rho_g u_g - \rho_l u_l}{\rho_g - \rho_l} - h_{evap,o}\right)$
z_{51}	$(c_p \rho V)_w \left(\frac{T_{1w} - T_{2w}}{L_1}\right)$
z_{55}	$(c_p \rho V)_w$
z_{66}	$(c_p \rho V)_w$

In this equation, K is a constant, dependent on the design conditions of the turbine. At design conditions, all parameters are known and K can be calculated. With known inlet and outlet conditions, the mass flow can be calculated for every situation.

For the calculation of the efficiency of the turbine, the correlation of Jüdes & Tsatsaronis [27] is used. Van Strijp [59] concludes that this correlation is the best to determine the efficiency. This correlation can be found in Equation (3.60).

$$\eta_{is} = \eta_{is,des}\left[-1.0176\left(\frac{\dot{m}}{\dot{m}_{des}}\right)^4 + 2.4443\left(\frac{\dot{m}}{\dot{m}_{des}}\right)^3 - 2.1812\left(\frac{\dot{m}}{\dot{m}_{des}}\right)^2 + 1.0535\left(\frac{\dot{m}}{\dot{m}_{des}}\right) + 0.701\right] \tag{3.60}$$

When the outlet quality of the turbine is lower than one, the correlation has to be corrected. This correction is done in Equation (3.61), where Δx is the change in quality in relation with the design value.

$$\eta_{is,corr} = \eta_{is} - \frac{1}{2}\Delta x \tag{3.61}$$

The quality used in Equation (3.61) is calculated from the enthalpy of the outlet. The enthalpy of the outlet is calculated using Equation (3.62). With this enthalpy, the quality is known, being dependent of enthalpy and pressure. Using the corrected isentropic efficiency, the new enthalpy is calculated, also using Equation (3.62).

$$h_o = h_i - (h_i - h_{o,is})\eta_{is} \tag{3.62}$$

The power generated by the turbine is given by Equation (3.63).

$$\dot{W}_{turb} = \dot{m}(h_i - h_o) \tag{3.63}$$

3.3.1. Generator

The mechanical energy generated in the turbine has to be converted into electrical energy. This is done by a generator. A generator converts the rotational energy from the turbine into AC current. To be able to deliver this current to the grid, it has to be at a frequency of 50 or 60 Hertz, depending on the grid. This corresponds

to 3000 or 3600 rpm. The generator has an efficiency, η_{gen}. According to Haglind [21], the losses are due to friction, electrical losses and copper losses. As friction and electrical losses are independent of the load that is generated, these values will be taken as a constant. The copper losses are dependent of the load. The equation for the generator efficiency at partial load can be seen in Equation (3.64). The value for F_{cu} is 0.43. This is the same as used by Haglind [21]. He states that it corresponds very well with experimental data. Therefore, it is assumed as a proper value.

$$\eta_{gen} = \frac{\eta_{gen,des} PL}{\eta_{gen,des} PL + (1 - \eta_{gen,des}) \left((1 - F_{cu}) + F_{cu} PL^2 \right)} \tag{3.64}$$

The partial load is given by Equation (3.65).

$$PL = \frac{\dot{W}_{turb}}{\dot{W}_{turb,des}} \tag{3.65}$$

3.4. Pumps

As mentioned earlier, the pumps will be modeled as static components, as the dynamics in the pump are negligible compared to the heat exchangers. They are implemented using an empirical relation, dependent on manufacturer data. When the impeller is known, the flow rate can be determined using the performance map. As the inlet pressure is known from the condenser and the outlet pressure is known from the evaporator, the map can be used to find the flow rate. This can be rewritten into a mass flow rate. This method is proposed by Colonna and van Putten [7].

According to Colonna and van Putten, the volume flow can be calculated which can be obtained using the pump characteristics. The method makes use of dimensionless parameters of the pump head and the volume flow, H_{nd} and $\dot{V}_{nd}$, defined in Equations (3.66) and (3.67).

$$H_{nd} = \frac{gH}{n^2 d^2} \tag{3.66}$$

$$\dot{V}_{nd} = \frac{\dot{V}}{nd^3} \tag{3.67}$$

These dimensionless parameters result in a parabolic pump characteristic, defined in Equation (3.68).

$$H_{nd} = a\dot{V}_{nd}^2 + b\dot{V}_{nd} + c \tag{3.68}$$

a, b and c can be found solving the following system of equations:

$$\begin{aligned} \frac{gH_{des}}{n_{des}^2 d_{des}^2} &= a\left(\frac{\dot{V}_{des}}{n_{des} d_{des}^3}\right)^2 + b\left(\frac{\dot{V}_{des}}{n_{des} d_{des}^3}\right) + c \\ 0 &= a\left(\frac{\dot{V}_0}{n_{des} d_{des}^3}\right)^2 + b\left(\frac{\dot{V}_0}{n_{des} d_{des}^3}\right) + c \\ \frac{gH_0}{n_{des}^2 d_{des}^2} &= c \end{aligned} \tag{3.69}$$

By substituting Equations (3.66) and (3.67) in Equation (3.68) and rewriting the equation, it becomes Equation (3.70).

$$\dot{V} = \frac{-\frac{bn}{gd_{des}} - \sqrt{\frac{b^2 n^2}{g^2 d_{des}^2} + \frac{4aH}{gd_{des}^4} - \frac{4acn^2}{g^2 d_{des}^2}}}{\frac{2a}{gd_{des}^4}} \tag{3.70}$$

In this equation, the head can be described by Equation (3.71).

$$H = \frac{p}{\rho g} \tag{3.71}$$

With the volume flow, the mass flow can be calculated using Equation (3.72).

$$\dot{m} = \overline{\rho}\dot{V} \tag{3.72}$$

where $\overline{\rho}$ is the average value of the in- and outlet density of the pump.
The efficiency is given in Equation (3.73).

$$\eta = \eta_{des}\left(1-\left(1-\frac{\dot{V}}{\dot{V}_{des}}\frac{n}{n_{des}}\right)^2\right) \tag{3.73}$$

With this efficiency, the outlet enthalpy can be calculated using Equation (3.74). Also, the pump power can be calculated using Equation (3.75).

$$h_o = h_i + \frac{h_{o,is}-h_i}{\eta} \tag{3.74}$$

$$\dot{W}_{pump} = \frac{\dot{V}\Delta p}{\eta} \tag{3.75}$$

3.5. Piping

The piping in the OTEC cycle is coupled with the mass flow. As the mass flow is an output of the steady-state components as the turbine and the pumps, the pipes will also be modeled as steady-state. The pipe model will have a pressure drop as output. The pump power is linearly dependent on the pressure drop. Therefore, it is important to keep the influence of the piping as low as possible. The pressure drop in the pipes can be divided into three major components: major losses, minor losses and hydrostatic losses. The major losses are the losses due to friction, the minor losses are the losses due to different components in the pipes such as pipe inlets, bends, etc. and the hydrostatic losses are the losses due to a difference in density as a result of a height difference.

3.5.1. Major losses

As said earlier, the major losses are the losses due to friction. The pressure drop can be described using the well-known Darcy-Weisbach formula [9][64], which can be found in Equation (3.76).

$$\Delta P_{maj} = f_D L\frac{\rho}{2}\frac{v^2}{D} \tag{3.76}$$

The Darcy friction factor f_D is different for laminar and turbulent flow. Laminar flow occurs at a Reynolds number smaller than 2000. For laminar flow, it is given by a small rewriting of the Hagen-Poiseuille equation [43], and can be found in Equation (3.77).

$$f_D = \frac{64}{Re} \tag{3.77}$$

For turbulent flow, the Reynolds number has to be larger than 4000. The Darcy friction factor for turbulent flow can be calculated using different methods. It can be read from the diagrams made by Moody [40], or calculated using an iterative method made by Colebrook [4]. As an iterative method is computationally unfavorable, especially with ever changing parameters, an approximation is used to calculate the Darcy friction factor. The approximation is done by Haaland [20]. This approximation can be found in Equation (3.78).

$$\frac{1}{\sqrt{f_D}} = -1.8\log\left[\left(\frac{\frac{\epsilon}{D}}{3.7}\right)^{1.11}+\frac{6.9}{Re}\right] \tag{3.78}$$

In an OTEC cycle, the flow is always turbulent. Only during start-up and shutdown procedures can the flow be laminar, but this is only for a short amount of time. Due to the very high flows, the velocity will be high and therefore the Reynolds number will be above 4000.

3.5.2. Minor losses

The minor losses are the losses due to non-uniform flow, caused by certain pipe components, such as bends, pipe inlets and tees. These losses are dependent on the minor loss coefficient of each component. The pressure drop is given by Equation (3.79).

$$\Delta P_{min} = K\frac{\rho v^2}{2} \tag{3.79}$$

The minor loss coefficient K is different for each component. Per component, it is also geometry and mass flow dependent. Maps including the different minor loss coefficients can be found in graphs made by Idel'chik [25] and Miller [39]. For simplicity, a constant value per component is assumed.

3.5.3. Hydrostatic losses

The hydrostatic losses occur due to a difference in density between the deep sea water and the water at the surface. The density changes with the depth of the water, due to a temperature change. For simplicity, the density profile is taken as a linear profile. This means that the hydrostatic losses can be given by the difference between the cold water density and the average density. As the density profile, in reality, tends to change only at the top, this is a conservative approach. The pressure loss is given in Equation (3.80), where ρ_m is given by Equation (3.81).

$$\Delta P_{hyd} = \left(\rho_{sw,cold} - \rho_m\right) g L_{depth} \tag{3.80}$$

$$\rho_{sw,m} = \frac{\rho_{sw,cold} + \rho_{sw,hot}}{2} \tag{3.81}$$

3.5.4. Total loss

To calculate the total loss, Equation (3.82) is used. The minor losses are added up as pipes can have multiple components.

$$\Delta P_{total} = \Delta P_{maj} + \sum \Delta P_{min} + \Delta P_{hyd} \tag{3.82}$$

As the hydrostatic pressure is dependent on the density difference between the pipe in- and outlet. As this is only relevant for the cold water pipe in the sea, the hydrostatic pressure is neglected for all pipes other than the cold water inlet pipe.

4

Validation

In the previous chapters, the choice for a model has been made and the physics and mathematics describing the model have been explained. In this chapter, the model will be validated using experimental data from an experimental set-up.

4.1. Experimental set-up

At the Process & Energy lab at the TU Delft, a small scale OTEC test set-up has been built. This set-up is known as the OTEC demo. The OTEC demo includes all components for both an Organic Rankine Cycle and a Kalina cycle. A Kalina cycle is a different power cycle, which is not in the scope of this thesis and therefore will not be discussed. A visualisation of the OTEC demo can be found in Figure 4.1a, with a list of components given in Table 4.1b. The recuperator from Table 4.1b is only applicable for a Kalina cycle and therefore not of interest for this thesis. The OTEC demo consists of sensors to measure temperature and pressure throughout the system, as well as flow sensors to measure the total flow, the re-circulation flow and the vapor flow through the orifice/valve.

4.1.1. Changes from original model

To validate the model, it has to be adjusted from the 3 MW scale to the scale of the experimental set-up. As can be seen from Table 4.1b, the OTEC demo does not include a turbine. This is because the original turbine in the set-up broke down and has been replaced by an orifice combined with a valve. This means that the turbine in the model described in Chapter 3 has to be replaced with a valve. The new equation for a valve becomes Equation (4.1).

$$\dot{m} = C_d A \sqrt{\rho_i (p_i - p_o)} \tag{4.1}$$

By changing the opening area of the valve, the pressure difference over the orifice changes. This makes it an extra input for the cycle. The valve is assumed to be isenthalpic, as done by Qiao and Rasmussen [46][48]. Stelwagen [52] also based his research on experiments from the OTEC demo and he states that the orifice is an ideal orifice, meaning there is no build-up of mass and the structure is adiabatic. From the mass- and energy balance, it follows that the inlet mass and enthalpy are equal to the outlet mass and enthalpy.

In the model, sea water is used as cooling medium. In the OTEC demo, the cold and hot water basin consist of normal water. Therefore, the properties for the cooling water are changed to water. This influences the heat transfer coefficient of the cooling medium and therefore also the overall heat transfer coefficient of the heat exchangers.

The working fluid pump is also different from the pump in the large-scale OTEC cycle. As stated in Section 2.3, the pumps in the large-scale model are centrifugal pumps. In the OTEC demo, the working fluid pump is a reciprocating pump, or positive displacement pump. By moving the liquid using a piston, the mass flow is determined. This piston is connected to a disc that rotates at a predetermined speed. With this type of pump, the pump curve is different than the one described in Section 3.4. As the piston is connected directly to the rotational disc, the mass flow is linearly dependent on the rotational speed. The new mass flow formula

becomes Equation (4.2).

$$\dot{m} = \frac{n}{n_{des}} \dot{m}_{des} \tag{4.2}$$

From Table 4.1b, it can be seen that there is no gear pump in the OTEC demo. Experiments were carried out with two types of pumps, but both broke down, presumably due to the ammonia. The separator separates the working fluid with gravity, so with natural recirculation. Natural recirculation can also be modeled in a different way. The mass flow through the working fluid pump is known from the buffer tank level, and the mass flow through the evaporator is known from the experiments. As the recirculation flow is $\dot{m}_{evap} - \dot{m}_{pump}$, the gear pump can be controlled to maintain the evaporator mass flow, resulting in a recirculation flow. This also determines the outlet quality.

(a) Experimental set-up of the OTEC demo

Number	Component
1	Evaporator
2	Separator
3	Orifice & Valve
4	Recuperator
5	Condenser
6	Cold water pump
7	Buffer tank
8	Working fluid pump
9	Hot water pump

(b) OTEC demo component list

Figure 4.1: OTEC demo in the lab at the TU Delft

As stated before, the valve is isenthalpic. As the pressure decreases, but the enthalpy stays the same, the saturated vapor becomes superheated. Therefore, a new state has to be included in the equations from Section 3.2.1. These equations are derived the same way as the sub-cooled region of the evaporator. The new set of equations can be found in Equation (4.3). The values for Z can be found in Table 4.1. A full derivation can be found in Appendix A.

$$\begin{bmatrix} z_{11} & z_{12} & 0 & 0 & 0 & 0 \\ z_{21} & z_{22} & z_{23} & z_{24} & 0 & 0 \\ z_{31} & z_{32} & z_{33} & z_{34} & 0 & 0 \\ 0 & z_{42} & 0 & z_{44} & 0 & 0 \\ z_{51} & 0 & 0 & 0 & z_{55} & 0 \\ 0 & 0 & 0 & 0 & 0 & z_{66} \end{bmatrix} \begin{bmatrix} \frac{dL_1}{dt} \\ \frac{dp}{dt} \\ \frac{d\overline{\gamma}}{dt} \\ \frac{d\dot{m}_{bt}}{dt} \\ \frac{dT_{1w}}{dt} \\ \frac{dT_{2w}}{dt} \end{bmatrix} = \begin{bmatrix} \dot{m}_i(h_i - h_g) + \alpha_1 A_{wf} \frac{L_1}{L}(T_{1w} - T_{1wf}) \\ \dot{m}_o(h_g - h_o) + \alpha_2 A_{wf} \frac{L_2}{L}(T_{2w} - T_{2wf}) \\ \dot{m}_i - \dot{m}_o \\ \dot{m}_o(h_o - h_l) \\ \alpha_1 A_{wf}(T_{1wf} - T_{1w}) + \alpha_{sw} A_{sw}(T_{1sw} - T_{1w}) \\ \alpha_2 A_{wf}(T_{2wf} - T_{2w}) + \alpha_{sw} A_{sw}(T_{2sw} - T_{2w}) \end{bmatrix} \tag{4.3}$$

Table 4.1: Matrix elements of Z(x,u) for the condenser, including the buffer tank, in the OTEC demo

z_{11}	$(\rho_1 (h_1 - h_g) A_{cs}$
z_{12}	$\left[\left(\frac{\partial \rho_1}{\partial p} + \frac{1}{2}\frac{\partial \rho_1}{\partial h_1}\frac{dh_g}{dp}\right)(h_1 - h_g) + \left(\frac{1}{2}\frac{dh_g}{dp}\right)\rho_1 - 1\right] A_{cs} L_1$
z_{21}	$[\rho_l (h_g - h_l)] A_{cs}(1 - \overline{\gamma})$
z_{22}	$\left[\left(\frac{\partial(\rho_g h_g)}{\partial p} - \frac{\partial \rho_g}{\partial p} h_l\right)\overline{\gamma} + (1 - \overline{\gamma})\frac{\partial h_l}{\partial p}\rho_l - 1\right] A_{cs} L_2$
z_{23}	$\rho_g (h_g - h_l) A_{cs} L_2$
z_{24}	$h_o - h_g$
z_{31}	$[\rho_1 - \rho_l(1 - \overline{\gamma}) + \rho_g \overline{\gamma}] A_{cs}$
z_{32}	$\left[\left(\frac{\partial \rho_1}{\partial p} + \frac{1}{2}\frac{\partial \rho_1}{\partial h_1}\frac{dh_g}{dp}\right) L_1 + \left(\frac{d\rho_l}{dp}(1 - \overline{\gamma}) + \frac{d\rho_g}{dp}\overline{\gamma}\right) L_2\right] A_{cs}$
z_{33}	$(\rho_g - \rho_l) A_{cs} L_2$
z_{34}	1
z_{42}	$\left(\frac{d\rho_g}{dp} V_g u_g + \frac{d\rho_l}{dp} V_l u_l + \frac{du_g}{dp} V_g \rho_g + \frac{du_l}{dp} V_l \rho_l\right) - \left(\frac{\rho_g u_g - \rho_l u_l}{\rho_g - \rho_l}\right)\left(\frac{d\rho_g}{dp} V_g + \frac{d\rho_l}{dp} V_l\right)$
z_{44}	$\left(\frac{\rho_g u_g - \rho_l u_l}{\rho_g - \rho_l} - h_{evap,o}\right)$
z_{51}	$(c_p \rho V)_w \left(\frac{T_{1w} - T_{2w}}{L_1}\right)$
z_{55}	$(c_p \rho V)_w$
z_{66}	$(c_p \rho V)_w$

All changes from the original model to the experimental set-up scale can be seen in Table 4.2

Table 4.2: Changes from the 3 MW scale into experimental set-up scale

Component	Changed from	Changed into
Turbine	Turbine	Orifice
Working fluid pump	Centrifugal pump	Reciprocating pump
Gear pump	Centrifugal pump	Controlled natural re-circulation
Condenser	Single state (two-phase)	Two states (superheat & two-phase)
Seawater	Thermodynamic seawater properties	Thermodynamic water properties

4.1.2. Data reduction

Data from the OTEC demo is captured by different type of sensors. The placement of these sensors can be seen from the process & instrumentation diagram, or P&ID. This can be found in Appendix C. The data is logged in an Excel file, and can be visualized using an in-house tool. An example is given in Figure 4.2. In this figure the pressure level can be seen before and after the orifice. As the experiments were conducted to measure different steady-state levels, the pressure levels are constant for a longer period of time. On the x-axis, it is possible to see the time. On the y-axis, the pressure levels are shown. From these data, both the

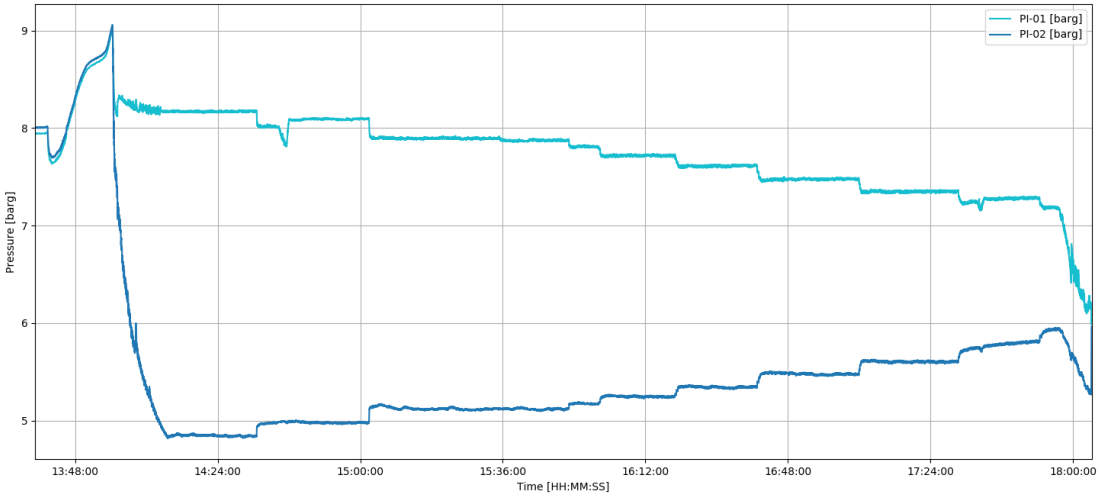

Figure 4.2: Example of data plot showing the pressure before (light blue) and after (dark blue) the orifice

steady-state as the dynamics of the model can be validated. As the only parameters measured are pressure, temperature and mass flow, other parameters have to be calculated from these parameters. The thermodynamic properties are calculated using REFPROP for the ammonia and CoolProp for the cooling water.

The flow meter of the evaporator is not accurate enough, as it fluctuates between 0 and 0.008 $\frac{g}{s}$ while the real value is around 0.005 $\frac{g}{s}$. Therefore, the mass flow of the working fluid has to be calculated. This can be done by adding the liquid and vapor flow from the separator, coming from sensors FI-201 and FI-202. With both the mass flow through the condenser and through the gear pump known, the mass flow through the evaporator can be calculated for steady-state using Equation (4.4).

$$\dot{m}_{evap} = \dot{m}_{gear} + \dot{m}_{cond} \tag{4.4}$$

To calculate the heat transfer through the heat exchangers, a steady energy balance is used. The heat transfer is calculated using the sea water mass flow and temperatures, using Equation (4.5), where the specific heat capacity c_p is a function of the pressure and temperature.

$$\dot{Q} = \dot{m} c_p \Delta T \tag{4.5}$$

The inlet enthalpy is obtained using the inlet temperature and pressure. With the heat transfer, mass flow and inlet enthalpy known, the outlet enthalpy can be calculated using Equation (4.6). With this outlet enthalpy, the outlet quality can be calculated using REFPROP using the outlet pressure.

$$\dot{Q} = \dot{m} \Delta h \tag{4.6}$$

The steady-state value for the outlet quality of the evaporator can also be calculated using Equation (4.7), which is an equation that only works in steady-state conditions.

$$x_{o,evap} = \frac{\dot{m}_{valve}}{\dot{m}_{evap}} \tag{4.7}$$

4.2. Steady-state Validation

First, a steady-state validation is done. This is done on the small-scale model, using the OTEC demo. The OTEC demo set-up has the following inputs:

- Cooling water mass flow (cold and warm)
- Cooling water temperature (cold and warm)
- Pressure drop over the orifice

These parameters can be controlled, and therefore used as input for the set-up. Stelwagen [52] conducted his experiments with the inputs found in Table 4.3. The cooling water parameters are constant and the pressure drop over the orifice is varied. In his model, there was no buffer tank present, nor was there any accumulation of liquid. The experiments do show a liquid level in the buffer tank, which is controlled. This extra input is used as an input for the model.

Table 4.3: Input values for the OTEC demo experiments. The pressure drop is changed for each experiment, the rest is a constant

dp_{valve} [bar]	$T_{cw,h}$ [°C]	$\dot{m}_{cw,h}\left[\frac{kg}{s}\right]$	$T_{cw,c}$ [°C]	$\dot{m}_{cw,c}\left[\frac{kg}{s}\right]$	BT level [%]
1.48-3.32	27	0.3	5	0.225	20

To match the experiments done by Stelwagen, the mass flow of the ammonia through the evaporator in the model is controlled for each step. The resulting inputs for the model can be seen in Table 4.4. The opening of the valve is calculated by using a controller for the opening to match the required pressure drop over the valve. This way, the steady-state values should match the experimental values.

Table 4.4: Model inputs for steady-state validation, generated from the experiments

#	$\dot{m}_{evap,i}\left[\frac{kg}{s}\right]$	dp_{valve} [bar]	$T_{cw,h}$ [°C]	$\dot{m}_{cw,h}\left[\frac{kg}{s}\right]$	$T_{cw,c}$ [°C]	$\dot{m}_{cw,c}\left[\frac{kg}{s}\right]$	BT level [%]
1	0.00378	3.32	27	0.3	5	0.225	20
2	0.00394	3.11	27	0.3	5	0.225	20
3	0.00449	2.75	27	0.3	5	0.225	20
4	0.00472	2.46	27	0.3	5	0.225	20
5	0.00485	2.26	27	0.3	5	0.225	20
6	0.00491	2.00	27	0.3	5	0.225	20
7	0.00507	1.74	27	0.3	5	0.225	20
8	0.00512	1.48	27	0.3	5	0.225	20

After running a preliminary validation, some results became apparent. When looking at these results in Figure 4.3, it can be seen that there is a large gap between the experiments and the model output regarding the heat transfer in the condenser. The theoretical heat transfer in the evaporator should be the almost the same, as the system is in steady-state. Why this is not the case in the experiments will be elaborated in Section 4.4.

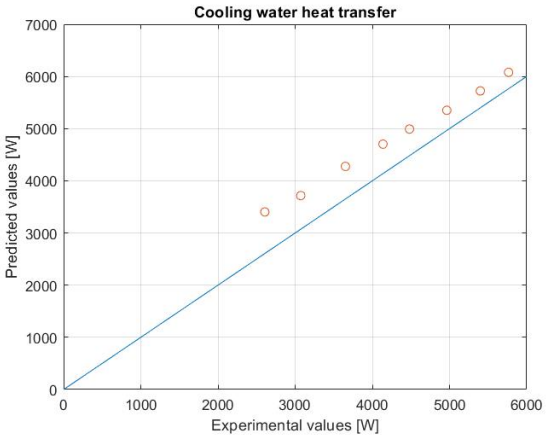

Figure 4.3: Preliminary cooling water validation for the heat transfer in the condenser. The simulations (red circle) should be on the experimental line (cyan), but the heat transfer is overpredicted, and therefore is above the experimental line

When looking deeper into this gap, it can be seen that the heat transfer correlation is not correctly predicting the heat transfer. The cooling water correlation used in the model is validated on the OTEC set-up with the same flow as used in the experiments and is therefore deemed valid. The two-phase correlations used in the model are the correlations by Khan [29] for the evaporator and Tao [55] for the condenser. The correlation of Tao is also valid for the area the experiments are done in, but for the correlation of Khan, this is outside the boundary. As the heat transfer in the condenser is almost equal to the heat transfer in the evaporator as the

system is at steady-state, an overprediction of the heat transfer coefficient in the evaporator can result in a overprediction of the heat transfer in de condenser. The correlation of Khan is valid between an equivalent Reynolds number of 1225 < Re_{eq} < 3000, where the experiments have an equivalent Reynolds number of 400 as maximum. Therefore, the correlation can be inaccurate for the experiments of the OTEC demo. The experiments are done in an unusual area, as the mass flux is very low, and with it the Reynolds number. Therefore, there are no correlations for the evaporator that are tested between the boundaries of the experiments.

From the thesis of Stelwagen [52], the correlation of Khan is the best predictor when the mass flow through the evaporator varies between 7 to 13 g/s. In this area, the correlation is overpredicting the heat transfer with an average of 7.34%. This is mainly because the correlation overpredicts the heat transfer at low outlet quality, but is almost perfect at higher outlet quality. As the outlet quality in the OTEC cycle will be around 70%, this correlation is deemed valid for an OTEC cycle.
However, when looking at the experiments done for a full cycle, the mass flow is much lower, namely between 3.8 and 5.1 g/s. This results in a large overprediction of the heat transfer coefficient. This overprediction can be calculated from the experiments, by using the LMTD method, or Logarithmic Mean Temperature Difference. This method calculates the overall heat transfer coefficient U using Equation (4.8).

$$\dot{Q} = UA\Delta\overline{T}_{LTMD} \tag{4.8}$$

where Q is the heat transfer in the heat exchanger, A is the heat transfer area of the heat exchanger and $\overline{T}_{LMTD}$ is the logarithmic mean temperature difference. The heat transfer is calculated using Equation (4.5). The LMTD is calculated using Equation (4.9). This calculation is valid for a counter-current heat exchanger.

$$\Delta\overline{T}_{LMTD} = \frac{(T_{h,i} - T_{c,o}) - (T_{h,o} - T_{c,i})}{\ln \frac{(T_{h,i} - T_{c,o})}{(T_{h,o} - T_{c,i})}} \tag{4.9}$$

The LMTD method is easy with only single phase fluids, but as the evaporator has a sub-cooled region and a two-phase region, this has to be separated. The sub-cooled heat transfer can be calculated using Equation (4.5). From this heat transfer, the UA-value of the sub-cooled region can be calculated using Equation (4.8). The overall heat transfer coefficient can be calculated using Equation (4.10), as the single-phase heat transfer coefficient is known from the correlation in Table 3.3. From this overall heat transfer coefficient, the single-phase area can be calculated.

$$U = \left(\frac{1}{\alpha_{sw}} + \frac{d_{plate}}{\lambda} + \frac{1}{\alpha_{wf}} \right)^{-1} \tag{4.10}$$

The two-phase heat transfer and area can be found using $\dot{Q}_{tp} = \dot{Q} - \dot{Q}_{sp}$ and the same reasoning for the area. With this new heat transfer and area, the overall heat transfer coefficient can be calculated using Equation (4.8). Using Equation (4.10), the heat transfer coefficient of the working fluid can be calculated. The calculated heat transfer coefficient according to the LMTD method is compared with the heat transfer coefficient according to Khan in Table 4.5. From this table, it can be seen that the heat transfer coefficient is strongly overpredicted by the correlation made by Khan. Stelwagen showed that a correlation made by Taboas [54] could predict the experimental data set better. This correlation can be seen in Equation (4.11). The values from the correlation are also compared with the experimental value in Table 4.5.

$$\alpha_{tp} = \begin{cases} 5Bo^{0.15}\alpha_{sp} & v_g < -111.88v_l + 11.848 \\ \max\left(5Bo^{0.15}\alpha_{sp}, \left(1 + \frac{3}{X_{tt}} + \frac{1}{X_{tt}^2}\right)^{0.2}\right) & v_g > -111.88v_l + 11.848 \end{cases} \tag{4.11}$$

$$v_g = \frac{Gx_m}{\rho_g} \quad v_l = \frac{G(1-x_m)}{\rho_l} \quad X_{tt} = \frac{(1-x_m)\dot{m}}{x_m\dot{m}} \left(\frac{\rho_g}{\rho_l}\right)^{0.5}$$

From Table 4.5, it can be seen that the correlation made by Khan is not correctly predicting the heat transfer. The correlation made by Taboas is better at predicting the heat transfer. It also follows the same pattern as the experiments, as the heat transfer coefficient is rising with rising mass flow. Therefore, the correlation of Taboas will be used in the steady-state and dynamic validation. The steady-state validation of case number 7 from Table 4.4 can be found in Table 4.6. The rest of the steady-state validation can be found in Appendix D.

Table 4.5: Comparison of the heat transfer coefficient in the evaporator between the experiments, the heat transfer correlation of Khan [29] and the heat transfer correlation of Taboas [54]

Heat transfer coefficient evaporator $\left[\frac{W}{m^2K}\right]$					
Δ p	Experiments	Khan	Deviation [%]	Taboas	Deviation [%]
3.32	1700	5250	208.8	2500	47.1
3.11	2050	5050	146.3	2600	26.8
2.75	2200	4950	125.0	2900	31.8
2.46	2300	4725	105.4	3050	32.6
2.26	2400	4600	91.7	3150	31.3
2.00	2600	4350	67.3	3200	23.1
1.74	2800	4200	50.0	3300	17.9
1.48	3000	4000	33.3	3375	12.5
Average deviation			**103.5**		**27.9**

As can be seen from Table 4.6, the heat transfer is not balanced in the OTEC demo. This implies either that the measurements are inaccurate, or that the system is not fully insulated. From other experiments done with the OTEC demo, a similar result can be found. Therefore, the assumption that the system is not fully insulated will be made. This also explains the hotter inlet temperature of the evaporator. For the dynamic validation, the heat transfer of the condenser is used as comparison with the model, to eliminate most of the error, as the heat transfer in the evaporator will be lower due to the insulation error.

Table 4.6: Steady-state validation with a pressure drop over the orifice of 1.74 bar

			Experiment	**Model**	
Component	Variable	Unit	Value	Value	Deviation [%]
Evaporator	$\dot{m}_i$	$\left[\frac{kg}{s}\right]$	0.00507	0.00507	0.00
	P_i	[bar]	8.48	8.50	0.33
	P_o	[bar]	8.46	8.49	0.45
	T_i	[°C]	14.85	13.31	-10.35
	T_o	[°C]	19.66	19.70	0.21
	$T_{sw,o}$	[°C]	22.93	22.71	-0.94
	x_o	[-]	0.88	0.87	-1.45
	$\dot{Q}$	[W]	5101.35	5374.66	5.36
Orifice	P_i	[bar]	8.35	8.39	0.52
	P_o	[bar]	6.62	6.65	0.58
	T_o	[°C]	14.85	14.11	-4.96
Condenser	P_o	[bar]	6.58	6.61	0.58
	T_o	[°C]	11.60	12.12	4.45
	$T_{sw,o}$	[°C]	10.74	10.68	-0.52
	$\dot{Q}$	[W]	5426.07	5378.29	-0.88

From Table 4.6, it can be seen that all values from the model are within 2% of the experiments, with a few exceptions. These exceptions will be discussed in Section 4.4. Because all values are within 2%, the steady-state is deemed valid.

4.3. Dynamic Validation

From Section 4.2, it can be said that the steady-state is well predicted, as almost all values are within 2% of the experiments. The same experiments are used to check whether the dynamics of the system can also be well predicted. The experiments from Section 4.2 are done by constantly adjusting the valve until a new pressure drop is reached. As every second is logged, the dynamics of the system are also logged and will be used for the dynamic validation.

The model adjusts both the valve opening and the set value for the inlet mass flow of the evaporator every 900 seconds. As stated earlier, the inlet mass flow of the evaporator is controlled to have the same values as

the steady-state values from the experiments. These step changes can be seen in Figure 4.4.

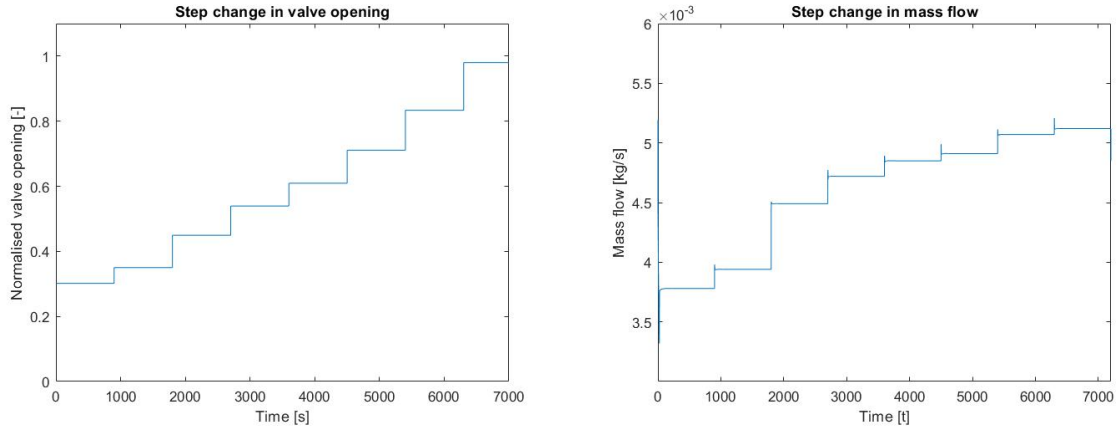

(a) Step change in valve opening

(b) Step change in mass flow

Figure 4.4: Step change inputs for model. The valve is an input, where the mass flow is set by using a controller on the gear pump

These step changes simulate the changes in the OTEC demo set-up. The data from the model have been compared with the data from the OTEC demo set-up. One comparison can be seen in Figure 4.5. The experimental data have been adjusted so that the time frame matches the model.

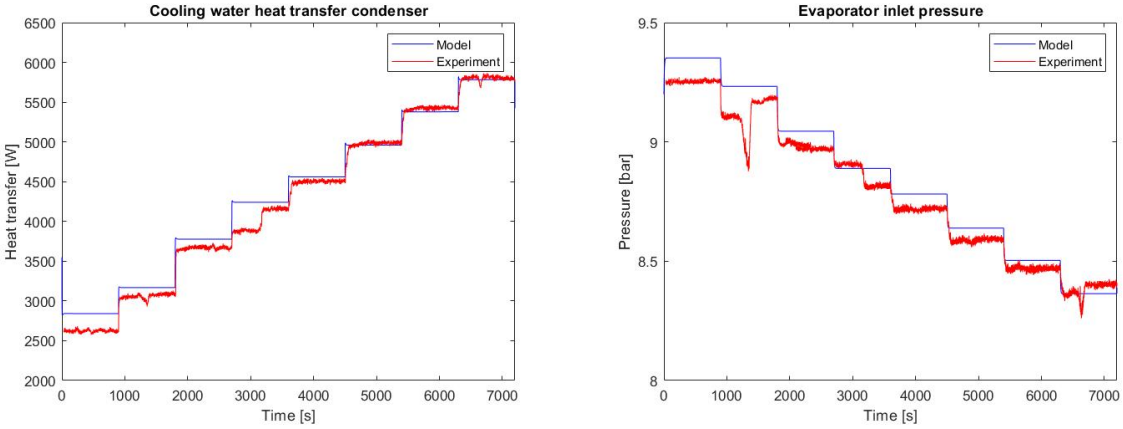

(a) Seawater heat transfer in condenser

(b) Inlet pressure of evaporator

Figure 4.5: Comparison of the dynamic data, with the model (blue) compared with the experiments (red). The time frame of the experimental data have been adjusted to investigate the dynamics

Figure 4.5 shows the steady-state error, found in Section 4.2. It also shows that the dynamics of the system are very fast. The step changes in mass flow can be seen in the heat transfer and the pressure curves. To see clearly what is happening at these step changes, a closer look is taken at the time frame between 5000 and 6000 seconds.

First, the mass flow over the orifice is checked. This comparison can be seen in Figure 4.6a. From this figure, it can be seen that the mass flow is not a step change, but a gradually changing parameter. Also, in reality there is no large peak, as can be seen in Figure 4.6a. To simulate the slowly rising mass flow, the opening of the valve is changed from step change to a ramp. This can be seen in Figure 4.6b. This also removes most of the peak.

The results using Figure 4.6b as an input, can be found in Figure 4.7. From these figures, a few things can be identified. It can be seen that the dynamics are matching very well. By matching the mass flow, the transient time, or the time between the steady-states, is the same. The heat transfer from Figure 4.7e shows a similar

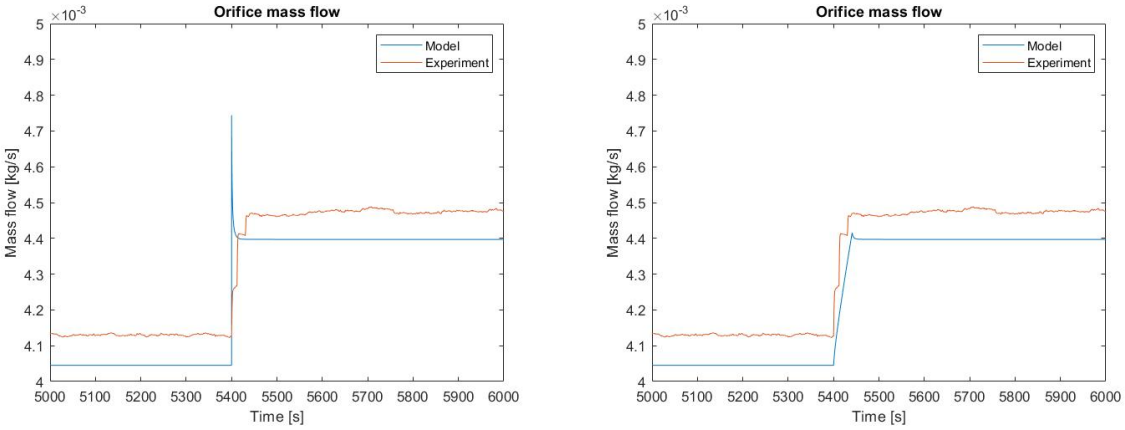

(a) Orifice mass flow when a step change is used

(b) Orifice mass flow when a ramp is used

Figure 4.6: Orifice mass flow with different modeling mechanisms. The model (blue) follows the experiment (orange) better when using a ramp, almost fully erasing the large peak present with a step change

path, no overshoot and only a small steady-state error, that can be found in Table 4.6 and Appendix D. It is dependent on the mass flow and follows the exact path that the mass flow does.

4.4. Discussion

In this chapter, the validation of the model has been discussed. It has been tested using an experimental set-up of an OTEC cycle. The model needed some adjustments, but could predict reality within reasonable accuracy. First, the steady-state validation will be discussed and than the dynamic validation.

Steady-state

From Section 4.2, it can be seen that the model can predict reality within reasonable accuracy for the steady-state. The error with the heat transfer in the evaporator and in the inlet temperature of the evaporator show that the experimental set-up is not perfectly insulated, which is the case in the model.
The error in the outlet temperature of the orifice is also due to an assumption made in the model. The model assumes that saturated vapor exits the separator and enters the valve/orifice. But due to a pressure drop in the pipe, the saturation temperature will drop in the model, which results in a lower enthalpy. In the experiments, the pipes are isenthalpic. Therefore, the inlet enthalpy is lower in the model than in the experiments. Because of the energy balance discussed in Section 4.1.1, the inlet enthalpy is equal to the outlet enthalpy and therefore the outlet temperature is not the same. The error looks large with 5%, but when it is transformed into a heat transfer error, the error becomes only 7 W, and is therefore negligible.
The error of the condenser outlet temperature is also due to an assumption. The outlet of the buffer tank is saturated liquid in the model, where in reality, sub-cooling is present. The thermodynamic equilibrium is at the boundary between vapor and liquid at the liquid level, but the liquid exits the buffer tank at the bottom, where the liquid is slightly sub-cooled as the heavier liquid falls down and the density increases with increasing pressure. In the bottom, the pressure will be higher due to a liquid column. Again, this error looks large with 4.5% but when transformed into heat transfer, it becomes only 7 W and is therefore negligible. That this amount is the same is by chance and uncorrelated.

All other errors are within 1% and can be deemed acceptable. The slight error can be due to the different heat transfer coefficient, which can be seen in Table 4.5. Also, the inaccuracies of the sensors can influence the results a bit. As a conclusion, it can be said that the model can predict the steady-state within reasonable accuracy.

Dynamics

When looking at the dynamics, it can be seen that almost every parameter follows the path of the condenser mass flow. This can be seen from Figure 4.6b and Figure 4.7. The transient region is the same for all parameters, approximately 40 seconds. This seems fast, but it represents reality within a very good accuracy. There

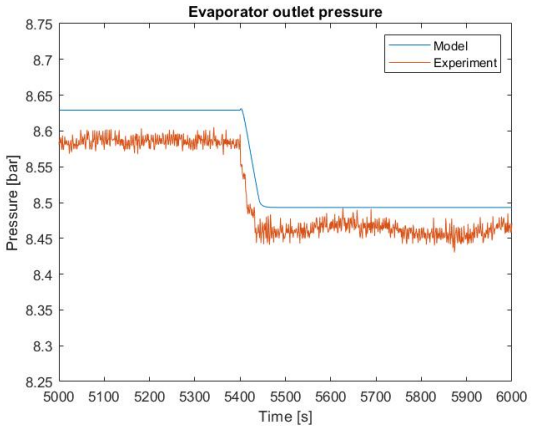

(a) Evaporator outlet pressure

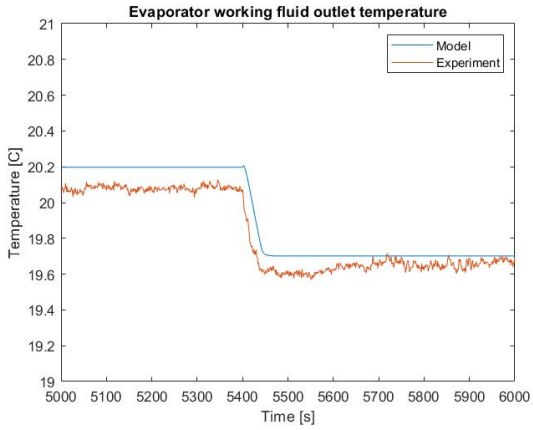

(b) Evaporator outlet temperature of working fluid

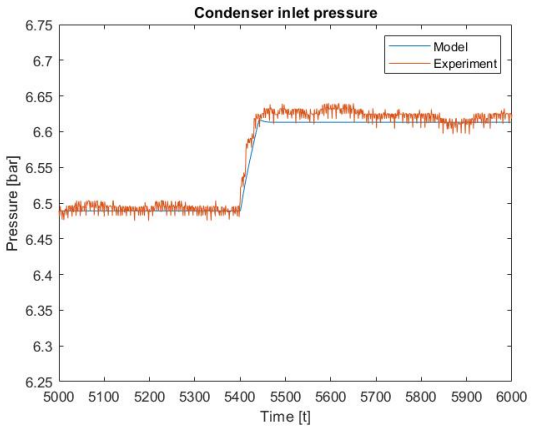

(c) Condenser inlet pressure

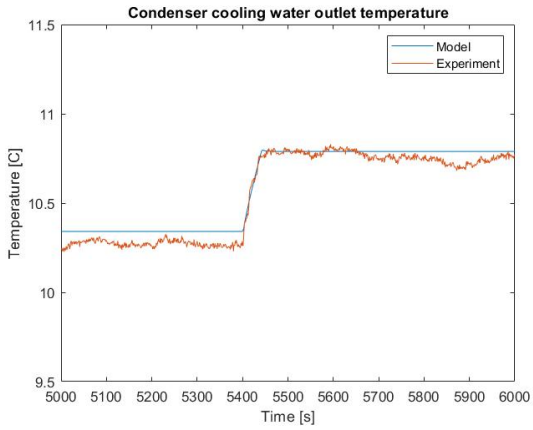

(d) Condenser outlet temperature of seawater

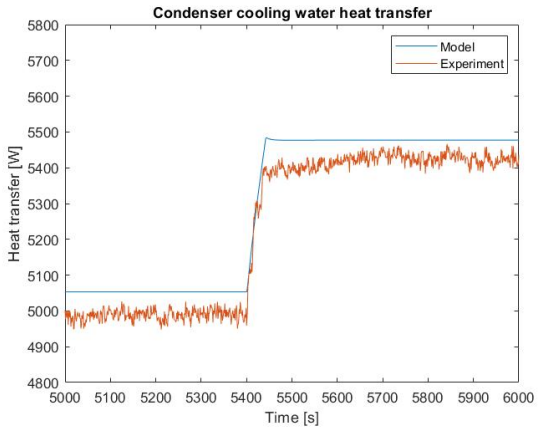

(e) Condenser seawater heat transfer

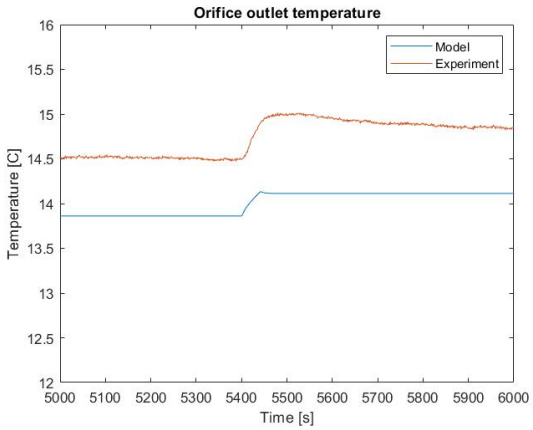

(f) Orifice outlet temperature

Figure 4.7: Dynamic response to the step changes between 5000 and 6000 seconds, comparing the model (blue) with experiments (red)

are still some parameters not the same. This is due to the difference in recirculation. Where the experiments state a slowly rising recirculation rate, the model operates differently. It changes the recirculation rate at the moment the valve is twisted, by adjusting the pump's rotational speed to match the evaporator's design mass flow.

However, when looking at the influence on the dynamics of the system, it can be seen that the influence is not very significant. The dynamics of the system are followed in a good manner with this error, which can be seen in Figures 4.7a and 4.7b.

Another parameter that is not matching well dynamically is the outlet quality. But this is dependent on the mass flow of the evaporator, and therefore the error can be defined as the same as the evaporator mass flow. Again, the error has a minor influence on the dynamics and is therefore not important for the dynamic validation.
As a conclusion, it can be said that the model is dynamically validated.

Overall validation

As stated before, it can be concluded that the model is both in steady-state and dynamically validated on the experimental set-up. But in order to do so, the model had to be slightly modified. The heat transfer correlation of the evaporator has been changed, as the correlation made by Khan [29] proved insufficient. When scaling the system to the 3 MW option, it has better potential than the correlation made by Taboas [54], used in the validation. The correlation made by Khan was validated inside the operating range of the 3 MW plant. But as this cannot be proven with real data, the correlation of Taboas will still be used for the scaled size. Further research is needed to confirm this is a good choice.

Looking at other changes, the change of component from turbine to valve/orifice is an important change. Although the valve is a validated component and the turbine model is not very different from the valve model, it is not safe to say that the turbine is also a validated component. Therefore, when changing the model back to the 3 MW configuration, the model is not validated anymore.
The absence of a gear pump in the OTEC demo configuration also represents an important change. It can be seen from Section 4.4 that it has a minor influence on the dynamics, but the mass flow and therefore the vapor quality are ill-predicted. To be able to use the model for a 3 MW scale, the gear pump was still included in this report. But when a full validation is wanted, this is something that should be investigated.
The working fluid pump in the model has been modified to the type of pump present in the experimental set-up. Where in the 3 MW model a centrifugal pump is used and its parameters are derived from the pump curve, the pump in the experimental set-up model is a reciprocating pump where the characteristics are linearly dependent on the rotational speed.

The model is validated on the small scale with some changes. All dynamic components have not been changed from the large scale, with the exception of the extra state in the condenser and the heat transfer correlation of the evaporator. The extra state in the condenser has a small impact and can also be used when the model is used in other working conditions. The other heat transfer correlation can have a small effect on the steady-state of the higher scale, but this will be checked further in this report. The dynamics will stay the same, even with another correlation. Therefore, it can be said that the dynamics are validated for all conditions.
When looking at the static components, it can be seen that they have all been changed. The turbine has changed to a valve and the pumps have become a reciprocating pump instead of a centrifugal pump. Therefore, when scaling the model up to the 3 MW scale, these components are not validated. Therefore, it can be said that the steady-state is not validated for all conditions.

5
Results

In the previous chapter, the model has been validated on a small-scale experimental set-up. In this chapter, the model will be used to generate results. This will be done by first scaling up to the 3 MW scale, by undoing all the changes from Table 4.2 and using multiple heat exchangers in parallel. A full Process Flow Diagram (PFD) can be found in Appendix C. After the model has been scaled up to the desired input, different scenarios are implemented to see what will happen in the transient region. All simulations are done with the same input values and the same control strategy. This control strategy is further checked in Chapter 6, but is deemed sufficient for this chapter. The control strategy consists of two P-controllers that control the change in the liquid levels of both the separator and the buffer tank.

5.1. Start-up and Shutdown

Important transient conditions are the start-up and shutdown. These are the largest transients that will occur in the system, and therefore can challenge the model. The model can not start from zero or reach a final output of zero, due to the fact that all correlations depend on the Reynolds number, and the Reynolds number becomes zero at zero velocity or mass flow. Therefore, the start or end of the start-up/shutdown procedure are near zero values.

Start-up

For a start-up sequence, the rotational speed of the seawater pumps are changed with a ramp from 12.5% to 100% in 30 minutes. This is done by using a controller on the cold seawater mass flow and an increasing ramp in the rotational speed of the hot seawater pump. This is done because the mass flow from the seawater pump is dependent on the pressure drop and the rotational speed, as can be seen from Equation (3.70). At the hot seawater side, the pressure drop is also dependent on the rotational speed, and therefore the rotational speed can be used as an input. At the cold seawater side, there is also a hydrostatic pressure drop. This pressure drop is not dependent on the rotational speed, and therefore the rotational speed can not be used as the single input. In reality, during start-up, the hydrostatic pressure drop will be close to zero, as the fluid in the cold water pipe will be at ambient temperature. It will take about 10 minutes for the cold water to reach the cycle, after which the rotational speed changes linear with the seawater mass flow. By using a controller for the cold seawater mass flow, this can be simulated. The input for the start-up can be seen in Figure 5.1a. This is the only input that is changed at the start-up, as the mass flow through the pumps is controlled and the mass flow through the turbine is dependent on the pressure ratio. The results can be seen in Figure 5.1.

Shutdown

A shutdown sequence is a start-up sequence, but negative. The controller is still used for the cold water mass flow. The input can be seen in Figure 5.2a. The results can be seen in Figure 5.2.

5.2. Temperature

The temperature of the ocean is always changing. For the steady-state models made by Allseas, three scenarios are calculated. The best case scenario is a hot seawater temperature of 29 °C, a worst case scenario of 25 °C and a design case of 27 °C. To simulate how the system reacts to changing temperature, the temperature is

modeled as a sine function with a base of 27 °C, an amplitude of 2 and a phase of $\frac{50000}{2\pi}$ rad. This input can be seen in Figure 5.3a. The results can be seen in Figure 5.3.

5.3. Failure

The scenarios above are scenarios that are scheduled or occur naturally. But it can also happen that certain components break down during operation. To simulate these scenarios, there are certain step changes done in the system.

5.3.1. Pumps

The pumps are very important components in the system, as the flows through the system are very high. Redundant pumps are in place in case a pump breaks down, but there will still be a small loss of power. The pumps will be modeled using a step change to simulate the loss of a pump, and the start-up of the redundant pump is modeled as a ramp of 15 minutes.

Sea water

The seawater pumps are the same for the hot and the cold side. The difference is the amount of pumps. The input for the hot and cold seawater pump can be seen in Figure 5.4a and 5.5a. The results can be seen in Figure 5.4 and 5.5.

Working fluid

For the working fluid pump, the situation is slightly different. The pump is limited at a certain rotational speed, slightly above the design point. With the failure of one pump, the rest of the pumps can not pump enough to compensate this loss. Therefore, the redundant pump has to be turned on in 150 seconds and it also has to be fully operational in 150 seconds, otherwise the buffer tank will be full. This input can be seen in Figure 5.6a. The results can be seen in Figure 5.6.

5.3.2. Heat Exchangers

The heat exchangers need cleaning or maintenance at a certain time, or a heat exchanger breaks down. In that case, a row of heat exchangers is closed from mass flow. The orientation of the heat exchangers can be seen in Appendix C. This is modeled as a step change in the geometry of the heat exchangers. The re-connection of these heat exchangers is also simulated.

Evaporator

All evaporators are lined up in five rows. Therefore, a step change from 1 to 0.8 times the geometry is simulated. This input can be seen in Figure 5.7a. The results can be found in Figure 5.7.

Condenser

The condensers are lined up in three rows. Therefore, a step change from 1 to 0.667 times the geometry is simulated. This input can be seen in Figure 5.8a. The results can be found in Figure 5.8.

5.4. Discussion

When looking at the results, a few things can be seen. The influence of the temperature change is almost linear. Higher temperature means higher output. As the modeled time scale is less than a day, it can be assumed that the real temperature changes can be regarded as insignificant.

It can also be seen that when a hot seawater pump breaks down, the net output of the system goes up. When looking at Figure 5.4e, it can be seen that the pressure drop decreases by almost 33%. As the rotational speed is the same and the volume flow per pump does not change very much, the efficiency also stays fairly constant. When looking at Equation (3.75), the large change in pump power can be explained. As the pressure drop decreases by 33%, the total volume flow decreases by 25% , because the total amount of pumps drops from 4 to 3, and the efficiency stays the same, the pump power decreases by roughly 50%. As the heat transfer does not change very much, the turbine output does not drop more than the seawater pump and the net output goes up. Whether this new configuration is a new optimum point should be researched further.

What can also be seen, is that when a working fluid pump failure occurs, the redundant pump has only 2.5 minutes to be started up and be fully operational, otherwise the buffer tank will overflow. This can be prevented by either using three pumps with one redundant pump instead of two pumps with one redundant pump. It can be seen from Figure 5.6d that the pressure in the evaporator drops, which is due to less mass coming in the evaporator, but the outlet quality rises, as can be seen in Figure 5.6c. This is also because less mass is inside the evaporator, but the heat transfer is still nearly the same.
In reality, an overflowing buffer tank will result into a pressure increase in the condenser, and therefore a lower performance of the condenser, a lower mass flow through the turbine, and eventually the problem will resolve itself. In the model, the buffer tank has dimensions but these are not limiting the state equation. Therefore, in the model the buffer tank can overflow and this needs to be researched further.

When looking at the start-up and shutdown sequences, it can be seen from Figure 5.1c and 5.2c that the evaporator and condenser start and stop from a relatively high temperature and pressure. In reality, this will be slightly higher, as it will go near ambient temperature. This is not included in the model.

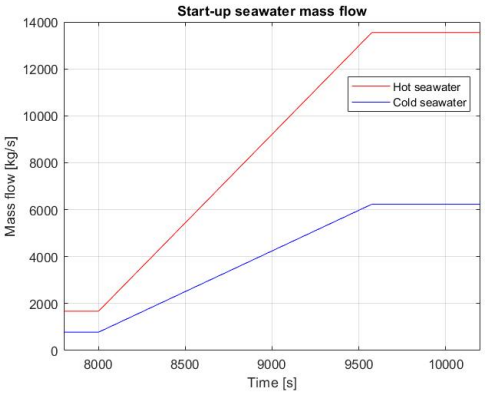

(a) Seawater mass flow

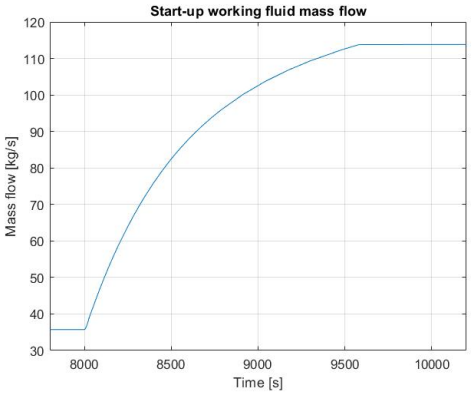

(b) Working fluid mass flow

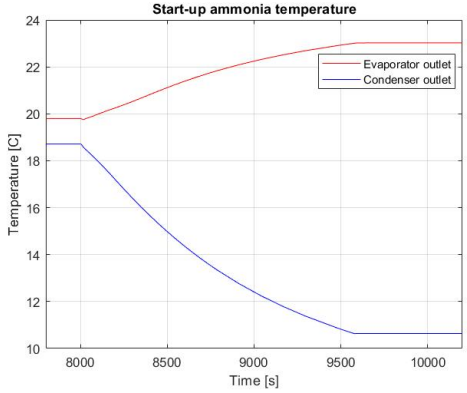

(c) Working fluid temperature

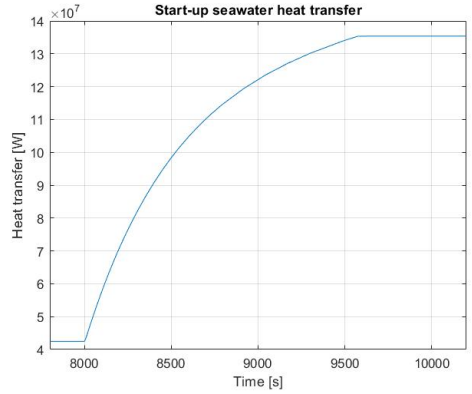

(d) Heat transfer

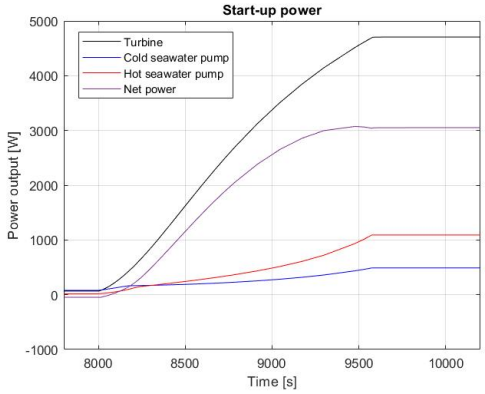

(e) Power

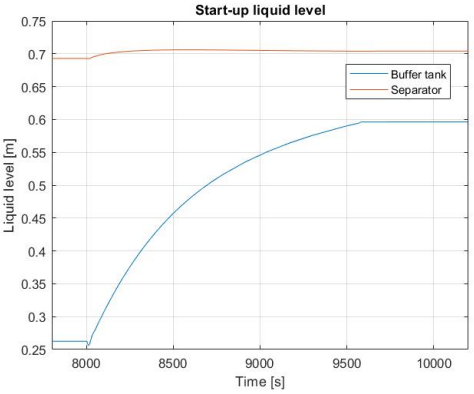

(f) Liquid level

Figure 5.1: Results of a start-up sequence. Figure 5.1a is the input, where the hot seawater (red) and cold seawater (blue) rise linearly to operating level. It can be seen that the linear rising mass flow results in a non-linear temperature profile (5.1c) and power profile (5.1e). Also, it can be seen that it results in a non-linear working fluid mass flow (5.1b) and a similar heat transfer (5.1d) profile.

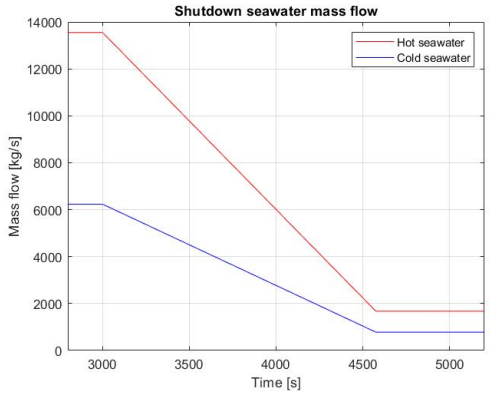

(a) Seawater mass flow

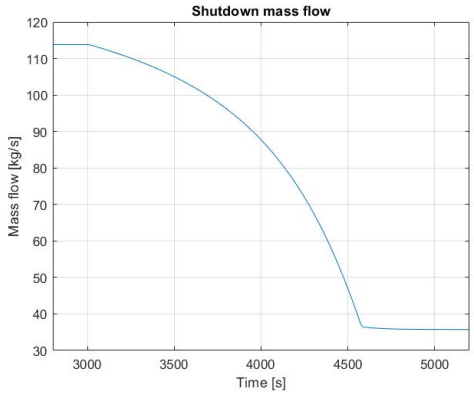

(b) Working fluid mass flow

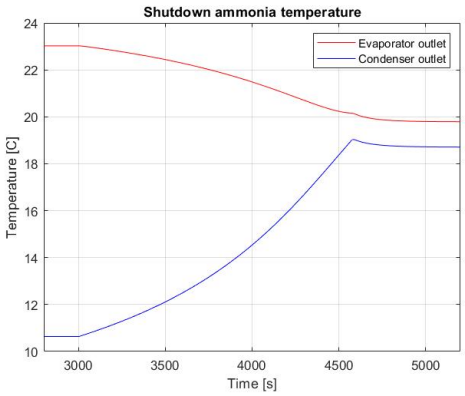

(c) Working fluid temperature

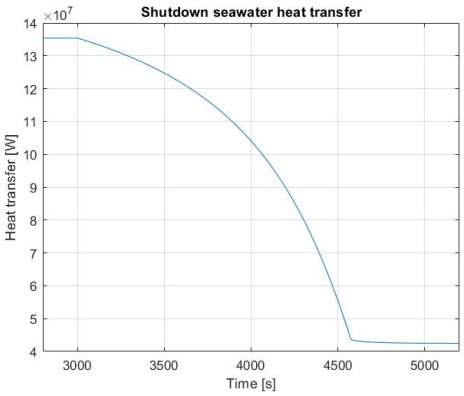

(d) Heat transfer

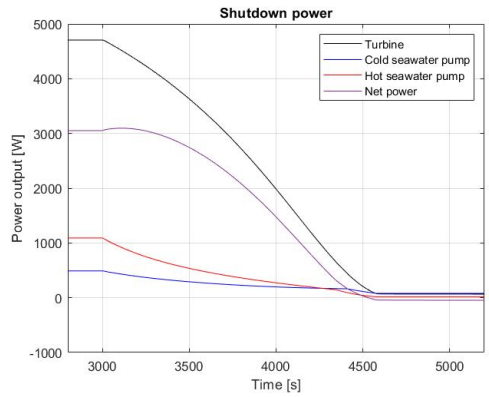

(e) Power

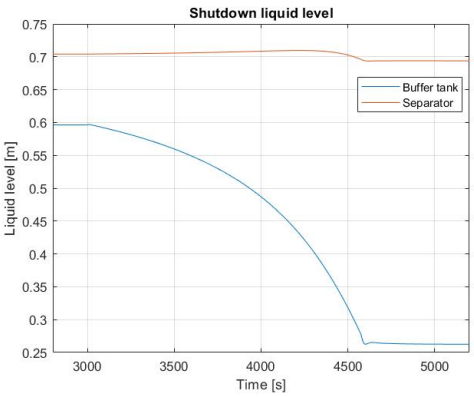

(f) Liquid level

Figure 5.2: Results of a shutdown sequence. Figure 5.2a is the input, where the hot seawater (red) and cold seawater (blue) decrease linearly from operating level to near-zero. It can be seen that the linear decreasing mass flow results in a non-linear temperature profile (5.2c) and power profile (5.2e). Also, it can be seen that it results in a non-linear working fluid mass flow (5.2b) and a similar heat transfer (5.2d) profile. It is a mirrored version of a start-up.

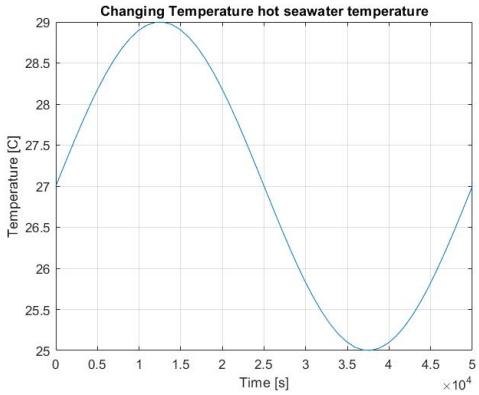

(a) Seawater inlet temperature

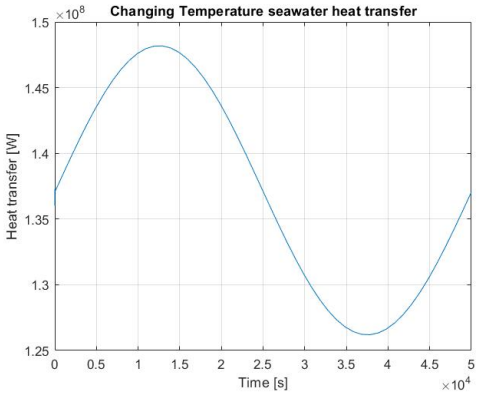

(b) Heat transfer

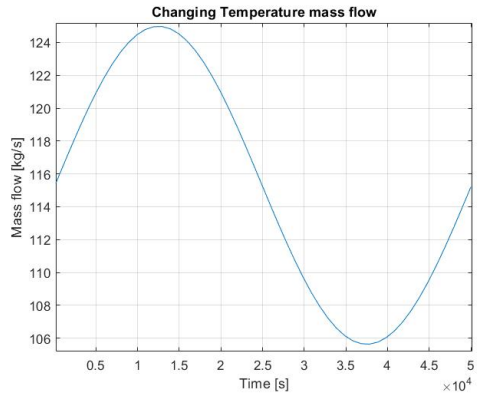

(c) Working fluid mass flow

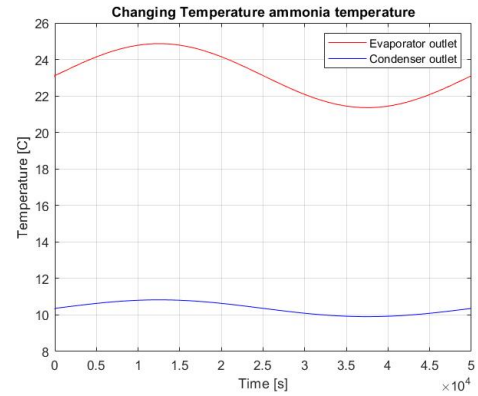

(d) Working fluid temperature

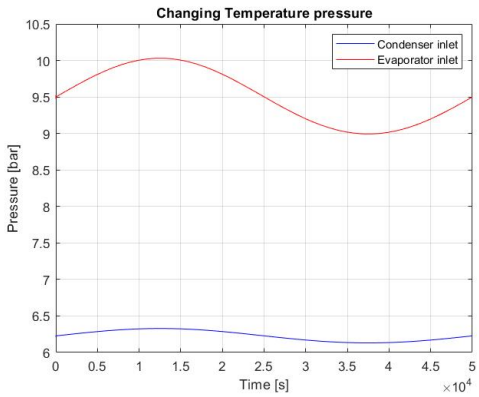

(e) Pressure

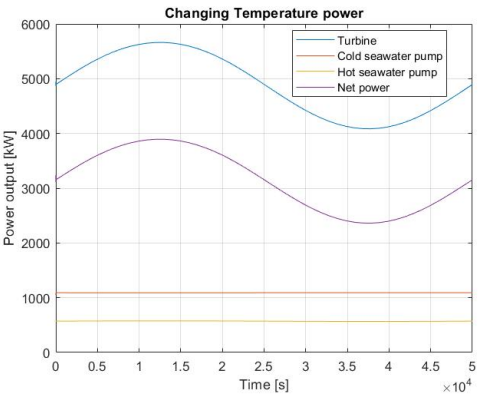

(f) Power

Figure 5.3: Results of a year-round changing temperature. Figure 5.3a is the input, where the temperature changes sinusoidally between 25 and 29. It can be seen that the heat transfer (5.3b) and the working fluid mass flow (5.3c) follow the same path. It can also be seen that the working fluid pressure (5.3e) and temperature (5.3d) follow the same path, but that the change is larger in the evaporator (red) than in the condenser (blue). This results in a sinusoidal change in power (5.3f), that follows the hot seawater inlet temperature path.

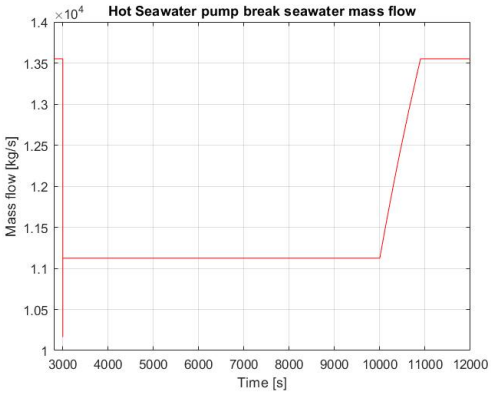

(a) Seawater mass flow

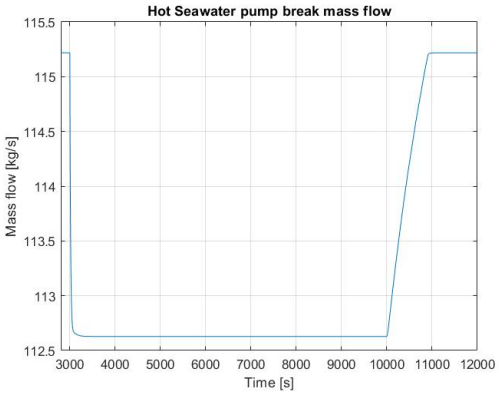

(b) Working Fluid

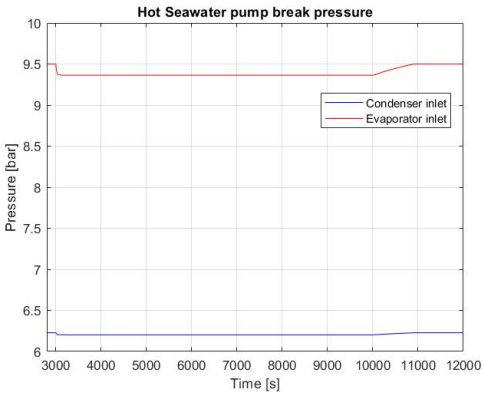

(c) Pressure

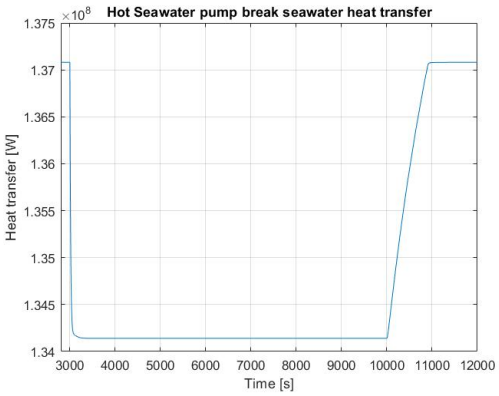

(d) Heat transfer

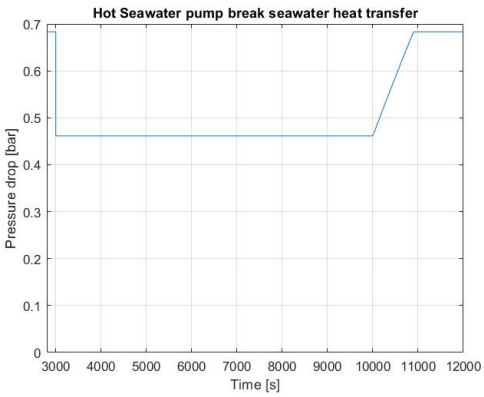

(e) Pressure drop

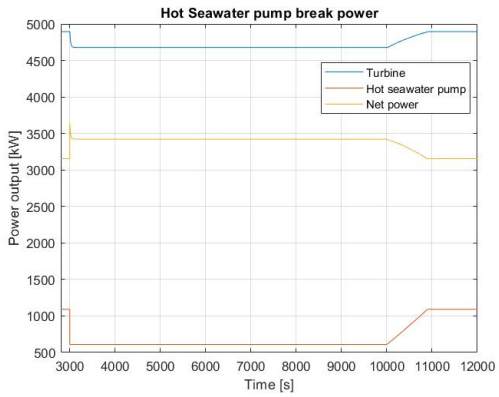

(f) Power

Figure 5.4: Results of a hot seawater pump failure sequence. Figure 5.4a is the input. It can be seen that the working fluid mass flow (5.4b) does not decrease very much, and therefore the heat transfer (5.4d) also does not decrease very much. It can also be seen that it has a larger impact on the evaporator (red) than on the condenser (blue) (5.4c). It can also be seen that the pressure drop decreases (5.4e). This results in a large decrease in pump power, which results in a higher net output (5.4f).

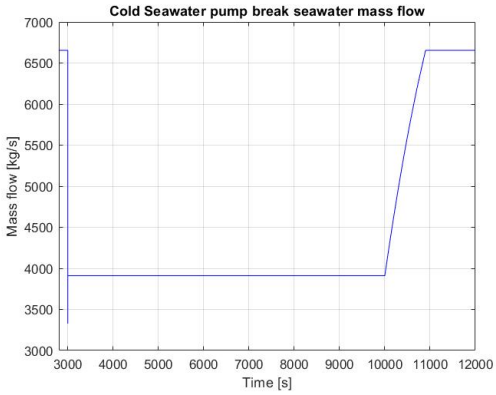

(a) Seawater mass flow

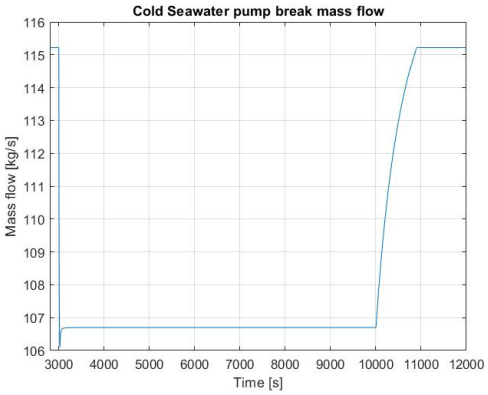

(b) Working Fluid

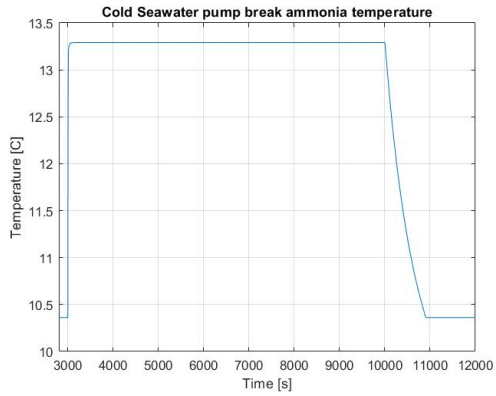

(c) Working fluid temperature

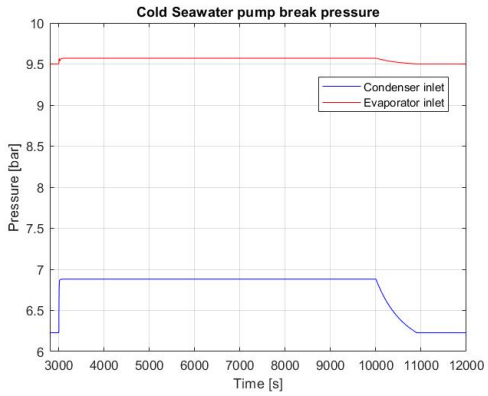

(d) Pressure

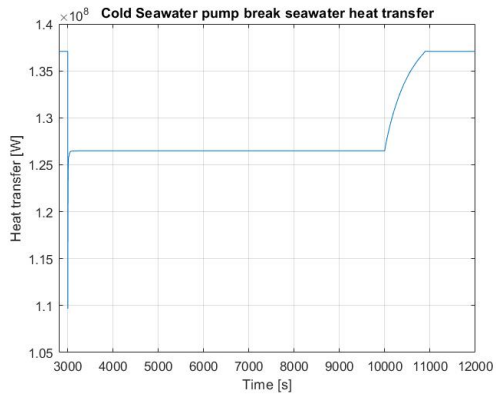

(e) Heat transfer

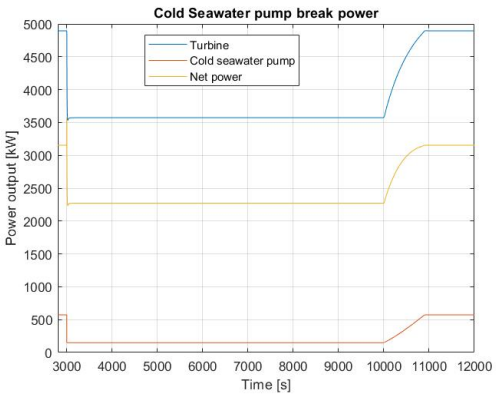

(f) Power

Figure 5.5: Results of a cold seawater pump failure sequence. Figure 5.5a is the input. It can be seen that the working fluid mass flow (5.5b) follows the same path, but does not decrease much. The heat transfer (5.5e) also follows this path. The impact on the pressure (5.5d) of the condenser (blue) is much larger than that of the evaporator (red). This results in a smaller pressure drop, which results in a smaller turbine output (5.5f). Therefore, the net output is lower.

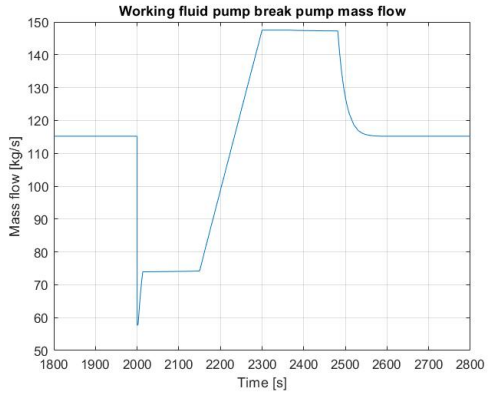

(a) Working fluid mass flow

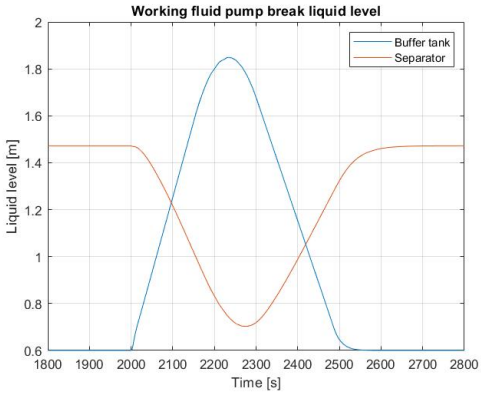

(b) Liquid level

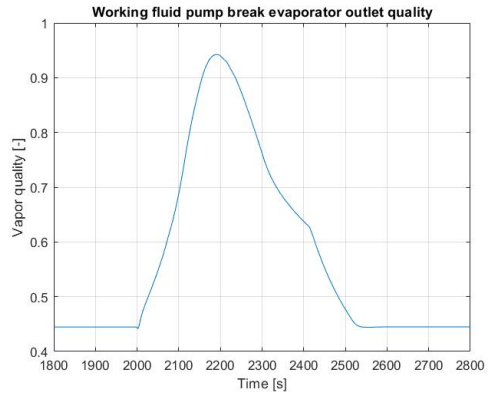

(c) Working fluid evaporator outlet quality

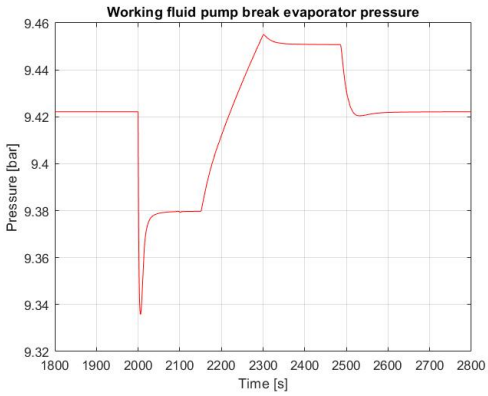

(d) Pressure

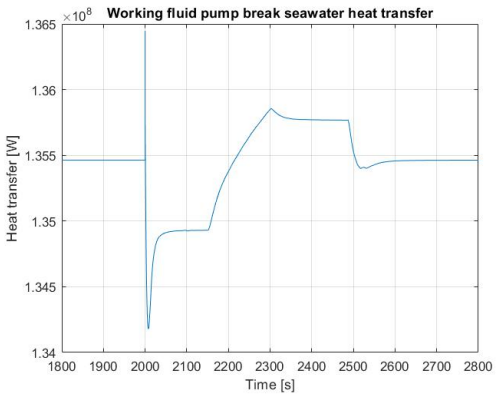

(e) Heat transfer

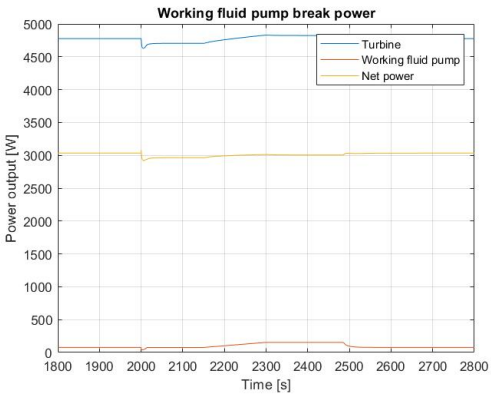

(f) Power

Figure 5.6: Results of a working fluid pump failure sequence. Figure 5.6a is the input. It can be seen that to stabilize the liquid level in the tanks (5.6b), a redundant pump has to be turned on after 150 seconds. It can also be seen that the heat transfer (5.6e) does not decrease much. Due to lower mass flow but similar heat transfer, the outlet quality (5.6c) rises fast. As the pressure (5.6d) does not change much, the power (5.6f) also stays fairly constant.

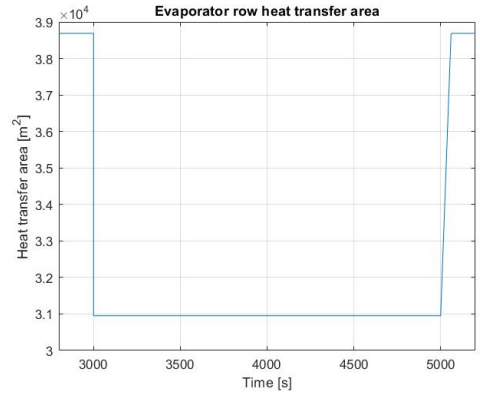

(a) Heat transfer area

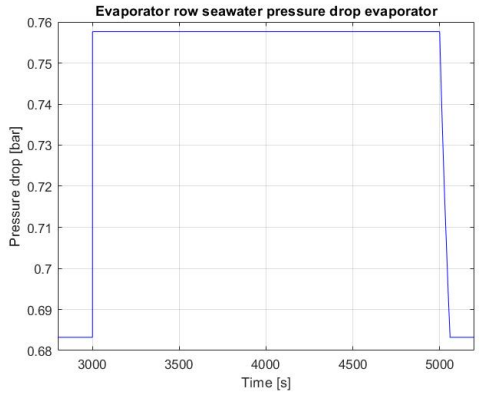

(b) Pressure drop

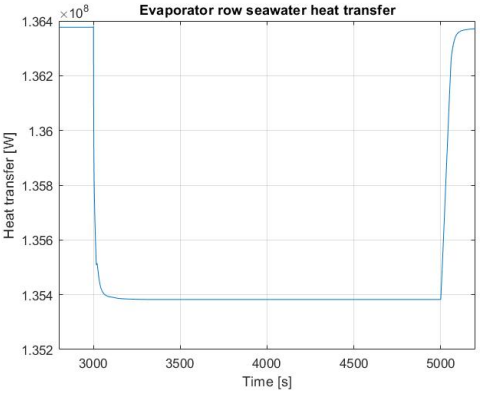

(c) Heat transfer

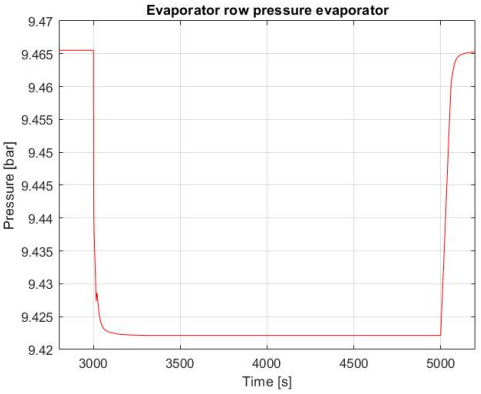

(d) Pressure

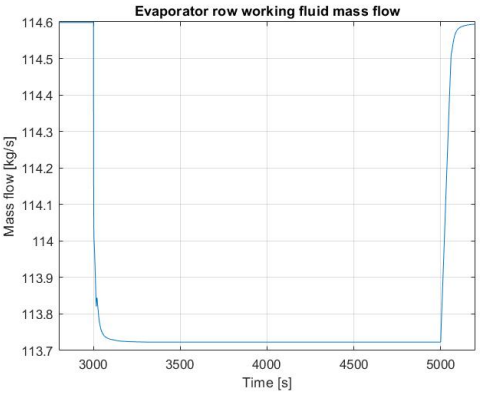

(e) Working fluid mass flow

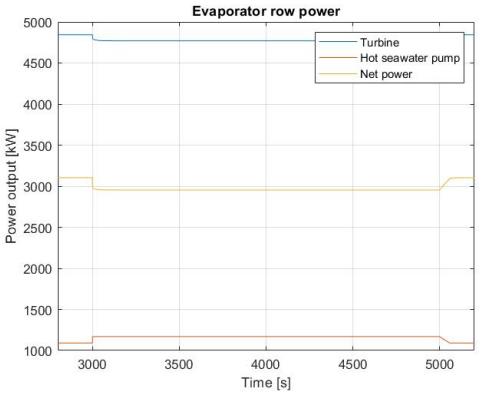

(f) Power

Figure 5.7: Results of an evaporator row failure sequence. Figure 5.7a is the input. This results in an immediate increase in pressure drop (5.7b). There is a small decrease in heat transfer (5.7c) and working fluid mass flow (5.7e), which results in a decrease in evaporator pressure (5.7d). The increased pressure drop in combination with the decreased evaporator pressure results in a lower turbine output and a higher pump power (5.7f). Therefore, the net output will be lower.

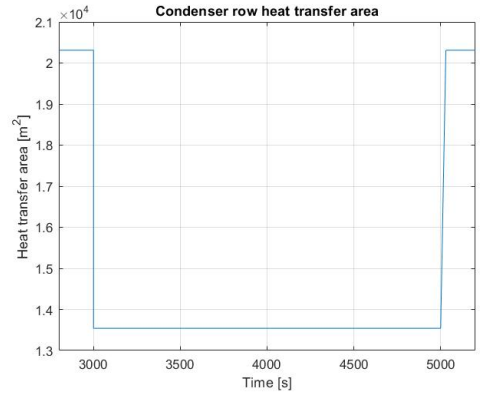

(a) Heat transfer area

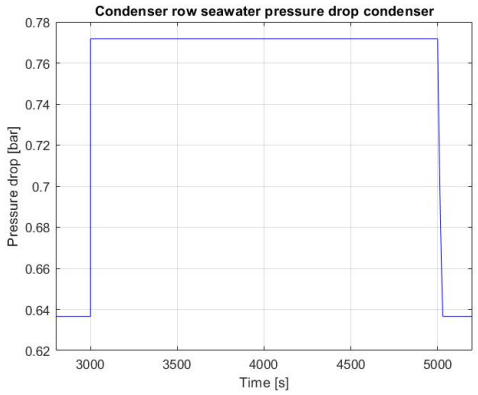

(b) Pressure drop

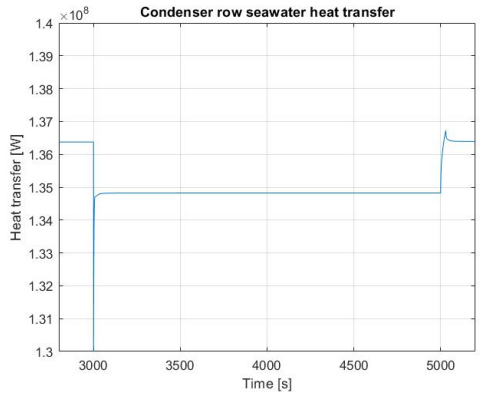

(c) Heat transfer

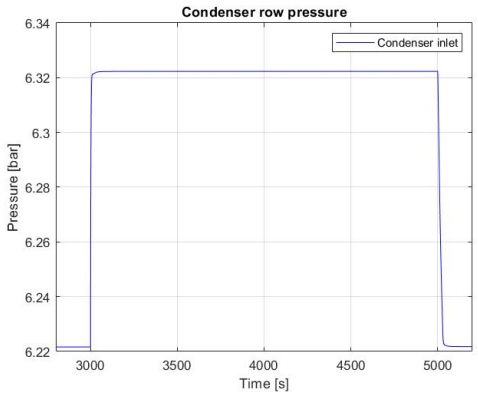

(d) Pressure

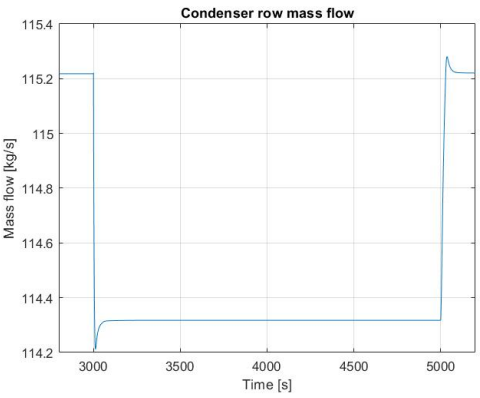

(e) Working fluid mass flow

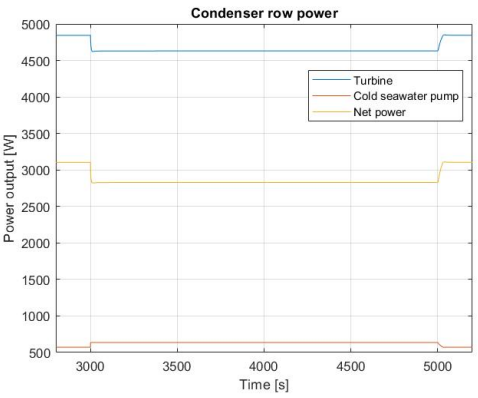

(f) Power

Figure 5.8: Results of a condenser row failure sequence. Figure 5.8a is the input. This results in an immediate increase in pressure drop (5.8b). The working fluid mass flow (5.8e) decreases very little, as does the heat transfer (5.8c). Due to the heat transfer decrease, the pressure in the condenser rises (5.8d). This pressure rise decreases the turbine output (5.8f), while the increase in pressure drop increases the pump power. This results in an decrease in net output.

6

Control

In Chapter 5, the results of different scenarios are displayed. These results are based on single inputs that change, where the output of the system is investigated. In this chapter, a control strategy will be constructed for the entire system, so not for single inputs. There are a few controllers in the system already, but in this chapter the control strategy will be optimised.

6.1. Input variables

First, the controllable variables have to be found. Only the quick adjustable variables are taken into account. In some situations, it can be beneficial to reduce the total heat transfer area or the amount of pumps, but these changes are not taken into account. When looking at the variables that can be adjusted in the system, there are only a few variables. The inputs apply mainly for the pumps: the rotational speed can be adjusted to change the mass flow of all pumps. Van Strijp [59] states that the vanes of the turbine can also be adjusted to change the vapor mass flow. This is done by adding a factor to Equation (3.59). The new equation becomes Equation (6.1).

$$\dot{m} = f_{VTG} K \sqrt{\rho_i p_i \left(1 - \left(\frac{p_o}{p_i}\right)\right)} \tag{6.1}$$

where the correction factor f_{VTG} is the Variable Turbine Geometry (VTG) factor. By adjusting this factor, the pressure ratio can be controlled. This is the same as the opening of the orifice in Chapter 4, which was used for validating the model. The inlet temperature for the cold and hot seawater can also be controlled, but this would require extra equipment for the cycle, and as the influence has been deemed negligible in Chapter 5, these will not be taken into account.

6.2. Control purpose

The reason for control is to ensure the highest possible output at all times, but also to keep the system from going into unsafe conditions. The unsafe conditions are determined using boundary conditions. These boundary conditions are mostly dependent on the conditions that manufacturers give. They can consist of pressure levels, temperature levels or the liquid level in the tanks.

To ensure the best output at all times, a few things are important:

- Steady-state. The system has an optimum state, and it is important that this state is kept during small changes.
- The outlet quality of the evaporator. As stated in Section 1.2, the heat transfer coefficient is the highest between a vapor quality of 0.4 and 0.7. Therefore, this is an important parameter to control.
- The heat transfer of the evaporator. If the heat transfer of the evaporator can be at its optimum point, more vapor can be produced by the evaporator using the same seawater mass flow, and therefore increase the net output. This result can also be achieved by reducing the mass flow of seawater, reducing

the pump work and receiving a higher net output as the reduction in pump power is higher than the losses in the turbine output.

- The heat transfer of the condenser. If the heat transfer of the condenser can be at its optimum point, the vapor can be fully condensed with less seawater mass flow, this will increase the net output. This result can also be achieved by reducing the mass flow of seawater as the reduction in pump power can be higher than the losses in the turbine output.
- Turbine power. It is important to maximize the output of the turbine, while minimizing the work of the pumps. As the turbine power is defined as $\dot{m}\Delta h$ in Equation (3.63), a trade-off between vapor mass flow and pressure ratio has to be found.

These five purposes can be controlled by the five inputs described in Section 6.1. The hypothesis is that the steady-state is best controlled by the working fluid pump, the outlet quality by the gear pump, the heat transfer of the evaporator by the hot seawater pump, the heat transfer of the condenser by the cold seawater pump and the turbine output can be best controlled by the VTG. An overview of this hypothesis can be found in Table 6.1, and will be checked by a sensitivity analysis.

Table 6.1: Hypothesis for the control strategy, stating which input variable to control to reach the optimum output of the purposes

Purpose	Variable
Steady-state	n_{pump}
Evaporator outlet quality	n_{gear}
Evaporator heat transfer	$n_{swpump\ hot}$
Condenser heat transfer	$n_{swpump\ cold}$
Turbine output	f_{VTG}

6.3. Sensitivity Analysis

As stated in Section 6.2, the hypothesis of Table 6.1 will be tested with a sensitivity analysis. According to Jørgensen and Endoricchio [26], a sensitivity analysis makes it possible to distinguish high-leverage variables, whose values have a significant impact on the system behaviour, and low-leverage variables, whose values have minimal impact on the system. The sensitivity analysis is conducted according to Equation (6.2). Jørgensen and Endoricchio also state that the relationship between an input variable and an output variable is rarely linear, so multiple points should be investigated.

$$S = \frac{\frac{\Delta y}{y}}{\frac{\Delta x}{x}} \tag{6.2}$$

where S is the sensitivity, y is the output and x is the input. The choice has been made to take an average of a step forward and a step backward from the nominal operating point. This gives a good representation how the system reacts to all possible changes from its nominal point. A summary of the nominal operating points and the step sizes can be found in Table 6.2. Between each step size, 500 seconds was taken to ensure steady-state before the step size.

Table 6.2: Inputs for the sensitivity analysis

Component	**Variable**	**Starting point**	**Step size**	**Unit**
Turbine	f_{VTG}	1	0.05	-
Pump	n_{pump}	50	3	rps
	n_{gear}	32	5	rps
	$n_{swpump\ hot}$	5.7	0.5	rps
	$n_{swpump\ cold}$	5.7	0.5	rps

The full result of the sensitivity analysis can be found in Appendix E. The most important parameters can be found in Table 6.3. This table can be read as follows: the value at a certain spot means that a change in the input parameter of 1% result in a change for the output parameter of the number inside the table. For

Table 6.3: Result of the sensitivity analysis, where Δx represents the step size, and the total is the mean of a step size forward and backward. If the sensitivity is negative, this means that the output changes in the opposite direction of the step size. For example, an increase of n_{gear} results in a decrease of $x_{out,evap}$.

Component	Input	Output	$-\Delta x$	Δx	Total
Turbine	f_{VTG}	$\frac{d\dot{m}_{bt}}{dt}$	-152.90	-148.23	-150.56
		$\dot{Q}_{cond}$	0.77	0.75	0.77
		$\dot{Q}_{evap}$	0.78	0.75	0.77
		$x_{out,evap}$	0.69	0.66	0.68
		W_{turb}	0.21	0.11	0.16
		W_{net}	0.35	0.18	0.26
Working fluid Pump	n_{pump}	$\frac{d\dot{m}_{bt}}{dt}$	340.45	327.57	334.01
		$\dot{Q}_{cond}$	0.01	0.01	0.01
		$\dot{Q}_{evap}$	0.01	0.01	0.01
		$x_{out,evap}$	-1.31	-1.09	-1.2
		W_{turb}	0.06	0.05	0.06
		W_{net}	0.06	0.03	0.05
Recirculation pump	n_{gear}	$\frac{d\dot{m}_{bt}}{dt}$	-2.33	-2.27	-2.30
		$\dot{Q}_{cond}$	0.01	0.01	0.01
		$\dot{Q}_{evap}$	0.01	0.01	0.01
		$x_{out,evap}$	-0.17	-0.17	-0.17
		W_{turb}	0.01	0.01	0.01
		W_{net}	0.02	0.02	0.02
Hot seawater pump	$n_{sw,hot}$	$\frac{d\dot{m}_{bt}}{dt}$	-24.30	-20.76	-22.53
		$\dot{Q}_{cond}$	0.11	0.09	0.10
		$\dot{Q}_{evap}$	0.11	0.09	0.10
		$x_{out,evap}$	0.15	0.13	0.14
		W_{turb}	0.23	0.19	0.21
		W_{net}	-0.95	-0.49	-0.42
Cold seawater pump	$n_{sw,cold}$	$\frac{d\dot{m}_{bt}}{dt}$	-34.36	-23.10	-28.73
		$\dot{Q}_{cond}$	0.16	0.11	0.14
		$\dot{Q}_{evap}$	0.16	0.10	0.13
		$x_{out,evap}$	0.22	0.15	0.19
		W_{turb}	0.63	0.44	0.53
		W_{net}	0.51	0.07	0.29

example, a sensitivity of 0.5 means that a change of the input variable of 1% results in a change in output of 0.5%.

From Table 6.3, a few conclusions can be made. The first one is that the system's steady-state is best controlled by the working fluid pump. This can be seen by looking at the high sensitivity of the changing mass of the buffer tank. The system is in steady-state if the change of mass in the tanks is 0. Therefore, the working fluid pump will be used to control the steady-state.

What also can be seen, is that the gearpump rotation is nearly insensitive to everything, except the outlet quality of the evaporator. This can be explained by the fact that, in steady-state, the outlet quality of the evaporator is defined by $\frac{\dot{m}_{turb}}{\dot{m}_{evap}}$, where $\dot{m}_{evap}$ is the sum of $\dot{m}_{gear} + \dot{m}_{turb}$. Therefore, the gear pump mass flow has a strong impact on the outlet quality and will be used to control this quality.

For the other input variables, it can seen that they are not running at an optimum. From Figure 5.4, it could be seen that when reducing the number of hot seawater pumps, the net output would rise. This also follows from the sensitivity analysis, as the net output has a negative sensitivity related to the rotational speed of the hot seawater pump. Therefore, an optimum point should be found and controlled at that point. In the cold seawater pump, the sensitivity is also non-zero. When increasing the rotational speed with the step size, the net output increases slightly, with a sensitivity of 0.07. But when decreasing the rotational speed with the step size, the net output decreases quite significant, with a sensitivity of 0.5. This implies that the optimum point is nearly reached and should be found and controlled.

When looking at the turbine, the net output has a small sensitivity. An increase in the opening of the vanes gives a small increase in the net output, but a decrease in the opening of the vanes give a larger decrease of the net output, as was the case with the cold seawater pump. Therefore, it can be concluded that the optimum point is not reached. What also can be seen is that the opening of the vanes has a higher influence on the heat transfer than the seawater pumps.

The pressure drop over the turbine is very influential for the heat transfer, and a measurable parameter. Therefore, this will be used as input for the control mechanism. For the rotational speed of the seawater pumps, the mass flow of the optimum point will be used as the input for the control mechanism, as this is a direct response to the rotational speed and is a good measurable parameter. For the gear pump, the outlet quality is a difficult to measure parameter. Dorfman and Fridman [14] use a calorimeter inside a throttling valve, but this is an time consuming process and can not be used for real-time control. In the model, the outlet quality can be used as an input for the optimum point. For the control mechanism, the change of the liquid level inside the separator will be used as an input, as this can be easily measured and is quite good in controlling the outlet quality. For the working fluid pump, the height of the buffer tank liquid level will be taken as an input for the control mechanism, as this is easily measurable.

6.4. Optimum point

As stated in Section 6.3, the system is not running at an optimum point. Therefore, the system will be optimised using the described control mechanisms. The outlet quality will be controlled at 0.7 and the change in the liquid level of the buffer tank will be controlled to ensure steady-state. From Figure 5.4f, it can be seen that the net output rises with a reduction of number of hot seawater pumps. Therefore, the first step has been to reduce the number of hot seawater pumps by 1.
The optimum point for a single parameter can be found by simulating a large number of step changes above and below the nominal operating point. But the optimum point of the first parameter is not necessarily the optimum point when combined with another parameter. Therefore, the search for a total optimum is done as follows:

- The optimum point of the variable turbine geometry is searched.
- At this optimum point, the optimum point of the hot seawater pump is searched.
- At this point, the optimum point of the cold seawater pump is searched.
- As a check, the sensitivity of the variable turbine geometry and the hot seawater pump are checked at this point to see if it is at its optimum. If not, these steps repeat themselves.

The results of these steps can be found in Figure 6.1.
From Figure 6.1, it can be seen that the influence of control is large. The reduction of the number of hot seawater pumps gives a positive change of 10% in net output. By optimising only the turbine, this increases to 12%, and with the control of the seawater pumps, this number even further increases up to 15%, with a total net output of 3435.3 kW. From Figure 6.1a, the optimum point is 1.08. But when optimising the other parameters, a slightly higher result was reached with 1.09 as an optimum. Therefore, this point has been chosen as the new optimum point. The full input for the optimum point can be found in Table 6.4.

Table 6.4: Optimum point of the model at 27 °C hot seawater temperature

Input variable	Optimum value	Original value	Unit
Turbine geometry	1.09	1	-
Hot seawater pump rotation	5.1	5.7	rps
Cold seawater pump rotation	6.1	5.7	rps

6.5. Discussion

The importance of control in an OTEC cycle is shown. Small changes can give a big change in the net output, as the margins are very small. How the system can be controlled, has been tested with a sensitivity analysis. An optimum point has to be found for each given seawater inlet temperature. This is the nominal case, so this

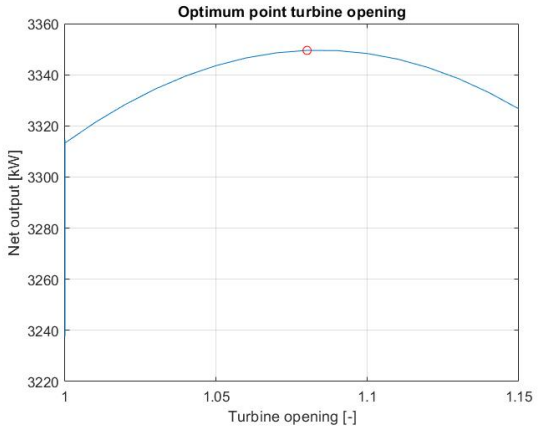

(a) Optimum point of the variable turbine geometry, with nominal seawater pump rotation

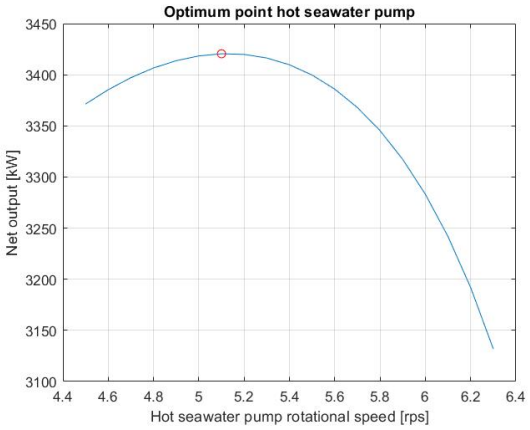

(b) Optimum point of the hot seawater pump rotation, with optimised turbine geometry and nominal cold seawater pump rotation

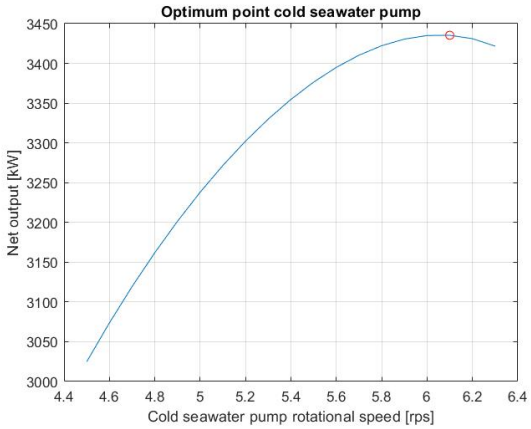

(c) Optimum point of the cold seawater pump rotation

Figure 6.1: Optimum point analysis of the three input variables. The red circle implies the optimum point of that variable

gives a good example of a new control strategy. That it is beneficial is shown in Figure 6.1, with an increase of 15% of the net output from the original case. This optimum point can be controlled for small transients, but when large transients occur, as is the case with the results from Chapter 5, a new strategy should be used.
In the case of a large transient, the optimum point will change. For example, when a row of evaporators is closed, either for maintenance or due to a component failure, it can be beneficial to slow all pumps down and change the turbine geometry accordingly. The optimum strategy for each case should be further investigated.

In the model, 5 input variables are used as the control variables. The turbine geometry is a changeable variable for the turbine and is used in this thesis, but not all turbines have a changeable geometry. In that case, the rotational speed of the turbine can be adjusted by adding more or less resistance on the shaft that is connected with the generator. As the rotational speed is a given constant for the turbine used, this is not investigated but can result in a different strategy.
For the optimum point in this report, the turbine vanes have to be opened further than the design case. The assumption is that this is possible, as the design case is not the hottest inlet seawater temperature. To ensure a higher output with the higher inlet seawater temperature, the turbine vanes can be opened further. This is an assumption, and should be confirmed by the manufacturer.

7

Conclusions and Recommendations

In this chapter, the conclusions of this research are presented by answering the research questions. The results will be discussed and recommendations for future research will be mentioned.

7.1. Conclusions

The main objective of this research was to find the impact of the transient regions of an OTEC cycle and how this cycle can be optimally controlled. In order to do so, a new mathematical model has been constructed and validated on an experimental set-up. The model has been scaled up to a 3 MW plant, where simulations have been done to find the impact of the transient regions and to implement a control strategy.

Controllable variables

Several input variables have been identified. The geometry of the plant and the number of components are chosen for a design case and can hardly be changed during operation. Also, the inlet temperature of the seawater is an input variable, which is given by nature and can not be controlled in an easy way. For the controllable input variables, the rotating equipment, such as the pumps and turbine, are important. By changing the rotational speed of the pumps or the opening of the vanes in the turbine, the operating conditions can be changed. Therefore, the controllable variables in an OTEC cycle are the rotational speed of the seawater pumps, the working fluid pump and the recirculation pump, as well as the opening of the vanes of the turbine.

Seawater temperature

To find the impact of the transient regions, a few scenarios have been investigated. The first scenario is the changing inlet temperature of the seawater. As the temperature of the ocean changes during the year, this is a realistic but slow transient. The result of the experiment showed that the output changes linearly with the the input, even when the the yearly changes were compressed into 14 hours. As this occurs with the small time step used for the model, it can be concluded that the influence of the temperature change of the surface water on the transient regions is very limited.

Mass flows

The next scenario is that of changing mass flows. Three different cases were investigated: hot seawater mass flow, cold seawater mass flow and working fluid mass flow. These scenarios each consist of a large change in mass flow, and therefore the impact of the transient region can be seen more clearly. When looking at the hot seawater mass flow, it could be seen that a decrease in hot seawater mass flow gives an increase in net output. This is due to a large pressure drop dependency, especially in comparison with the heat transfer output. This means that the loss in turbine power output is less than the reduction in pump power. This also implies that the system is not running at an optimum, and therefore control could make a large impact.
For the cold seawater pump, a decrease in mass flow resulted in a decrease in output. As the heat transfer in the condenser decreases, the pressure in the condenser rises. This also decreases the pressure drop over the turbine, resulting in a lower power output. There is also a reduction in the pump power, but this is smaller than the power loss in the turbine.
For the working fluid pump, the transient impact is very large for the cycle. The results showed that when the mass flow is reduced due to a working pump failure, the system has only 2.5 minutes to start the redundant

pump, otherwise the buffer tank would overflow. As the model does not have a volume limit in the buffer tank, the pressure does not rise like it would in reality. Therefore, the result shows the right initial reaction of the model, but, in reality, the prolonged reaction will be different.

Start-up and shutdown

The largest transient condition in the system is when the system starts or shuts down. This condition is interesting to see if the model can cope with large transients and to see how long a start-up sequence has to be to ensure no extreme values that can make the system fail. The results showed that the system can cope with the large transients, and that the transients are followed in a logical way. The pressure levels start to level, the power output decreases in a slow but steady way and the tanks do not overflow or run dry.

Failure of components

The last scenario that was simulated is how fast the system reacts to a failure of components. As said earlier, the system has to react in 2.5 minutes when a working fluid pump fails by turning on the redundant pump. If not, the buffer tank would overflow. In other cases, such as the failure of a row of evaporators or condensers, it reacts immediately, with a lower net output as a result.

Control

That control can have an influence has been proven, if only by the fact that a reduction in hot seawater mass flow results in a higher net output. A sensitivity analysis has been conducted on the system, with the previously mentioned controllable variables as input variables. From this analysis, it was shown that by controlling the working fluid pump rotation, fast steady-state was obtained. By controlling the gear pump rotation, the outlet quality of the evaporator could be controlled. Moreover, without a control strategy, the system was not running at an optimum. A three parameter optimum point has been found using the vanes of the turbine and the rotation of the seawater pumps at 3453.3 kW net output. This is an 15% increase in net output from the original case, which strongly shows the need for control. Using the control strategy of controlling the working fluid pump for steady-state, the gear pump for the quality and the optimum point, small transients can be negated and the output can be maximised.

The impact of the transient regions can be regarded as small, except for scenarios as maintenance and failure of components. The small transients were optimised using a derived control strategy to improve the systems net power output by 15%.

7.2. Recommendations

The research shows the impact of the transient region and implies a control strategy. A few recommendations are given for further studies.

Heat transfer coefficient

The heat transfer coefficient of the ammonia on the condenser side is very high in the model compared to the data of manufacturers. The data from manufacturers states the heat transfer coefficient has to be almost 7 times lower to match their values. As the heat transfer correlation used is made specifically for ammonia and is tested on the same set-up as the model, the correlation is deemed valid for the system. Whether the correlation from the manufacturer is very different or the correlation used in this research is not applicable at the large scale should be investigated, as well as the influence of this heat transfer correlation.

Finite volume model

The model has been made with the thought of real-time control as a boundary condition. Therefore, it could be possible that the accuracy of the model is lower than when a finite volume model with a large amount of control volumes would be used. To check the accuracy of the model in this research, a finite volume model could be used.

Tank influence

As there is no limit of the tank, the pressure in the tank does not rise when the tank is overflowing. In reality, the pressure does rise and the performance of the condenser decreases. This influence can be significant and should therefore be researched further.

Large-scale experiments

The model has been validated on the OTEC demo. But in this experimental set-up, there is no gear pump present and the re-circulation occurs due to a liquid pressure column. Also, when scaling the model to the 3 MW scale, the pump models change, the orifice changed into a turbine and the seawater pumps are not controlled. To validate the large-scale experiments, tests should be done with the large scale system when it is ready.

Control strategies

The control strategy should be tested for each large transient, such as the failure of a pump or shutting down a row of heat exchangers. This probably asks for a different strategy or an extended version of the proposed strategy. By implementing different control strategies, the system can be optimised for all situations.

Turbine rotational speed

When a different turbine is used without a fixed rotational speed, the rotational speed can be used as input for the control strategy. The influence and the implementation of this should be investigated.

Vanes opening

In the control strategy, the assumption is made that the turbine vanes can be opened further than in the design case. Whether this is true, could be investigated together with a manufacturer.

A

Dynamic model derivation

The generalized Navier-Stokes equations can be used for dynamic modelling of heat exchangers. They can describe the conservation of mass and energy of the working fluid as well as the conservation of energy of the wall of the heat exchanger. These are derived from MacArthur and Grald [35]. They can be found in Equations (A.1), (A.2) and (A.3).

$$\frac{\partial \rho}{\partial t} + \frac{\partial (\rho u)}{\partial z} = 0 \tag{A.1}$$

$$\frac{\partial (\rho h - p)}{\partial t} + \frac{\partial (\rho u h)}{\partial z} = \alpha_{wf} \frac{\pi D_{wf}}{A} (T_w - T_{wf}) \tag{A.2}$$

$$\left(c_p \rho A\right)_w \frac{\partial T_w}{\partial t} = \alpha_{wf} \pi D_{wf} \left(T_{wf} - T_w\right) + \alpha_{sw} \pi D_{sw} \left(T_{sw} - T_w\right) \tag{A.3}$$

By integrating these equations by the length of the fluid phase they describe, the spatial dependence can be removed. When doing this, the Leibniz's rule can be used to rewrite the PDE's to ODE's.

$$\int_{z_1(t)}^{z_2(t)} \frac{\partial f(z,t)}{\partial t} = \frac{d}{dt}\left(\int_{z_1(t)}^{z_2(t)} f(z,t) dz \right) + f\big(z_1(t),t\big) \frac{d(z_1(t))}{dt} - f\big(z_2(t),t\big) \frac{d(z_2(t))}{dt} \tag{A.4}$$

A.1. Evaporator

A.1.1. Mass conservation sub-cooled region

The PDE is given in Equation (A.1). Multiplying this equation by the cross-sectional area, the equation becomes Equation (A.5).

$$\frac{\partial (\rho A_{cs})}{\partial t} + \frac{\partial \dot{m}}{\partial z} \tag{A.5}$$

This equation is then integrated over the length of the sub-cooled region, so from z = 0 to z = L_1. By integrating the first part and assuming a constant cross-sectional area, it becomes:

$$\int_0^{L_1} \frac{\partial (\rho A_{cs})}{\partial t} dz = A_{cs} \int_0^{L_1} \left(\frac{\partial \rho}{\partial t} dz \right) \tag{A.6}$$

By applying the Leibniz rule, it becomes:

$$\int_0^{L_1} \frac{\partial (\rho A_{cs})}{\partial t} dz = A_{cs} \left(\frac{d}{dt} \int_0^{L_1} \rho dz - \rho_l \frac{dL_1}{dt} \right) \tag{A.7}$$

By assuming an average density in the sub-cooled region and performing the integration, it becomes:

$$\int_0^{L_1} \frac{\partial (\rho A_{cs})}{\partial t} dz = A_{cs} \left(\frac{d}{dt} (\rho_1 L_1) - \rho_l \frac{dL_1}{dt} \right) \tag{A.8}$$

By taking the time derivative, it becomes:

$$\int_0^{L_1} \frac{\partial(\rho A_{cs})}{\partial t} dz = A_{cs}\left(\rho_1 \frac{dL_1}{dt} + L_1 \frac{d\rho_1}{dt} - \rho_l \frac{dL_1}{dt}\right) \tag{A.9}$$

By choosing pressure and enthalpy as state variables, it becomes:

$$\int_0^{L_1} \frac{\partial(\rho A_{cs})}{\partial t} dz = A_{cs}\left[\left(\left.\frac{\partial \rho_1}{\partial p}\right|_{h_1} \frac{dp}{dt} + \left.\frac{\partial \rho_1}{\partial h_1}\right|_{p} \frac{dh_1}{dt}\right) L_1 + (\rho_1 - \rho_l)\frac{dL_1}{dt}\right] \tag{A.10}$$

By stating that $h_1 = \frac{h_{in}+h_l}{2}$, $\frac{dh_1}{dt} = \frac{1}{2}\left(\frac{dh_{in}}{dt} + \frac{dh_l}{dt}\right)$, it becomes:

$$\int_0^{L_1} \frac{\partial(\rho A_{cs})}{\partial t} dz = \left(\left.\frac{\partial \rho_1}{\partial p}\right|_{h_1} \frac{dp}{dt} + \left.\frac{\partial \rho_1}{\partial h_1}\right|_{p} \frac{1}{2}\left(\frac{dh_l}{dt} + \frac{dh_{in}}{dt}\right)\right) L_1 A_{cs} + (\rho_1 - \rho_l)\frac{dL_1}{dt} A_{cs} \tag{A.11}$$

Because saturated enthalpy is only dependent on pressure, it becomes:

$$\int_0^{L_1} \frac{\partial(\rho A_{cs})}{\partial t} dz = \left(\left(\left.\frac{\partial \rho_1}{\partial p}\right|_{h_1} + \frac{1}{2}\left.\frac{\partial \rho_1}{\partial h_1}\right|_{p} \frac{\partial h_l}{\partial p}\right)\frac{dp}{dt} + \frac{1}{2}\left.\frac{\partial \rho_1}{\partial h_1}\right|_{p} \frac{dh_{in}}{dt}\right) L_1 A_{cs} + (\rho_1 - \rho_l)\frac{dL_1}{dt} A_{cs} \tag{A.12}$$

By integrating the second term over the length of the sub-cooled region, it becomes:

$$\int_0^{L_1} \frac{\partial \dot{m}}{\partial z} dz = \dot{m}_{12} - \dot{m}_{in} \tag{A.13}$$

By combining Equations (A.12) and (A.13), it becomes:

$$\left(\left(\left.\frac{\partial \rho_1}{\partial p}\right|_{h_1} + \frac{1}{2}\left.\frac{\partial \rho_1}{\partial h_1}\right|_{p} \frac{\partial h_l}{\partial p}\right)\frac{dp}{dt} + \frac{1}{2}\left.\frac{\partial \rho_1}{\partial h_1}\right|_{p} \frac{dh_{in}}{dt}\right) L_1 A_{cs} + (\rho_1 - \rho_l)\frac{dL_1}{dt} A_{cs} + \dot{m}_{12} - \dot{m}_{in} = 0 \tag{A.14}$$

A.1.2. Mass conservation two-phase region

The PDE is given in Equation (A.1). Multiplying this equation by the cross-sectional area, the equation becomes Equation (A.5). By integrating the first part over the length of the two-phase region, from z = L_1 to z = L and assuming constant cross-sectional area, this becomes:

$$\int_{L_1}^{L} \frac{\partial(\rho A_{cs})}{\partial t} dz = A_{cs} \int_{L_1}^{L} \frac{\partial \rho}{\partial t} \tag{A.15}$$

By applying the Leibniz rule, it becomes:

$$\int_{L_1}^{L} \frac{\partial(\rho A_{cs})}{\partial t} dz = A_{cs}\left(\frac{d}{dt}\int_{L_1}^{L} \rho dz + \rho_l \frac{dL_1}{dt}\right) \tag{A.16}$$

By applying void fraction, it becomes:

$$\int_{L_1}^{L} \frac{\partial(\rho A_{cs})}{\partial t} dz = A_{cs}\left(\frac{d}{dt}\int_{L_1}^{L} \left(\rho_l(1-\gamma) + \rho_g \gamma\right) dz + \rho_l \frac{dL_1}{dt}\right) \tag{A.17}$$

By doing the integration and by L = L_1 + L_2, it becomes:

$$\int_{L_1}^{L} \frac{\partial(\rho A_{cs})}{\partial t} dz = A_{cs}\left(\frac{d}{dt}\left(\rho_l(1-\overline{\gamma}) + \rho_g \overline{\gamma}\right) L_2 + \rho_l \frac{dL_1}{dt}\right) \tag{A.18}$$

Taking the time derivative, it becomes:

$$\int_{L_1}^{L} \frac{\partial(\rho A_{cs})}{\partial t} dz = A_{cs}\left(\left(\frac{d\rho_l}{dt}(1-\overline{\gamma}) + \frac{d\rho_g}{dt}\overline{\gamma}\right)L_2 + \left(\rho_l(1-\overline{\gamma}) + \rho_g\overline{\gamma}\right)\frac{dL_2}{dt} + \left(\rho_g - \rho_l\right)L_2\frac{d\overline{\gamma}}{dt} + \rho_l\frac{dL_1}{dt}\right) \tag{A.19}$$

Because saturated densities are only dependent on pressure, it becomes:

$$\int_{L_1}^{L} \frac{\partial(\rho A_{cs})}{\partial t} dz = A_{cs}\left(\left(\frac{\partial\rho_l}{\partial p}(1-\overline{\gamma}) + \frac{\partial\rho_g}{\partial p}\overline{\gamma}\right)L_2\frac{dp}{dt} + \left(\rho_l(1-\overline{\gamma}) + \rho_g\overline{\gamma}\right)\frac{dL_2}{dt} + \left(\rho_g - \rho_l\right)L_2\frac{d\overline{\gamma}}{dt} + \rho_l\frac{dL_1}{dt}\right) \tag{A.20}$$

By $\frac{dL_2}{dt} = -\frac{dL_1}{dt}$ and rewriting Equation (A.20), it becomes:

$$\int_{L_1}^{L} \frac{\partial(\rho A_{cs})}{\partial t} dz = A_{cs}\left(\left(\frac{\partial\rho_l}{\partial p}(1-\overline{\gamma}) + \frac{\partial\rho_g}{\partial p}\overline{\gamma}\right)L_2\frac{dp}{dt} + \left(\rho_g - \rho_l\right)L_2\frac{d\overline{\gamma}}{dt} + \left(\rho_l - \rho_g\right)\overline{\gamma}\frac{dL_1}{dt}\right) \tag{A.21}$$

By integrating the second term of Equation (A.5), it becomes:

$$\int_{L_1}^{L} \frac{\partial\dot{m}}{\partial z} dz = \dot{m}_o - \dot{m}_{12} \tag{A.22}$$

By combining Equations (A.21) and (A.22), it becomes:

$$\left(\frac{\partial\rho_l}{\partial p}(1-\overline{\gamma}) + \frac{\partial\rho_g}{\partial p}\overline{\gamma}\right)A_{cs}L_2\frac{dp}{dt} + \left(\rho_g - \rho_l\right)A_{cs}L_2\frac{d\overline{\gamma}}{dt} + \left(\rho_l - \rho_g\right)\overline{\gamma}A_{cs}\frac{dL_1}{dt} + \dot{m}_o - \dot{m}_{12} = 0 \tag{A.23}$$

A.1.3. Energy conservation of sub-cooled region

The PDE is given in Equation (A.2). Multiplying this equation by the cross-sectional area, the equation becomes:

$$\frac{\partial(\rho h A_{cs} - A_{cs}p)}{\partial t} + \frac{\partial(\dot{m}h)}{\partial z} = \alpha_{wf}\pi D\left(T_w - T_{wf}\right) \tag{A.24}$$

By integrating the first term over the length of the sub-cooled region, from z = 0 to z = L_1, it becomes:

$$\int_{0}^{L_1} \frac{\partial(\rho h A_{cs})}{\partial t} dz = A_{cs}\int_{0}^{L_1} \frac{\partial(\rho h)}{\partial t} dz \tag{A.25}$$

By applying the Leibniz rule, it becomes:

$$\int_{0}^{L_1} \frac{\partial(\rho h A_{cs})}{\partial t} dz = A_{cs}\left(\frac{d}{dt}\int_{0}^{L_1} \rho h\, dz - \rho_l h_l\frac{dL_1}{dt}\right) \tag{A.26}$$

By assuming an average density and enthalpy and doing the integration, it becomes:

$$\int_{0}^{L_1} \frac{\partial(\rho h A_{cs})}{\partial t} dz = A_{cs}\left(\frac{d}{dt}\left(\rho_1 h_1 L_1\right)dz - \rho_l h_l\frac{dL_1}{dt}\right) \tag{A.27}$$

By taking the time derivative, it becomes:

$$\int_{0}^{L_1} \frac{\partial(\rho h A_{cs})}{\partial t} dz = A_{cs}\left(h_1 L_1\frac{d\rho_1}{dt} + \rho_1 L_1\frac{dh_1}{dt} + \rho_1 h_1\frac{dL_1}{dt} - \rho_l h_l\frac{dL_1}{dt}\right) \tag{A.28}$$

By choosing pressure and enthalpy as state variables, it becomes:

$$\int_{0}^{L_1} \frac{\partial(\rho h A_{cs})}{\partial t} dz = A_{cs}\left(\left(\left.\frac{\partial\rho_1}{\partial h_1}\right|_p\frac{dh_1}{dt} + \left.\frac{\partial\rho_1}{\partial p}\right|_{h_1}\frac{dp}{dt}\right)h_1 L_1 + \rho_1 L_1\frac{dh_1}{dt} + \rho_1 h_1\frac{dL_1}{dt} - \rho_l h_l\frac{dL_1}{dt}\right) \tag{A.29}$$

By rewriting Equation (A.29), it becomes:

$$\int_0^{L_1} \frac{\partial(\rho h A_{cs})}{\partial t} dz = \left(\left.\frac{\partial \rho_1}{\partial h_1}\right|_p h_1 + \rho_1 \right) L_1 A_{cs} \frac{dh_1}{dt} + \left.\frac{\partial \rho_1}{\partial p}\right|_{h_1} h_1 L_1 A_{cs} \frac{dp}{dt} + (\rho_1 h_1 - \rho_l h_l) A_{cs} \frac{dL_1}{dt} \tag{A.30}$$

By stating that $h_1 = \frac{h_{in}+h_l}{2}$, $\frac{dh_1}{dt} = \frac{1}{2}\left(\frac{dh_{in}}{dt} + \frac{dh_l}{dt}\right)$, it becomes:

$$\int_0^{L_1} \frac{\partial(\rho h A_{cs})}{\partial t} dz = \left(\left.\frac{\partial \rho_1}{\partial h_1}\right|_p h_1 + \rho_1 \right) L_1 A_{cs} \frac{1}{2}\left(\frac{dh_{in}}{dt} + \frac{dh_l}{dt}\right) + \left.\frac{\partial \rho_1}{\partial p}\right|_{h_1} h_1 L_1 A_{cs} \frac{dp}{dt} + (\rho_1 h_1 - \rho_l h_l) A_{cs} \frac{dL_1}{dt} \tag{A.31}$$

As saturated enthalpy is only dependent on pressure, it becomes:

$$\int_0^{L_1} \frac{\partial(\rho h A_{cs})}{\partial t} dz = \left(\left.\frac{\partial \rho_1}{\partial h_1}\right|_p h_1 + \rho_1 \right) L_1 A_{cs} \frac{1}{2}\left(\frac{dh_{in}}{dt} + \frac{\partial h_l}{\partial p}\frac{dp}{dt}\right) + \left.\frac{\partial \rho_1}{\partial p}\right|_{h_1} h_1 L_1 A_{cs} \frac{dp}{dt} + (\rho_1 h_1 - \rho_l h_l) A_{cs} \frac{dL_1}{dt} \tag{A.32}$$

By rewriting this equation, it becomes:

$$\begin{aligned} \int_0^{L_1} \frac{\partial(\rho h A_{cs})}{\partial t} dz = & \left(\left.\frac{\partial \rho_1}{\partial h_1}\right|_p h_1 + \rho_1 \right) L_1 A_{cs} \frac{1}{2} \frac{dh_{in}}{dt} + (\rho_1 h_1 - \rho_l h_l) A_{cs} \frac{dL_1}{dt} \\ & + \left(\frac{1}{2}\left(\left.\frac{\partial \rho_1}{\partial h_1}\right|_p \frac{\partial h_l}{\partial p} h_1 + \rho_1 \frac{\partial h_l}{\partial p} \right) + \left.\frac{\partial \rho_1}{\partial p}\right|_{h_1} h_1 \right) L_1 A_{cs} \frac{dp}{dt} \end{aligned} \tag{A.33}$$

By integrating the second term of Equation (A.24) from z = 0 to z = L_1, it becomes:

$$\int_0^{L_1} -\frac{\partial(A_{cs} p)}{\partial t} dz = -A_{cs} \int_0^{L_1} \frac{\partial p}{\partial t} dz \tag{A.34}$$

By applying the Leibniz rule, it becomes:

$$\int_0^{L_1} -\frac{\partial(A_{cs} p)}{\partial t} dz = -A_{cs} \left(\frac{d}{dt} \int_0^{L_1} p \, dz - p \frac{dL_1}{dt} \right) \tag{A.35}$$

By performing the integration, it becomes:

$$\int_0^{L_1} -\frac{\partial(A_{cs} p)}{\partial t} dz = -A_{cs} \left(\frac{d}{dt} p L_1 - p \frac{dL_1}{dt} \right) \tag{A.36}$$

By taking the time derivative, it becomes:

$$\int_0^{L_1} -\frac{\partial(A_{cs)} p}{\partial t} dz = -A_{cs} \left(\frac{dp}{dt} L_1 + \frac{dL_1}{dt} p - p \frac{dL_1}{dt} \right) = -A_{cs} \frac{dp}{dt} L_1 \tag{A.37}$$

By integrating the third term of the PDE from z = 0 to z = L_1, it becomes:

$$\int_0^{L_1} \frac{\partial \dot{m} h}{\partial z} dz = \dot{m}_{12} h_l - \dot{m}_{in} h_{in} \tag{A.38}$$

By integrating the right hand side of Equation (A.24), it becomes:

$$\int_0^{L_1} \alpha_{wf} \pi D_{wf} \left(T_w - T_{wf} \right) dz = \alpha_{1wf} \pi D_{wf} L_1 \left(T_{1w} - T_{1wf} \right) \tag{A.39}$$

By multiplying the equation with $\frac{L}{L}$, it becomes:

$$\int_0^{L_1} \alpha_{wf} \pi D_{wf} \left(T_w - T_{wf}\right) dz = \alpha_{1wf} A_{wf} \frac{L_1}{L} \left(T_{1w} - T_{1wf}\right) \tag{A.40}$$

Combining Equations (A.33), (A.37), (A.38) and (A.40), it becomes:

$$\begin{aligned} &\left(\left.\frac{\partial \rho_1}{\partial h_1}\right|_p h_1 + \rho_1\right) L_1 A_{cs} \frac{1}{2} \frac{dh_{in}}{dt} + (\rho_1 h_1 - \rho_l h_l) A_{cs} \frac{dL_1}{dt} + \left(\frac{1}{2}\left(\left.\frac{\partial \rho_1}{\partial h_1}\right|_p \frac{\partial h_l}{\partial p} h_1 + \rho_1 \frac{\partial h_l}{\partial p}\right) + \left.\frac{\partial \rho_1}{\partial p}\right|_{h_1} h_1\right) L_1 A_{cs} \frac{dp}{dt} \\ &- A_{cs} \frac{dp}{dt} L_1 + \dot{m}_{12} h_l - \dot{m}_{in} h_{in} = \alpha_{1wf} A_{wf} \frac{L_1}{L} \left(T_{1w} - T_{1wf}\right) \end{aligned} \tag{A.41}$$

By rewriting this equation, it becomes:

$$\begin{aligned} &\left(\left.\frac{\partial \rho_1}{\partial h_1}\right|_p h_1 + \rho_1\right) L_1 A_{cs} \frac{1}{2} \frac{dh_{in}}{dt} + \left(\frac{1}{2}\left(\left.\frac{\partial \rho_1}{\partial h_1}\right|_p \frac{\partial h_l}{\partial p} h_1 + \rho_1 \frac{\partial h_l}{\partial p}\right) + \left.\frac{\partial \rho_1}{\partial p}\right|_{h_1} h_1 - 1\right) L_1 A_{cs} \frac{dp}{dt} \\ &+ (\rho_1 h_1 - \rho_l h_l) A_{cs} \frac{dL_1}{dt} + \dot{m}_{12} h_l - \dot{m}_{in} h_{in} = \alpha_{1wf} A_{wf} \frac{L_1}{L} \left(T_{1w} - T_{1wf}\right) \end{aligned} \tag{A.42}$$

A.1.4. Energy conservation in the two-phase region

By integrating the first part of Equation (A.24) over the length of the two-phase region, it becomes:

$$\int_{L_1}^{L} \frac{\partial \rho h A_{cs}}{\partial t} dz = A_{cs} \int_{L_1}^{L} \frac{\partial \rho h}{\partial t} \tag{A.43}$$

By applying the Leibniz rule, it becomes:

$$\int_{L_1}^{L} \frac{\partial \rho h A_{cs}}{\partial t} dz = A_{cs} \left(\frac{d}{dt} \int_{L_1}^{L} \rho h dz + \rho_l h_l \frac{dL_1}{dt}\right) \tag{A.44}$$

By assuming void fraction, it becomes:

$$\int_{L_1}^{L} \frac{\partial \rho h A_{cs}}{\partial t} dz = A_{cs} \left(\frac{d}{dt} \int_{L_1}^{L} \left(\rho_l h_l (1-\gamma) + \rho_g h_h \gamma\right) dz + \rho_l h_l \frac{dL_1}{dt}\right) \tag{A.45}$$

By performing the integration, it becomes:

$$\int_{L_1}^{L} \frac{\partial \rho A_{cs}}{\partial t} dz = A_{cs} \left(\frac{d}{dt} \left(\rho_l h_l (1-\overline{\gamma}) + \rho_g h_g \overline{\gamma}\right) L_2 + \rho_l h_l \frac{dL_1}{dt}\right) \tag{A.46}$$

By taking the time derivative, it becomes:

$$\begin{aligned} \int_{L_1}^{L} \frac{\partial \rho h A_{cs}}{\partial t} dz = A_{cs} \Bigg[&\left(\frac{d\left(\rho_l h_l\right)}{dt} (1-\overline{\gamma}) + \frac{d\left(\rho_g h_g\right)}{dt} \overline{\gamma}\right) L_2 \\ &+ \left(\rho_l h_l (1-\overline{\gamma}) + \rho_g h_g \overline{\gamma}\right) \frac{dL_2}{dt} + \left(\rho_g h_g - \rho_l h_l\right) L_2 \frac{d\overline{\gamma}}{dt} + \rho_l h_l \frac{dL_1}{dt} \Bigg] \end{aligned} \tag{A.47}$$

As saturated properties are only dependent on pressure, it becomes:

$$\begin{aligned} \int_{L_1}^{L} \frac{\partial \rho h A_{cs}}{\partial t} dz = A_{cs} \Bigg[&\left(\frac{\partial\left(\rho_l h_l\right)}{\partial p} (1-\overline{\gamma}) + \frac{\partial\left(\rho_g h_g\right)}{\partial p} \overline{\gamma}\right) L_2 \frac{dp}{dt} \\ &+ \left(\rho_l h_l (1-\overline{\gamma}) + \rho_g h_g \overline{\gamma}\right) \frac{dL_2}{dt} + \left(\rho_g h_g - \rho_l h_l\right) L_2 \frac{d\overline{\gamma}}{dt} + \rho_l h_l \frac{dL_1}{dt} \Bigg] \end{aligned} \tag{A.48}$$

As $\frac{dL_2}{dt} = -\frac{dL_1}{dt}$, it becomes, after rewriting:

$$\begin{aligned}\int_{L_1}^{L} \frac{\partial \rho h A_{cs}}{\partial t} dz = &\left(\frac{\partial \left(\rho_l h_l\right)}{\partial p}(1-\overline{\gamma}) + \frac{\partial \left(\rho_g h_g\right)}{\partial p}\overline{\gamma} \right) A_{cs} L_2 \frac{dp}{dt} \\ &+ \left(\rho_l h_l - \rho_g h_g\right)\overline{\gamma} A_{cs} \frac{dL_1}{dt} + \left(\rho_g h_g - \rho_l h_l\right) A_{cs} L_2 \frac{d\overline{\gamma}}{dt}\end{aligned} \tag{A.49}$$

By integrating the second term of Equation (A.24) over the length of the two-phase region, it becomes:

$$\int_{L_1}^{L} -\frac{\partial p A_{cs}}{\partial t} dz = -A_{cs} \int_{L_1}^{L} \frac{\partial p}{\partial t} dz \tag{A.50}$$

By applying the Leibniz rule, it becomes:

$$\int_{L_1}^{L} -\frac{\partial p A_{cs}}{\partial t} dz = -A_{cs} \left(\frac{d}{dt} \int_{L_1}^{L} p + p \frac{dL_1}{dt} \right) \tag{A.51}$$

By performing the integration, it becomes:

$$\int_{L_1}^{L} -\frac{\partial p A_{cs}}{\partial t} dz = -A_{cs} \left(\frac{d}{dt}\left(p L_2\right) + p \frac{dL_1}{dt} \right) \tag{A.52}$$

By taking the time derivative, it becomes:

$$\int_{L_1}^{L} -\frac{\partial p A_{cs}}{\partial t} dz = -A_{cs} \left(L_2 \frac{dp}{dt} + p \frac{dL_2}{dt} + p \frac{dL_1}{dt} \right) \tag{A.53}$$

With $\frac{dL_2}{dt} = -\frac{dL_1}{dt}$, it becomes:

$$\int_{L_1}^{L} -\frac{\partial p A_{cs}}{\partial t} dz = -A_{cs} L_2 \frac{dp}{dt} \tag{A.54}$$

By integrating the third term of Equation (A.24) over the length of the two-phase region, it becomes:

$$\int_{L_1}^{L} \frac{\partial \dot{m} h}{\partial z} = \dot{m}_o h_o - \dot{m}_{12} h_l \tag{A.55}$$

By integrating the right hand side of Equation (A.24) over the length of the sub-cooled region, it becomes:

$$\int_{L_1}^{L} \alpha_{wf} \pi D_{wf} \left(T_w - T_{wf}\right) = \alpha_{2wf} \pi D L_2 \left(T_{2w} - T_{2wf}\right) \tag{A.56}$$

By multiplying this equation by $\frac{L}{L}$, it becomes:

$$\int_{L_1}^{L} \alpha_{wf} \pi D_{wf} \left(T_w - T_{wf}\right) = \alpha_{2wf} A_{wf} \frac{L_2}{L} \left(T_{2w} - T_{2wf}\right) \tag{A.57}$$

By combining Equations (A.49), (A.54), (A.55) and (A.57), it becomes:

$$\begin{aligned}&\left(\frac{\partial \left(\rho_l h_l\right)}{\partial p}(1-\overline{\gamma}) + \frac{\partial \left(\rho_g h_g\right)}{\partial p}\overline{\gamma} - 1 \right) A_{cs} L_2 \frac{dp}{dt} + \left(\rho_l h_l - \rho_g h_g\right)\overline{\gamma} A_{cs} \frac{dL_1}{dt} + \left(\rho_g h_g - \rho_l h_l\right) A_{cs} L_2 \frac{d\overline{\gamma}}{dt} \\ &+ \dot{m}_o h_o - \dot{m}_{12} h_l = \alpha_{2wf} A_{wf} \frac{L_2}{L} \left(T_{2w} - T_{2wf}\right)\end{aligned} \tag{A.58}$$

A.1.5. Structure conservation in the sub-cooled region

The PDE is given in Equation (A.3). By multiplying this equation by the length of the heat exchanger, it becomes:

$$\left(c_p \rho V\right)_w \frac{\partial T_w}{\partial t} = \alpha_{wf} A_{wf} \left(T_{wf} - T_w\right) + \alpha_{sw} A_{sw} \left(T_{sw} - T_w\right) \tag{A.59}$$

By integrating the left part over arbitrary length from a to b and applying the Leibniz rule, this becomes:

$$\int_a^b \left(c_p \rho V\right)_w \frac{\partial T_w}{\partial t} dz = \left(c_p \rho V\right)_w \frac{d}{dt} \int_a^b T_w dz + T_w(a) \frac{da}{dt} - T_w(b) \frac{db}{dt} \tag{A.60}$$

By performing the integration, it becomes:

$$\int_a^b \left(c_p \rho V\right)_w \frac{\partial T_w}{\partial t} dz = \left(c_p \rho V\right)_w \left(\frac{d}{dt}(b-a) T_{w(a-b)} + T_w(a) \frac{da}{dt} - T_w(b) \frac{db}{dt}\right) \tag{A.61}$$

By taking the time derivative, it becomes:

$$\int_a^b \left(c_p \rho V\right)_w \frac{\partial T_w}{\partial t} dz = \left(c_p \rho V\right)_w \left(\frac{d(b-a)}{dt} T_{w(a-b)} + (b-a) \frac{dT_{w(a-b)}}{dt} + T_w(a) \frac{da}{dt} - T_w(b) \frac{db}{dt}\right) \tag{A.62}$$

For the sub-cooled region, a = 0 and b = L_1. With this, it becomes:

$$\int_0^{L_1} \left(c_p \rho V\right)_w \frac{\partial T_w}{\partial t} dz = \left(c_p \rho V\right)_w \left(\frac{dL_1}{dt} T_{1w} + L_1 \frac{dT_{1w}}{dt} - T_{w(L_1)} \frac{dL_1}{dt}\right) \tag{A.63}$$

In literature, different values for $T_{w(L_1)}$ are taken. As it is assumed a lumped temperature, it is a discontinuous function at the boundary. In reality, the temperature at the wall will be closer to the two-phase region than to the single-phase region, as stated by Willatzen, He and Weerstra [65][22][62]. Therefore, $T_{w(L_1)} = T_{2w}$. With this, it becomes:

$$\int_0^{L_1} \left(c_p \rho V\right)_w \frac{\partial T_w}{\partial t} dz = \left(c_p \rho V\right)_w \left(L_1 \frac{dT_{1w}}{dt} + (T_{1w} - T_{2w}) \frac{dL_1}{dt}\right) \tag{A.64}$$

Integrating the right hand side of Equation (A.59), it becomes:

$$\int_0^{L_1} \left(\alpha_{wf} A_{wf} \left(T_{wf} - T_w\right) + \alpha_{sw} A_{sw} \left(T_{sw} - T_w\right)\right) dz = \alpha_{wf} A_{wf} L_1 \left(T_{wf} - T_w\right) + \alpha_{sw} A_{sw} L_1 \left(T_{sw} - T_w\right) \tag{A.65}$$

Combining Equations (A.64) and (A.65) and dividing left and right by L_1, it becomes:

$$\left(c_p \rho V\right)_w \left(\frac{dT_{1w}}{dt} + \frac{T_{1w} - T_{2w}}{L_1} \frac{dL_1}{dt}\right) = \alpha_{wf} A_{wf} \left(T_{wf} - T_w\right) + \alpha_{sw} A_{sw} \left(T_{sw} - T_w\right) \tag{A.66}$$

A.1.6. Structure conservation in the two-phase region

By using Equation (A.62) for the two-phase region, a = L_1 and b = L_2, L = L_1 + L_2 and $T_{w(L_1)} = T_{2w}$, it becomes:

$$\int_{L_1}^{L} \left(c_p \rho V\right)_w \frac{\partial T_w}{\partial t} dz = \left(c_p \rho V\right)_w \left(T_{2w} \frac{dL_2}{dt} + L_2 \frac{dT_{2w}}{dt} + T_{2w} \frac{dL_1}{dt}\right) \tag{A.67}$$

As $\frac{dL_1}{dt} = -\frac{dL_2}{dt}$, it becomes:

$$\int_{L_1}^{L} \left(c_p \rho V\right)_w \frac{\partial T_w}{\partial t} dz = \left(c_p \rho V\right)_w \left(L_2 \frac{dT_{2w}}{dt}\right) \tag{A.68}$$

By integrating the right hand side of equation (A.59) from L_1 to L, it becomes:

$$\int_{L_1}^{L} \left(\alpha_{wf} A_{wf} \left(T_{wf} - T_w\right) + \alpha_{sw} A_{sw} \left(T_{sw} - T_w\right)\right) dz = \alpha_{wf} A_{wf} L_2 \left(T_{wf} - T_w\right) + \alpha_{sw} A_{sw} L_2 \left(T_{sw} - T_w\right) \tag{A.69}$$

By combining Equations (A.68) and (A.69) and dividing it by L_2, it becomes:

$$\left(c_p \rho V\right)_w \left(\frac{dT_{2w}}{dt}\right) = \alpha_{wf} A_{wf} \left(T_{wf} - T_w\right) + \alpha_{sw} A_{sw} \left(T_{sw} - T_w\right) \tag{A.70}$$

A.1.7. Governing time derivatives

The six equations have five explicit time derivatives: $\frac{dL_1}{dt}, \frac{dp}{dt}, \frac{d\overline{\gamma}}{dt}, \frac{dT_{1w}}{dt} and \frac{dT_{2w}}{dt}$. Using Equations (A.13) and (A.22), $\dot{m}_{12}$ can be eliminated. This can be done by rewriting these equations. This is done in Equations (A.71) and (A.72).

$$\dot{m}_{12} = m_{in} - \left(\left(\left.\frac{\partial \rho_1}{\partial p}\right|_{h_1} + \frac{1}{2}\left.\frac{\partial \rho_1}{\partial h_1}\right|_p \frac{\partial h_l}{\partial p}\right)\frac{dp}{dt} + \frac{1}{2}\left.\frac{\partial \rho_1}{\partial h_1}\right|_p \frac{dh_{in}}{dt}\right) L_1 A_{cs} - \left(\rho_1 - \rho_l\right)\frac{dL_1}{dt} A_{cs} \tag{A.71}$$

$$\dot{m}_{12} = \left(\frac{\partial \rho_l}{\partial p}\left(1 - \overline{\gamma}\right) + \frac{\partial \rho_g}{\partial p}\overline{\gamma}\right) L_2 A_{cs} \frac{dp}{dt} + \left(\rho_g - \rho_l\right) L_2 A_{cs} \frac{d\overline{\gamma}}{dt} + \left(\rho_l - \rho_g\right)\overline{\gamma} A_{cs} \frac{dL_1}{dt} + \dot{m}_o \tag{A.72}$$

By using Equation (A.71) to rewrite Equation (A.42), it becomes:

$$\begin{aligned}&\left(\left.\frac{\partial \rho_1}{\partial h_1}\right|_p \left(h_1 - h_l\right) + \rho_1\right) L_1 A_{cs} \frac{1}{2}\frac{dh_{in}}{dt} + \left(\frac{1}{2}\left(\left.\frac{\partial \rho_1}{\partial h_1}\right|_p \frac{\partial h_l}{\partial p}\left(h_1 - h_l\right) + \rho_1 \frac{\partial h_l}{\partial p}\right) + \left.\frac{\partial \rho_1}{\partial p}\right|_{h_1} \left(h_1 - h_l\right) - 1\right) L_1 A_{cs} \frac{dp}{dt} \\ &+ \left(\rho_1 \left(h_1 - h_l\right)\right) A_{cs} \frac{dL_1}{dt} + \dot{m}_{in} \left(h_l - h_{in}\right) = \alpha_{1wf} A_{wf} \frac{L_1}{L} \left(T_{1w} - T_{1wf}\right)\end{aligned} \tag{A.73}$$

By using Equation (A.72) to rewrite Equation (A.58), it becomes:

$$\begin{aligned}&\left(\frac{\partial h_l}{\partial p}\rho_l(1 - \overline{\gamma}) + \left(\frac{\partial\left(\rho_g h_g\right)}{\partial p} - \frac{\partial \rho_g}{\partial p} h_l\right)\overline{\gamma} - 1\right) A_{cs} L_2 \frac{dp}{dt} + \rho_g \left(h_l - h_g\right)\overline{\gamma} A_{cs} \frac{dL_1}{dt} + \rho_g \left(h_g - h_l\right) A_{cs} L_2 \frac{d\overline{\gamma}}{dt} \\ &+ \dot{m}_o \left(h_o - h_l\right) = \alpha_{2wf} A_{wf} \frac{L_2}{L} \left(T_{2w} - T_{2wf}\right)\end{aligned} \tag{A.74}$$

Combining Equations (A.71) and (A.72), it becomes:

$$\begin{aligned}m_{in} - m_{out} = &\left[\left(\left.\frac{\partial \rho_1}{\partial p}\right|_{h_1} + \frac{1}{2}\left.\frac{\partial \rho_1}{\partial h_1}\right|_p \frac{\partial h_l}{\partial p}\right) L_1 A_{cs} + \left(\frac{\partial \rho_l}{\partial p}\left(1 - \overline{\gamma}\right) + \frac{\partial \rho_g}{\partial p}\overline{\gamma}\right) L_2 A_{cs}\right] \frac{dp}{dt} \\ &+ \left(\left(\rho_l - \rho_g\right)\overline{\gamma} + \left(\rho_1 - \rho_l\right)\right) A_{cs} \frac{dL_1}{dt} + \left(\rho_g - \rho_l\right) L_2 A_{cs} \frac{d\overline{\gamma}}{dt} + \frac{1}{2}\left.\frac{\partial \rho_1}{\partial h_1}\right|_p L_1 A_{cs} \frac{dh_{in}}{dt}\end{aligned} \tag{A.75}$$

A.1.8. Separator

By combining the separator and evaporator, Equation (A.75) and (A.74) have to be rewritten and an energy conservation of the separator has to be given. The mass conservation of the separator is given by:

$$\frac{dm_{sep}}{dt} = \dot{m}_{in} - \dot{m}_{turb} - \dot{m}_{gear} \tag{A.76}$$

As $\dot{m}_{in}$ of the separator is $\dot{m}_{out}$ of the evaporator, Equation (A.75) becomes:

$$\begin{aligned}m_{in} - \frac{dm_{sep}}{dt} - \dot{m}_{turb} - \dot{m}_{gear} = &\left[\left(\left.\frac{\partial \rho_1}{\partial p}\right|_{h_1} + \frac{1}{2}\left.\frac{\partial \rho_1}{\partial h_1}\right|_p \frac{\partial h_l}{\partial p}\right) L_1 A_{cs} + \left(\frac{\partial \rho_l}{\partial p}\left(1 - \overline{\gamma}\right) + \frac{\partial \rho_g}{\partial p}\overline{\gamma}\right) L_2 A_{cs}\right] \frac{dp}{dt} \\ &+ \left(\left(\rho_l - \rho_g\right)\overline{\gamma} + \left(\rho_1 - \rho_l\right)\right) A_{cs} \frac{dL_1}{dt} + \left(\rho_g - \rho_l\right) L_2 A_{cs} \frac{d\overline{\gamma}}{dt} + \frac{1}{2}\left.\frac{\partial \rho_1}{\partial h_1}\right|_p L_1 A_{cs} \frac{dh_{in}}{dt}\end{aligned} \tag{A.77}$$

Using Equation (A.76), Equation (A.74) becomes:

$$\left(\frac{\partial h_l}{\partial p}\rho_l(1-\overline{\gamma})+\left(\frac{\partial(\rho_g h_g)}{\partial p}-\frac{\partial \rho_g}{\partial p}h_l\right)\overline{\gamma}-1\right)A_{cs}L_2\frac{dp}{dt}+\rho_g\left(h_l-h_g\right)\overline{\gamma}A_{cs}\frac{dL_1}{dt}+\rho_g\left(h_g-h_l\right)A_{cs}L_2\frac{d\overline{\gamma}}{dt} \\ +\left(\frac{dm_{sep}}{dt}+\dot{m}_{turb}+\dot{m}_{gear}\right)(h_o-h_l)=\alpha_{2wf}A_{wf}\frac{L_2}{L}\left(T_{2w}-T_{2wf}\right) \tag{A.78}$$

The energy conservation of the separator is:

$$\frac{d\left(m_{sep}u_{sep}\right)}{dt}=\dot{m}_{evap,out}h_{evap,out}-\dot{m}_{gear}h_l-\dot{m}_{turb}h_g \tag{A.79}$$

The left hand side of Equation (A.79) becomes:

$$\frac{d\left(m_{sep}u_{sep}\right)}{dt}=\frac{d\left(m_g u_g+m_l u_l\right)}{dt} \tag{A.80}$$

As $m=\rho V$, it becomes:

$$\frac{d\left(m_{sep}u_{sep}\right)}{dt}=\frac{d\left(\rho_g V_g u_g+\rho_l V_l u_l\right)}{dt} \tag{A.81}$$

By taking the derivative, it becomes:

$$\frac{d\left(m_{sep}u_{sep}\right)}{dt}=\dot{\rho}_g V_g u_g+\rho_g\dot{V}_g u_g+\rho_g V_g\dot{u}_g+\dot{\rho}_l V_l u_l+\rho_l\dot{V}_l u_l+\rho_l V_l\dot{u}_l \tag{A.82}$$

To solve this, we first need to find $\dot{V}_g$. This can be done in the following steps:

$$\frac{dm_{sep}}{dt}=\dot{\rho}_g V_g+\rho_g\dot{V}_g+\dot{\rho}_l V_l+\rho_l\dot{V}_l \tag{A.83}$$

As the total volume of the separator cannot change, $\dot{V}_l+\dot{V}_g=0$, or $\dot{V}_l=-\dot{V}_g$. Using this, it becomes:

$$\frac{dm_{sep}}{dt}=\left(\dot{\rho}_g V_g+\dot{\rho}_l V_l\right)+\left(\rho_g-\rho_l\right)\dot{V}_g \tag{A.84}$$

By rewriting Equation (A.84) and stating that saturated density is a function of pressure, it becomes:

$$\dot{V}_g=\frac{\frac{dm_{sep}}{dt}-\left(\frac{\partial\rho_g}{\partial p}V_g+\frac{\partial\rho_l}{\partial p}V_l\right)\dot{p}}{\left(\rho_g-\rho_l\right)} \tag{A.85}$$

By implementing Equation (A.85), using $\dot{V}_g=\dot{V}_l$ and stating that saturated density is only dependent on pressure, Equation (A.82) becomes:

$$\frac{d\left(m_{sep}u_{sep}\right)}{dt}=\left(\frac{\partial\rho_g}{\partial p}V_g u_g+\rho_g V_g\frac{\partial u_g}{\partial p}+\frac{\partial\rho_l}{\partial p}V_l u_l+\rho_l V_l\frac{\partial u_l}{\partial p}\right)+\left(\rho_g u_g-\rho_l u_l\right)\left(\frac{\frac{dm_{sep}}{dt}-\left(\frac{\partial\rho_g}{\partial p}V_g+\frac{\partial\rho_l}{\partial p}V_l\right)\dot{p}}{\left(\rho_g-\rho_l\right)}\right) \tag{A.86}$$

The right hand side of Equation (A.79), when using Equation (A.76), becomes:

$$\left(\frac{dm_{sep}}{dt}+\dot{m}_{gear}+\dot{m}_{turb}\right)h_{evap,out}-\dot{m}_{gear}h_l-\dot{m}_{turb}h_g \tag{A.87}$$

Combining Equations (A.86) and (A.87), it becomes:

$$\frac{d\left(m_{sep}u_{sep}\right)}{dt}=\left(\frac{\partial\rho_g}{\partial p}V_g u_g+\rho_g V_g\frac{\partial u_g}{\partial p}+\frac{\partial\rho_l}{\partial p}V_l u_l+\rho_l V_l\frac{\partial u_l}{\partial p}\right)+\left(\rho_g u_g-\rho_l u_l\right)\left(\frac{\frac{dm_{sep}}{dt}-\left(\frac{\partial\rho_g}{\partial p}V_g+\frac{\partial\rho_l}{\partial p}V_l\right)\dot{p}}{\left(\rho_g-\rho_l\right)}\right) \\ =\frac{dm_{sep}}{dt}h_{evap,out}+\dot{m}_{gear}\left(h_{evap,out}-h_l\right)+\dot{m}_{turb}\left(h_{evap,out}-h_g\right) \tag{A.88}$$

A.2. Condenser

A.2.1. Mass conservation

The PDE is given in Equation (A.1). By multiplying this equation by the cross-sectional area, this equation becomes:

$$\frac{\partial(\rho A_{cs})}{\partial t} + \frac{\partial \dot{m}}{\partial z} \tag{A.89}$$

This equation is integrated of the length of the heat exchanger, from 0 to L. The first part becomes:

$$\int_0^L \frac{\partial(\rho A_{cs})}{\partial t} dz = A_{cs} \int_0^L \frac{\partial \rho}{\partial t} dz \tag{A.90}$$

By applying the Leibniz rule, it becomes:

$$\int_0^L \frac{\partial(\rho A_{cs})}{\partial t} dz = A_c s \frac{d}{dt} \int_0^L \rho dz \tag{A.91}$$

By assuming void fraction, it becomes:

$$\int_0^L \frac{\partial(\rho A_{cs})}{\partial t} dz = A_{cs} \int_0^L \frac{d}{dt} \left(\rho_l (1-\gamma) + \rho_g \gamma\right) \tag{A.92}$$

By performing the integration, it becomes:

$$\int_0^L \frac{\partial(\rho A_{cs})}{\partial t} dz = V_{wf} \frac{d}{dt} \left(\rho_l (1-\overline{\gamma}) + \rho_g \overline{\gamma}\right) \tag{A.93}$$

By taking the time derivative, it becomes:

$$\int_0^L \frac{\partial(\rho A_{cs})}{\partial t} dz = V_{wf} \left(\frac{d\rho_l}{dt} (1-\overline{\gamma}) + \frac{d\rho_g}{dt} \overline{\gamma} + \left(\rho_g - \rho_l\right) \frac{d\overline{\gamma}}{dt} \right) \tag{A.94}$$

As saturated density is only dependent of pressure, it becomes:

$$\int_0^L \frac{\partial(\rho A_{cs})}{\partial t} dz = \left(\frac{\partial \rho_l}{\partial p} (1-\overline{\gamma}) + \frac{\partial \rho_g}{\partial p} \overline{\gamma} \right) V_{wf} \frac{dp}{dt} + \left(\rho_g - \rho_l\right) V_{wf} \frac{d\overline{\gamma}}{dt} \tag{A.95}$$

By integrating the second part of Equation (A.1) over the length of the heat exchanger, it becomes:

$$\int_0^L \frac{\partial \dot{m}}{\partial z} dz = \dot{m}_o - \dot{m}_i \tag{A.96}$$

By combining Equations (A.95) and (A.96), it becomes:

$$\left(\frac{\partial \rho_l}{\partial p} (1-\overline{\gamma}) + \frac{\partial \rho_g}{\partial p} \overline{\gamma} \right) V_{wf} \frac{dp}{dt} + \left(\rho_g - \rho_l\right) V_{wf} \frac{d\overline{\gamma}}{dt} + \dot{m}_o - \dot{m}_i = 0 \tag{A.97}$$

A.2.2. Energy conservation

The PDE is given in Equation (A.2). By multiplying the equation by the cross-sectional area, it becomes:

$$\frac{\partial(\rho h A_{cs} - A_{cs} p)}{\partial t} + \frac{\partial(\dot{m} h)}{\partial z} = \alpha_{wf} \pi D \left(T_w - T_{wf}\right) \tag{A.98}$$

By integrating the first part over the length of the heat exchanger, it becomes:

$$\int_0^L \frac{\partial(\rho h A_{cs})}{\partial t} dz = A_{cs} \int_0^L \frac{\partial(\rho h)}{\partial t} dz \tag{A.99}$$

By applying the Leibniz rule, it becomes:

$$\int_0^L \frac{\partial(\rho h A_{cs})}{\partial t} dz = A_{cs} \frac{d}{dt} \int_0^L \rho h dz \tag{A.100}$$

By assuming void fraction, it becomes:

$$\int_0^L \frac{\partial(\rho h A_{cs})}{\partial t} dz = A_{cs} \frac{d}{dt} \int_0^L \left(\rho_l h_l (1-\gamma) + \rho_g h_g \gamma\right) dz \tag{A.101}$$

By performing the integration, it becomes:

$$\int_0^L \frac{\partial(\rho h A_{cs})}{\partial t} dz = V_{wf} \frac{d}{dt} \left(\rho_l h_l (1-\overline{\gamma}) + \rho_g h_g \overline{\gamma}\right) \tag{A.102}$$

By taking the time derivative, it becomes:

$$\int_0^L \frac{\partial(\rho h A_{cs})}{\partial t} dz = V_{wf} \left(\frac{d(\rho_l h_l)}{dt} (1-\overline{\gamma}) + \frac{d(\rho_g h_g)}{dt} \overline{\gamma} + \left(\rho_g h_g - \rho_l h_l\right) \frac{d\overline{\gamma}}{dt} \right) \tag{A.103}$$

As saturated enthalpy and density are only dependent on pressure, it becomes:

$$\int_0^L \frac{\partial(\rho h A_{cs})}{\partial t} dz = \left(\frac{\partial(\rho_l h_l)}{\partial p} (1-\overline{\gamma}) + \frac{\partial(\rho_g h_g)}{\partial p} \overline{\gamma} \right) V_{wf} \frac{dp}{dt} + \left(\rho_g h_g - \rho_l h_l\right) V_{wf} \frac{d\overline{\gamma}}{dt} \tag{A.104}$$

By integrating the second part of Equation (A.98) over the length of the heat exchanger, it becomes:

$$\int_0^L \frac{-\partial(A_{cs} p)}{\partial t} dz = -A_{cs} \int_0^L \frac{\partial p}{\partial t} dz \tag{A.105}$$

By applying the Leibniz rule, it becomes:

$$\int_0^L \frac{-\partial(A_{cs} p)}{\partial t} dz = -A_{cs} \frac{d}{dt} \int_0^L p dz \tag{A.106}$$

By performing the integration and taking the time derivative, it becomes:

$$\int_0^L \frac{-\partial(A_{cs} p)}{\partial t} = -V_{wf} \frac{dp}{dt} \tag{A.107}$$

By integrating the third part of Equation (A.98) over the length of the heat exchanger, it becomes:

$$\int_0^L \frac{\partial \dot{m} h}{\partial z} dz = \dot{m}_o h_o - \dot{m}_i h_i \tag{A.108}$$

By integrating the right hand side of Equation (A.98) over the length of the heat exchanger, it becomes:

$$\int_0^L \alpha_{wf} \pi D_{wf} \left(T_w - T_{wf}\right) dz = \alpha_{wf} A_{wf} \left(T_w - T_{wf}\right) \tag{A.109}$$

By combining Equations (A.104), (A.107), (A.108) and (A.109), it becomes:

$$\left(\frac{\partial(\rho_l h_l)}{\partial p} (1-\overline{\gamma}) + \frac{\partial(\rho_g h_g)}{\partial p} \overline{\gamma} - 1 \right) V_{wf} \frac{dp}{dt} + \left(\rho_g h_g - \rho_l h_l\right) V_{wf} \frac{d\overline{\gamma}}{dt} + \dot{m}_o h_o - \dot{m}_i h_i = \alpha_{wf} A_{wf} \left(T_w - T_{wf}\right) \tag{A.110}$$

A.2.3. Structure conservation

The PDE is given in Equation (A.3). By integrating this equation over the length of the heat exchanger, so from 0 to L, it becomes:

$$\left(c_p \rho V\right)_w \frac{\partial T_w}{\partial t} = \alpha_{wf} A_{wf} \left(T_{wf} - T_w\right) + \alpha_{sw} A_{sw} \left(T_{sw} - T_w\right) \tag{A.111}$$

A.2.4. Buffer Tank

By combining the buffer tank and the condenser, Equations (A.96) and (A.110) have to be rewritten and an energy conservation of the separator has to be given. The mass conservation of the separator is given by:

$$\frac{dm_{bt}}{dt} = \dot{m}_{in} - \dot{m}_{out} \tag{A.112}$$

As $\dot{m}_{in}$ of the buffer tank is $\dot{m}_{out}$ of the condenser, Equation (A.96) becomes:

$$\left(\frac{\partial \rho_l}{\partial p}(1-\overline{\gamma}) + \frac{\partial \rho_g}{\partial p}\overline{\gamma}\right) V_{wf} \frac{dp}{dt} + \left(\rho_g - \rho_l\right) V_{wf} \frac{d\overline{\gamma}}{dt} + \dot{m}_{bt,o} + \frac{dm_{bt}}{dt} - \dot{m}_i = 0 \tag{A.113}$$

Using Equation (A.112), Equation (A.110) becomes:

$$\left(\frac{\partial(\rho_l h_l)}{\partial p}(1-\overline{\gamma}) + \frac{\partial(\rho_g h_g)}{\partial p}\overline{\gamma} - 1\right) V_{wf} \frac{dp}{dt} + \left(\rho_g h_g - \rho_l h_l\right) V_{wf} \frac{d\overline{\gamma}}{dt} + \left(\dot{m}_{bt,o} + \frac{dm_{bt}}{dt}\right) h_l - \dot{m}_i h_i = \alpha_{wf} A_{wf} \left(T_w - T_{wf}\right) \tag{A.114}$$

The energy conservation of the buffer tank is:

$$\frac{d\left(m_{bt} u_{bt}\right)}{dt} = \dot{m}_{cond,out} h_{cond,out} - \dot{m}_{bt,o} h_l \tag{A.115}$$

The left hand side of Equation (A.115) becomes:

$$\frac{d\left(m_{bt} u_{bt}\right)}{dt} = \frac{d\left(m_g u_g + m_l u_l\right)}{dt} \tag{A.116}$$

As $m = \rho V$, it becomes:

$$\frac{d\left(m_{bt} u_{bt}\right)}{dt} = \frac{d\left(\rho_g V_g u_g + \rho_l V_l u_l\right)}{dt} \tag{A.117}$$

By taking the derivative, it becomes:

$$\frac{d\left(m_{bt} u_{bt}\right)}{dt} = \dot{\rho}_g V_g u_g + \rho_g \dot{V}_g u_g + \rho_g V_g \dot{u}_g + \dot{\rho}_l V_l u_l + \rho_l \dot{V}_l u_l + \rho_l V_l \dot{u}_l \tag{A.118}$$

To solve this, we first need to find $\dot{V}_g$. This can be done in the following steps:

$$\frac{dm_{bt}}{dt} = \dot{\rho}_g V_g + \rho_g \dot{V}_g + \dot{\rho}_l V_l + \rho_l \dot{V}_l \tag{A.119}$$

As the total volume of the separator cannot change, $\dot{V}_l + \dot{V}_g = 0$, or $\dot{V}_l = -\dot{V}_g$. Using this, it becomes:

$$\frac{dm_{bt}}{dt} = \left(\dot{\rho}_g V_g + \dot{\rho}_l V_l\right) + \left(\rho_g - \rho_l\right) \dot{V}_g \tag{A.120}$$

By rewriting Equation (A.113) and stating that saturated density is a function of pressure, it becomes:

$$\dot{V}_g = \frac{fracdm_{bt}dt - \left(\frac{\partial \rho_g}{\partial p} V_g + \frac{\partial \rho_l}{\partial p} V_l\right) \dot{p}}{\left(\rho_g - \rho_l\right)} \tag{A.121}$$

By implementing Equation (A.121), using $\dot{V}_g = \dot{V}_l$ and stating that saturated density is only dependent on pressure, Equation (A.118) becomes:

$$\frac{d\left(m_{bt} u_{bt}\right)}{dt} = \left(\frac{\partial \rho_g}{\partial p} V_g u_g + \rho_g V_g \frac{\partial u_g}{\partial p} + \frac{\partial \rho_l}{\partial p} V_l u_l + \rho_l V_l \frac{\partial u_l}{\partial p}\right) + \left(\rho_g u_g - \rho_l u_l\right) \left(\frac{\frac{dm_{bt}}{dt} - \left(\frac{\partial \rho_g}{\partial p} V_g + \frac{\partial \rho_l}{\partial p} V_l\right) \dot{p}}{\left(\rho_g - \rho_l\right)}\right) \tag{A.122}$$

The right hand side of Equation (A.115), using Equation (A.112), becomes:

$$\left(\frac{dm_{bt}}{dt} + m_{bt,o}\right) h_{cond,o} - m_{bt,o} h_l \tag{A.123}$$

Combining Equations (A.122) and (A.123), it becomes:

$$\begin{aligned} \frac{d\left(m_{bt} u_{bt}\right)}{dt} &= \left(\frac{\partial \rho_g}{\partial p} V_g u_g + \rho_g V_g \frac{\partial u_g}{\partial p} + \frac{\partial \rho_l}{\partial p} V_l u_l + \rho_l V_l \frac{\partial u_l}{\partial p}\right) \\ &+ \left(\rho_g u_g - \rho_l u_l\right) \left(\frac{\frac{dm_{bt}}{dt} - \left(\frac{\partial \rho_g}{\partial p} V_g + \frac{\partial \rho_l}{\partial p} V_l\right) \dot{p}}{\left(\rho_g - \rho_l\right)}\right) = \frac{dm_{bt}}{dt} h_{cond,o} + \dot{m}_{bt,o} \left(h_{cond,o} - h_l\right) \end{aligned} \tag{A.124}$$

A.3. Seawater temperatures

The energy balance for a counter-current heat exchanger with an arbitrary length dz is given by Equation (A.125).

$$\dot{m}_{sw} c_{p,sw} \left(T_{sw,z} - T_{sw,z+dz}\right) = \alpha_{sw} A_{sw} \frac{dz}{L} \left(T_{sw,z} - T_w\right) \tag{A.125}$$

By rewriting this equation, it becomes:

$$\frac{-dT}{T_{sw,z} - T_w} = \frac{\alpha_{sw} A_{sw}}{m_{sw} c_{p,sw} L} \tag{A.126}$$

By integrating this equation, it becomes:

$$\int_{T_{sw,z}}^{T_{sw,z+dz}} \frac{-dT}{T_{sw,z} - T_w} = \int_{z}^{z+dz} \frac{\alpha_{sw} A_{sw}}{m_{sw} c_{p,sw} L} \tag{A.127}$$

By performing this integration, it becomes:

$$T_{sw,z+dz} = T_w + \left(T_{sw,z} - T_w\right) e^{\frac{\alpha_{sw} A_{sw} dz}{m_{sw} c_{p,sw} L}} \tag{A.128}$$

For the two-phase region of the evaporator, the outlet temperature becomes:

$$T_{sw,12} = T_{w,2} + \left(T_{sw,in} - T_{w,2}\right) e^{\frac{-\alpha_{sw} A_{sw} L_2}{m_{sw} c_{p,sw} L}} \tag{A.129}$$

For the sub-cooled region of the evaporator, the outlet temperature becomes:

$$T_{sw,out} = T_{w,1} + \left(T_{sw,12} - T_{w,1}\right) e^{\frac{-\alpha_{sw} A_{sw} L_1}{m_{sw} c_{p,sw} L}} \tag{A.130}$$

For the condenser, the outlet temperature becomes:

$$T_{sw,out} = T_w + \left(T_{sw,in} - T_w\right) e^{\frac{-\alpha_{sw} A_{sw}}{m_{sw} c_{p,sw}}} \tag{A.131}$$

To find the average temperature for each region, Equation (A.128) is integrated and it becomes:

$$\overline{T}_{sw} = \frac{\int_0^L \left(T_w + \left(T_{sw,z} - T_w\right) e^{\frac{-\alpha_{sw} A_{sw} dz}{m_{sw} c_{p,sw} L}}\right) dz}{\int_0^L dz} \tag{A.132}$$

For the sub-cooled region of the evaporator, this becomes:

$$\overline{T}_{sw,1} = T_{w,1} + \left(T_{sw,12} - T_{w,1}\right) \left(\frac{m_{sw} c_{p,sw} L}{\alpha_{sw} A_{sw} L_1}\right) \left(1 - e^{\frac{-\alpha_{sw} A_{sw} L_1}{m_{sw} c_{p,sw} L}}\right) \tag{A.133}$$

For the two-phase region of the evaporator, it becomes:

$$\overline{T}_{sw,2} = T_{w,2} + \left(T_{sw,in} - T_{w,2}\right) \left(\frac{m_{sw} c_{p,sw} L}{\alpha_{sw} A_{sw} L_2}\right) \left(1 - e^{\frac{-\alpha_{sw} A_{sw} L_2}{m_{sw} c_{p,sw} L}}\right) \tag{A.134}$$

For the condenser, it becomes:

$$\overline{T}_{sw} = T_w + \left(T_{sw,in} - T_w\right) \left(\frac{m_{sw} c_{p,sw}}{\alpha_{sw} A_{sw}}\right) \left(1 - e^{\frac{-\alpha_{sw} A_{sw}}{m_{sw} c_{p,sw}}}\right) \tag{A.135}$$

A.4. Condenser (OTEC demo)

As the OTEC demo has an extra state, the superheated state, a new set of equations is used.

A.4.1. Mass conservation superheated region

The PDE is given in Equation (A.1). Multiplying this equation by the cross-sectional area, the equation becomes Equation (A.136).

$$\frac{\partial(\rho A_{cs})}{\partial t} + \frac{\partial \dot{m}}{\partial z} \tag{A.136}$$

This equation is then integrated over the length of the superheated region, so from z = 0 to z = L_1. By integrating the first part and assuming a constant cross-sectional area, it becomes:

$$\int_0^{L_1} \frac{\partial(\rho A_{cs})}{\partial t} dz = A_{cs} \int_0^{L_1} \left(\frac{\partial \rho}{\partial t} dz \right) \tag{A.137}$$

By applying the Leibniz rule, it becomes:

$$\int_0^{L_1} \frac{\partial(\rho A_{cs})}{\partial t} dz = A_{cs} \left(\frac{d}{dt} \int_0^{L_1} \rho dz - \rho_l \frac{dL_1}{dt} \right) \tag{A.138}$$

By assuming an average density in the superheated region and performing the integration, it becomes:

$$\int_0^{L_1} \frac{\partial(\rho A_{cs})}{\partial t} dz = A_{cs} \left(\frac{d}{dt}(\rho_1 L_1) - \rho_g \frac{dL_1}{dt} \right) \tag{A.139}$$

By taking the time derivative, it becomes:

$$\int_0^{L_1} \frac{\partial(\rho A_{cs})}{\partial t} dz = A_{cs} \left(\rho_1 \frac{dL_1}{dt} + L_1 \frac{d\rho_1}{dt} - \rho_g \frac{dL_1}{dt} \right) \tag{A.140}$$

By choosing pressure and enthalpy as state variables, it becomes:

$$\int_0^{L_1} \frac{\partial(\rho A_{cs})}{\partial t} dz = A_{cs} \left[\left(\left. \frac{\partial \rho_1}{\partial p} \right|_{h_1} \frac{dp}{dt} + \left. \frac{\partial \rho_1}{\partial h_1} \right|_{p} \frac{dh_1}{dt} \right) L_1 + (\rho_1 - \rho_g) \frac{dL_1}{dt} \right] \tag{A.141}$$

By stating that $h_1 = \frac{h_{in}+h_g}{2}$, $\frac{dh_1}{dt} = \frac{1}{2}\left(\frac{dh_{in}}{dt} + \frac{dh_g}{dt}\right)$, it becomes:

$$\int_0^{L_1} \frac{\partial(\rho A_{cs})}{\partial t} dz = \left(\left. \frac{\partial \rho_1}{\partial p} \right|_{h_1} \frac{dp}{dt} + \left. \frac{\partial \rho_1}{\partial h_1} \right|_{p} \frac{1}{2} \left(\frac{dh_g}{dt} + \frac{dh_{in}}{dt} \right) \right) L_1 A_{cs} + (\rho_1 - \rho_g) \frac{dL_1}{dt} A_{cs} \tag{A.142}$$

Because saturated enthalpy is only dependent on pressure, it becomes:

$$\int_0^{L_1} \frac{\partial(\rho A_{cs})}{\partial t} dz = \left(\left(\left. \frac{\partial \rho_1}{\partial p} \right|_{h_1} + \frac{1}{2} \left. \frac{\partial \rho_1}{\partial h_1} \right|_{p} \frac{\partial h_g}{\partial p} \right) \frac{dp}{dt} + \frac{1}{2} \left. \frac{\partial \rho_1}{\partial h_1} \right|_{p} \frac{dh_{in}}{dt} \right) L_1 A_{cs} + (\rho_1 - \rho_g) \frac{dL_1}{dt} A_{cs} \tag{A.143}$$

By integrating the second term over the length of the superheated region, it becomes:

$$\int_0^{L_1} \frac{\partial \dot{m}}{\partial z} dz = \dot{m}_{12} - \dot{m}_{in} \tag{A.144}$$

By combining Equations (A.143) and (A.144), it becomes:

$$\left(\left(\left. \frac{\partial \rho_1}{\partial p} \right|_{h_1} + \frac{1}{2} \left. \frac{\partial \rho_1}{\partial h_1} \right|_{p} \frac{\partial h_g}{\partial p} \right) \frac{dp}{dt} + \frac{1}{2} \left. \frac{\partial \rho_1}{\partial h_1} \right|_{p} \frac{dh_{in}}{dt} \right) L_1 A_{cs} + (\rho_1 - \rho_g) \frac{dL_1}{dt} A_{cs} + \dot{m}_{12} - \dot{m}_{in} = 0 \tag{A.145}$$

A.4.2. Mass conservation two-phase region

The PDE is given in Equation (A.1). Multiplying this equation by the cross-sectional area, the equation becomes Equation (A.136). By integrating the first part over the length of the two-phase region, from z = L_1 to z = L and assuming constant cross-sectional area, this becomes:

$$\int_{L_1}^{L} \frac{\partial(\rho A_{cs})}{\partial t} dz = A_{cs} \int_{L_1}^{L} \frac{\partial \rho}{\partial t} \tag{A.146}$$

By applying the Leibniz rule, it becomes:

$$\int_{L_1}^{L} \frac{\partial(\rho A_{cs})}{\partial t} dz = A_{cs} \left(\frac{d}{dt} \int_{L_1}^{L} \rho dz + \rho_g \frac{dL_1}{dt} \right) \tag{A.147}$$

By applying void fraction, it becomes:

$$\int_{L_1}^{L} \frac{\partial(\rho A_{cs})}{\partial t} dz = A_{cs} \left(\frac{d}{dt} \int_{L_1}^{L} \left(\rho_l (1-\gamma) + \rho_g \gamma \right) dz + \rho_g \frac{dL_1}{dt} \right) \tag{A.148}$$

By doing the integration and by L = L_1 + L_2, it becomes:

$$\int_{L_1}^{L} \frac{\partial(\rho A_{cs})}{\partial t} dz = A_{cs} \left(\frac{d}{dt} \left(\rho_l (1-\overline{\gamma}) + \rho_g \overline{\gamma} \right) L_2 + \rho_g \frac{dL_1}{dt} \right) \tag{A.149}$$

Taking the time derivative, it becomes:

$$\int_{L_1}^{L} \frac{\partial(\rho A_{cs})}{\partial t} dz = A_{cs} \left(\left(\frac{d\rho_l}{dt} (1-\overline{\gamma}) + \frac{d\rho_g}{dt} \overline{\gamma} \right) L_2 + \left(\rho_l (1-\overline{\gamma}) + \rho_g \overline{\gamma} \right) \frac{dL_2}{dt} + \left(\rho_g - \rho_l \right) L_2 \frac{d\overline{\gamma}}{dt} + \rho_g \frac{dL_1}{dt} \right) \tag{A.150}$$

Because saturated densities are only dependent on pressure, it becomes:

$$\int_{L_1}^{L} \frac{\partial(\rho A_{cs})}{\partial t} dz = A_{cs} \left(\left(\frac{\partial \rho_l}{\partial p} (1-\overline{\gamma}) + \frac{\partial \rho_g}{\partial p} \overline{\gamma} \right) L_2 \frac{dp}{dt} + \left(\rho_l (1-\overline{\gamma}) + \rho_g \overline{\gamma} \right) \frac{dL_2}{dt} + \left(\rho_g - \rho_l \right) L_2 \frac{d\overline{\gamma}}{dt} + \rho_g \frac{dL_1}{dt} \right) \tag{A.151}$$

By $\frac{dL_2}{dt} = -\frac{dL_1}{dt}$ and rewriting Equation (A.151), it becomes:

$$\int_{L_1}^{L} \frac{\partial(\rho A_{cs})}{\partial t} dz = A_{cs} \left(\left(\frac{\partial \rho_l}{\partial p} (1-\overline{\gamma}) + \frac{\partial \rho_g}{\partial p} \overline{\gamma} \right) L_2 \frac{dp}{dt} + \left(\rho_g - \rho_l \right) L_2 \frac{d\overline{\gamma}}{dt} + \left(\rho_g - \rho_l + \left(\rho_l - \rho_g \right) \overline{\gamma} \right) \frac{dL_1}{dt} \right) \tag{A.152}$$

By integrating the second term of Equation (A.136), it becomes:

$$\int_{L_1}^{L} \frac{\partial \dot{m}}{\partial z} dz = \dot{m}_o - \dot{m}_{12} \tag{A.153}$$

By combining Equations (A.152) and (A.153), it becomes:

$$\left(\frac{\partial \rho_l}{\partial p} (1-\overline{\gamma}) + \frac{\partial \rho_g}{\partial p} \overline{\gamma} \right) A_{cs} L_2 \frac{dp}{dt} + \left(\rho_g - \rho_l \right) A_{cs} L_2 \frac{d\overline{\gamma}}{dt} + \left(\rho_g - \rho_l + \left(\rho_l - \rho_g \right) \overline{\gamma} \right) A_{cs} \frac{dL_1}{dt} + \dot{m}_o - \dot{m}_{12} = 0 \tag{A.154}$$

A.4.3. Energy conservation of superheated region

The PDE is given in Equation (A.2). Multiplying this equation by the cross-sectional area, the equation becomes:

$$\frac{\partial(\rho h A_{cs} - A_{cs} p)}{\partial t} + \frac{\partial(\dot{m} h)}{\partial z} = \alpha_{wf} \pi D \left(T_w - T_{wf} \right) \tag{A.155}$$

By integrating the first term over the length of the superheated region, from z = 0 to z = L_1, it becomes:

$$\int_0^{L_1} \frac{\partial(\rho h A_{cs})}{\partial t} dz = A_{cs} \int_0^{L_1} \frac{\partial(\rho h)}{\partial t} dz \tag{A.156}$$

By applying the Leibniz rule, it becomes:

$$\int_0^{L_1} \frac{\partial(\rho h A_{cs})}{\partial t} dz = A_{cs} \left(\frac{d}{dt} \int_0^{L_1} \rho h \, dz - \rho_g h_g \frac{dL_1}{dt} \right) \tag{A.157}$$

By assuming an average density and enthalpy and doing the integration, it becomes:

$$\int_0^{L_1} \frac{\partial(\rho h A_{cs})}{\partial t} dz = A_{cs} \left(\frac{d}{dt} \left(\rho_1 h_1 L_1 \right) dz - \rho_g h_g \frac{dL_1}{dt} \right) \tag{A.158}$$

By taking the time derivative, it becomes:

$$\int_0^{L_1} \frac{\partial(\rho h A_{cs})}{\partial t} dz = A_{cs} \left(h_1 L_1 \frac{d\rho_1}{dt} + \rho_1 L_1 \frac{dh_1}{dt} + \rho_1 h_1 \frac{dL_1}{dt} - \rho_g h_g \frac{dL_1}{dt} \right) \tag{A.159}$$

By choosing pressure and enthalpy as state variables, it becomes:

$$\int_0^{L_1} \frac{\partial(\rho h A_{cs})}{\partial t} dz = A_{cs} \left(\left(\left. \frac{\partial \rho_1}{\partial h_1} \right|_p \frac{dh_1}{dt} + \left. \frac{\partial \rho_1}{\partial p} \right|_{h_1} \frac{dp}{dt} \right) h_1 L_1 + \rho_1 L_1 \frac{dh_1}{dt} + \rho_1 h_1 \frac{dL_1}{dt} - \rho_g h_g \frac{dL_1}{dt} \right) \tag{A.160}$$

By rewriting Equation (A.160), it becomes:

$$\int_0^{L_1} \frac{\partial(\rho h A_{cs})}{\partial t} dz = \left(\left. \frac{\partial \rho_1}{\partial h_1} \right|_p h_1 + \rho_1 \right) L_1 A_{cs} \frac{dh_1}{dt} + \left. \frac{\partial \rho_1}{\partial p} \right|_{h_1} h_1 L_1 A_{cs} \frac{dp}{dt} + (\rho_1 h_1 - \rho_g h_g) A_{cs} \frac{dL_1}{dt} \tag{A.161}$$

By stating that $h_1 = \frac{h_{in} + h_g}{2}$, $\frac{dh_1}{dt} = \frac{1}{2} \left(\frac{dh_{in}}{dt} + \frac{dh_g}{dt} \right)$, it becomes:

$$\int_0^{L_1} \frac{\partial(\rho h A_{cs})}{\partial t} dz = \left(\left. \frac{\partial \rho_1}{\partial h_1} \right|_p h_1 + \rho_1 \right) L_1 A_{cs} \frac{1}{2} \left(\frac{dh_{in}}{dt} + \frac{dh_g}{dt} \right) + \left. \frac{\partial \rho_1}{\partial p} \right|_{h_1} h_1 L_1 A_{cs} \frac{dp}{dt} + (\rho_1 h_1 - \rho_g h_g) A_{cs} \frac{dL_1}{dt} \tag{A.162}$$

As saturated enthalpy is only dependent on pressure, it becomes:

$$\int_0^{L_1} \frac{\partial(\rho h A_{cs})}{\partial t} dz = \left(\left. \frac{\partial \rho_1}{\partial h_1} \right|_p h_1 + \rho_1 \right) L_1 A_{cs} \frac{1}{2} \left(\frac{dh_{in}}{dt} + \frac{\partial h_g}{\partial p} \frac{dp}{dt} \right) + \left. \frac{\partial \rho_1}{\partial p} \right|_{h_1} h_1 L_1 A_{cs} \frac{dp}{dt} + (\rho_1 h_1 - \rho_g h_g) A_{cs} \frac{dL_1}{dt} \tag{A.163}$$

By rewriting this equation, it becomes:

$$\begin{aligned} \int_0^{L_1} \frac{\partial(\rho h A_{cs})}{\partial t} dz = & \left(\left. \frac{\partial \rho_1}{\partial h_1} \right|_p h_1 + \rho_1 \right) L_1 A_{cs} \frac{1}{2} \frac{dh_{in}}{dt} + (\rho_1 h_1 - \rho_g h_g) A_{cs} \frac{dL_1}{dt} \\ & + \left(\frac{1}{2} \left(\left. \frac{\partial \rho_1}{\partial h_1} \right|_p \frac{\partial h_g}{\partial p} h_1 + \rho_1 \frac{\partial h_g}{\partial p} \right) + \left. \frac{\partial \rho_1}{\partial p} \right|_{h_1} h_1 \right) L_1 A_{cs} \frac{dp}{dt} \end{aligned} \tag{A.164}$$

By integrating the second term of Equation (A.155) from z = 0 to z = L_1, it becomes:

$$\int_0^{L_1} -\frac{\partial(A_{cs} p)}{\partial t} dz = -A_{cs} \int_0^{L_1} \frac{\partial p}{\partial t} dz \tag{A.165}$$

By applying the Leibniz rule, it becomes:

$$\int_0^{L_1} -\frac{\partial(A_{cs}p)}{\partial t}dz = -A_{cs}\left(\frac{d}{dt}\int_0^{L_1} p\,dz - p\frac{dL_1}{dt}\right) \tag{A.166}$$

By performing the integration, it becomes:

$$\int_0^{L_1} -\frac{\partial(A_{cs}p)}{\partial t}dz = -A_{cs}\left(\frac{d}{dt}pL_1 - p\frac{dL_1}{dt}\right) \tag{A.167}$$

By taking the time derivative, it becomes:

$$\int_0^{L_1} -\frac{\partial(A_{cs})p}{\partial t}dz = -A_{cs}\left(\frac{dp}{dt}L_1 + \frac{dL_1}{dt}p - p\frac{dL_1}{dt}\right) = -A_{cs}\frac{dp}{dt}L_1 \tag{A.168}$$

By integrating the third term of the PDE from z = 0 to z = L_1, it becomes:

$$\int_0^{L_1} \frac{\partial \dot{m}h}{\partial z}dz = \dot{m}_{12}h_g - \dot{m}_{in}h_{in} \tag{A.169}$$

By integrating the right hand side of Equation (A.155), it becomes:

$$\int_0^{L_1} \alpha_{wf}\pi D_{wf}\left(T_w - T_{wf}\right)dz = \alpha_{1wf}\pi D_{wf}L_1\left(T_{1w} - T_{1wf}\right) \tag{A.170}$$

By multiplying the equation with $\frac{L}{L}$, it becomes:

$$\int_0^{L_1} \alpha_{wf}\pi D_{wf}\left(T_w - T_{wf}\right)dz = \alpha_{1wf}A_{wf}\frac{L_1}{L}\left(T_{1w} - T_{1wf}\right) \tag{A.171}$$

Combining Equations (A.164), (A.168), (A.169) and (A.171), it becomes:

$$\begin{aligned}&\left(\left.\frac{\partial\rho_1}{\partial h_1}\right|_p h_1 + \rho_1\right)L_1A_{cs}\frac{1}{2}\frac{dh_{in}}{dt} + (\rho_1h_1 - \rho_gh_g)A_{cs}\frac{dL_1}{dt} + \left(\frac{1}{2}\left(\left.\frac{\partial\rho_1}{\partial h_1}\right|_p\frac{\partial h_g}{\partial p}h_1 + \rho_1\frac{\partial h_g}{\partial p}\right) + \left.\frac{\partial\rho_1}{\partial p}\right|_{h_1}h_1\right)L_1A_{cs}\frac{dp}{dt}\\ &- A_{cs}\frac{dp}{dt}L_1 + \dot{m}_{12}h_g - \dot{m}_{in}h_{in} = \alpha_{1wf}A_{wf}\frac{L_1}{L}\left(T_{1w} - T_{1wf}\right)\end{aligned} \tag{A.172}$$

By rewriting this equation, it becomes:

$$\begin{aligned}&\left(\left.\frac{\partial\rho_1}{\partial h_1}\right|_p h_1 + \rho_1\right)L_1A_{cs}\frac{1}{2}\frac{dh_{in}}{dt} + \left(\frac{1}{2}\left(\left.\frac{\partial\rho_1}{\partial h_1}\right|_p\frac{\partial h_g}{\partial p}h_1 + \rho_1\frac{\partial h_g}{\partial p}\right) + \left.\frac{\partial\rho_1}{\partial p}\right|_{h_1}h_1 - 1\right)L_1A_{cs}\frac{dp}{dt}\\ &+ (\rho_1h_1 - \rho_gh_g)A_{cs}\frac{dL_1}{dt} + \dot{m}_{12}h_g - \dot{m}_{in}h_{in} = \alpha_{1wf}A_{wf}\frac{L_1}{L}\left(T_{1w} - T_{1wf}\right)\end{aligned} \tag{A.173}$$

A.4.4. Energy conservation in the two-phase region

By integrating the first part of Equation (A.155) over the length of the two-phase region, it becomes:

$$\int_{L_1}^{L} \frac{\partial\rho hA_{cs}}{\partial t}dz = A_{cs}\int_{L_1}^{L}\frac{\partial\rho h}{\partial t} \tag{A.174}$$

By applying the Leibniz rule, it becomes:

$$\int_{L_1}^{L} \frac{\partial\rho hA_{cs}}{\partial t}dz = A_{cs}\left(\frac{d}{dt}\int_{L_1}^{L}\rho h dz + \rho_gh_g\frac{dL_1}{dt}\right) \tag{A.175}$$

By assuming void fraction, it becomes:

$$\int_{L_1}^{L} \frac{\partial \rho h A_{cs}}{\partial t} dz = A_{cs} \left(\frac{d}{dt} \int_{L_1}^{L} \left(\rho_l h_l (1-\gamma) + \rho_g h_h \gamma \right) dz + \rho_g h_g \frac{dL_1}{dt} \right) \tag{A.176}$$

By performing the integration, it becomes:

$$\int_{L_1}^{L} \frac{\partial \rho A_{cs}}{\partial t} dz = A_{cs} \left(\frac{d}{dt} \left(\rho_l h_l (1-\overline{\gamma}) + \rho_g h_g \overline{\gamma} \right) L_2 + \rho_g h_g \frac{dL_1}{dt} \right) \tag{A.177}$$

By taking the time derivative, it becomes:

$$\begin{aligned} \int_{L_1}^{L} \frac{\partial \rho h A_{cs}}{\partial t} dz = A_{cs} \Bigg[& \left(\frac{d\left(\rho_l h_l\right)}{dt} (1-\overline{\gamma}) + \frac{d\left(\rho_g h_g\right)}{dt} \overline{\gamma} \right) L_2 \\ & + \left(\rho_l h_l (1-\overline{\gamma}) + \rho_g h_g \overline{\gamma} \right) \frac{dL_2}{dt} + \left(\rho_g h_g - \rho_l h_l \right) L_2 \frac{d\overline{\gamma}}{dt} + \rho_g h_g \frac{dL_1}{dt} \Bigg] \end{aligned} \tag{A.178}$$

As saturated properties are only dependent on pressure, it becomes:

$$\begin{aligned} \int_{L_1}^{L} \frac{\partial \rho h A_{cs}}{\partial t} dz = A_{cs} \Bigg[& \left(\frac{\partial\left(\rho_l h_l\right)}{\partial p} (1-\overline{\gamma}) + \frac{\partial\left(\rho_g h_g\right)}{\partial p} \overline{\gamma} \right) L_2 \frac{dp}{dt} \\ & + \left(\rho_l h_l (1-\overline{\gamma}) + \rho_g h_g \overline{\gamma} \right) \frac{dL_2}{dt} + \left(\rho_g h_g - \rho_l h_l \right) L_2 \frac{d\overline{\gamma}}{dt} + \rho_g h_g \frac{dL_1}{dt} \Bigg] \end{aligned} \tag{A.179}$$

As $\frac{dL_2}{dt} = -\frac{dL_1}{dt}$, it becomes, after rewriting:

$$\begin{aligned} \int_{L_1}^{L} \frac{\partial \rho h A_{cs}}{\partial t} dz = & \left(\frac{\partial\left(\rho_l h_l\right)}{\partial p} (1-\overline{\gamma}) + \frac{\partial\left(\rho_g h_g\right)}{\partial p} \overline{\gamma} \right) A_{cs} L_2 \frac{dp}{dt} \\ & + \left(\rho_g h_g - \rho_l h_l + \left(\rho_l h_l - \rho_g h_g \right) \overline{\gamma} \right) A_{cs} \frac{dL_1}{dt} + \left(\rho_g h_g - \rho_l h_l \right) A_{cs} L_2 \frac{d\overline{\gamma}}{dt} \end{aligned} \tag{A.180}$$

By integrating the second term of Equation (A.155) over the length of the two-phase region, it becomes:

$$\int_{L_1}^{L} -\frac{\partial p A_{cs}}{\partial t} dz = -A_{cs} \int_{L_1}^{L} \frac{\partial p}{\partial t} dz \tag{A.181}$$

By applying the Leibniz rule, it becomes:

$$\int_{L_1}^{L} -\frac{\partial p A_{cs}}{\partial t} dz = -A_{cs} \left(\frac{d}{dt} \int_{L_1}^{L} p + p \frac{dL_1}{dt} \right) \tag{A.182}$$

By performing the integration, it becomes:

$$\int_{L_1}^{L} -\frac{\partial p A_{cs}}{\partial t} dz = -A_{cs} \left(\frac{d}{dt} \left(p L_2 \right) + p \frac{dL_1}{dt} \right) \tag{A.183}$$

By taking the time derivative, it becomes:

$$\int_{L_1}^{L} -\frac{\partial p A_{cs}}{\partial t} dz = -A_{cs} \left(L_2 \frac{dp}{dt} + p \frac{dL_2}{dt} + p \frac{dL_1}{dt} \right) \tag{A.184}$$

With $\frac{dL_2}{dt} = -\frac{dL_1}{dt}$, it becomes:

$$\int_{L_1}^{L} -\frac{\partial p A_{cs}}{\partial t} dz = -A_{cs} L_2 \frac{dp}{dt} \tag{A.185}$$

By integrating the third term of Equation (A.155) over the length of the two-phase region, it becomes:

$$\int_{L_1}^{L} \frac{\partial \dot{m} h}{\partial z} = \dot{m}_o h_o - \dot{m}_{12} h_g \tag{A.186}$$

By integrating the right hand side of Equation (A.155) over the length of the sub-cooled region, it becomes:

$$\int_{L_1}^{L} \alpha_{wf} \pi D_{wf} \left(T_w - T_{wf}\right) = \alpha_{2wf} \pi D L_2 \left(T_{2w} - T_{2wf}\right) \tag{A.187}$$

By multiplying this equation by $\frac{L}{L}$, it becomes:

$$\int_{L_1}^{L} \alpha_{wf} \pi D_{wf} \left(T_w - T_{wf}\right) = \alpha_{2wf} A_{wf} \frac{L_2}{L} \left(T_{2w} - T_{2wf}\right) \tag{A.188}$$

By combining Equations (A.180), (A.185), (A.186) and (A.188), it becomes:

$$\begin{aligned} &\left(\frac{\partial \left(\rho_l h_l\right)}{\partial p}(1-\overline{\gamma}) + \frac{\partial \left(\rho_g h_g\right)}{\partial p}\overline{\gamma} - 1\right) A_{cs} L_2 \frac{dp}{dt} + \left(\rho_g h_g - \rho_l h_l + \left(\rho_l h_l - \rho_g h_g\right)\overline{\gamma}\right) A_{cs} \frac{dL_1}{dt} + \left(\rho_g h_g - \rho_l h_l\right) A_{cs} L_2 \frac{d\overline{\gamma}}{dt} \\ &+ \dot{m}_o h_o - \dot{m}_{12} h_g = \alpha_{2wf} A_{wf} \frac{L_2}{L} \left(T_{2w} - T_{2wf}\right) \end{aligned} \tag{A.189}$$

A.4.5. Structure conservation in the sub-cooled region

The PDE is given in Equation (A.3). By multiplying this equation by the length of the heat exchanger, it becomes:

$$\left(c_p \rho V\right)_w \frac{\partial T_w}{\partial t} = \alpha_{wf} A_{wf} \left(T_{wf} - T_w\right) + \alpha_{sw} A_{sw} \left(T_{sw} - T_w\right) \tag{A.190}$$

By integrating the left part over arbitrary length from a to b and applying the Leibniz rule, this becomes:

$$\int_a^b \left(c_p \rho V\right)_w \frac{\partial T_w}{\partial t} dz = \left(c_p \rho V\right)_w \frac{d}{dt} \int_a^b T_w dz + T_w(a) \frac{da}{dt} - T_w(b) \frac{db}{dt} \tag{A.191}$$

By performing the integration, it becomes:

$$\int_a^b \left(c_p \rho V\right)_w \frac{\partial T_w}{\partial t} dz = \left(c_p \rho V\right)_w \left(\frac{d}{dt}(b-a) T_{w(a-b)} + T_w(a) \frac{da}{dt} - T_w(b) \frac{db}{dt}\right) \tag{A.192}$$

By taking the time derivative, it becomes:

$$\int_a^b \left(c_p \rho V\right)_w \frac{\partial T_w}{\partial t} dz = \left(c_p \rho V\right)_w \left(\frac{d(b-a)}{dt} T_{w(a-b)} + (b-a) \frac{dT_{w(a-b)}}{dt} + T_w(a) \frac{da}{dt} - T_w(b) \frac{db}{dt}\right) \tag{A.193}$$

For the superheated region, a = 0 and b = L_1. With this, it becomes:

$$\int_0^{L_1} \left(c_p \rho V\right)_w \frac{\partial T_w}{\partial t} dz = \left(c_p \rho V\right)_w \left(\frac{dL_1}{dt} T_{1w} + L_1 \frac{dT_{1w}}{dt} - T_{w(L_1)} \frac{dL_1}{dt}\right) \tag{A.194}$$

In literature, different values for $T_{w(L_1)}$ are taken. As it is assumed a lumped temperature, it is a discontinuous function at the boundary. In reality, the temperature at the wall will be closer to the two-phase region than to the single-phase region, as stated by Willatzen, He and Weerstra [65][22][62]. Therefore, $T_{w(L_1)} = T_{2w}$. With this, it becomes:

$$\int_0^{L_1} \left(c_p \rho V\right)_w \frac{\partial T_w}{\partial t} dz = \left(c_p \rho V\right)_w \left(L_1 \frac{dT_{1w}}{dt} + \left(T_{1w} - T_{2w}\right) \frac{dL_1}{dt}\right) \tag{A.195}$$

Integrating the right hand side of Equation (A.190), it becomes:

$$\int_0^{L_1} \left(\alpha_{wf} A_{wf} \left(T_{wf} - T_w\right) + \alpha_{sw} A_{sw} \left(T_{sw} - T_w\right)\right) dz = \alpha_{wf} A_{wf} L_1 \left(T_{wf} - T_w\right) + \alpha_{sw} A_{sw} L_1 \left(T_{sw} - T_w\right) \tag{A.196}$$

Combining Equations (A.195) and (A.196) and dividing left and right by L_1, it becomes:

$$\left(c_p \rho V\right)_w \left(\frac{dT_{1w}}{dt} + \frac{T_{1w} - T_{2w}}{L_1} \frac{dL_1}{dt}\right) = \alpha_{wf} A_{wf} \left(T_{wf} - T_w\right) + \alpha_{sw} A_{sw} \left(T_{sw} - T_w\right) \tag{A.197}$$

A.4.6. Structure conservation in the two-phase region

By using Equation (A.193) for the two-phase region, a = L_1 and b = L_2, L = L_1 + L_2 and $T_{w(L_1)} = T_{2w}$, it becomes:

$$\int_{L_1}^{L} \left(c_p \rho V\right)_w \frac{\partial T_w}{\partial t} dz = \left(c_p \rho V\right)_w \left(T_{2w} \frac{dL_2}{dt} + L_2 \frac{dT_{2w}}{dt} + T_{2w} \frac{dL_1}{dt}\right) \tag{A.198}$$

As $\frac{dL_1}{dt} = -\frac{dL_2}{dt}$, it becomes:

$$\int_{L_1}^{L} \left(c_p \rho V\right)_w \frac{\partial T_w}{\partial t} dz = \left(c_p \rho V\right)_w \left(L_2 \frac{dT_{2w}}{dt}\right) \tag{A.199}$$

By integrating the right hand side of equation (A.190) from L_1 to L, it becomes:

$$\int_{L_1}^{L} \left(\alpha_{wf} A_{wf} \left(T_{wf} - T_w\right) + \alpha_{sw} A_{sw} \left(T_{sw} - T_w\right)\right) dz = \alpha_{wf} A_{wf} L_2 \left(T_{wf} - T_w\right) + \alpha_{sw} A_{sw} L_2 \left(T_{sw} - T_w\right) \tag{A.200}$$

By combining Equations (A.199) and (A.200) and dividing it by L_2, it becomes:

$$\left(c_p \rho V\right)_w \left(\frac{dT_{2w}}{dt}\right) = \alpha_{wf} A_{wf} \left(T_{wf} - T_w\right) + \alpha_{sw} A_{sw} \left(T_{sw} - T_w\right) \tag{A.201}$$

A.4.7. Governing time derivatives

The six equations have five explicit time derivatives: $\frac{dL_1}{dt}, \frac{dp}{dt}, \frac{d\overline{\gamma}}{dt}, \frac{dT_{1w}}{dt} and \frac{dT_{2w}}{dt}$. Using Equations (A.144) and (A.153), $\dot{m}_{12}$ can be eliminated. This can be done by rewriting these equations. This is done in Equations (A.202) and (A.203).

$$\dot{m}_{12} = m_{in} - \left(\left(\left.\frac{\partial \rho_1}{\partial p}\right|_{h_1} + \frac{1}{2} \left.\frac{\partial \rho_1}{\partial h_1}\right|_p \frac{\partial h_g}{\partial p}\right) \frac{dp}{dt} + \frac{1}{2} \left.\frac{\partial \rho_1}{\partial h_1}\right|_p \frac{dh_{in}}{dt}\right) L_1 A_{cs} - \left(\rho_1 - \rho_g\right) \frac{dL_1}{dt} A_{cs} \tag{A.202}$$

$$\dot{m}_{12} = \left(\frac{\partial \rho_l}{\partial p} \left(1 - \overline{\gamma}\right) + \frac{\partial \rho_g}{\partial p} \overline{\gamma}\right) L_2 A_{cs} \frac{dp}{dt} + \left(\rho_g - \rho_l\right) L_2 A_{cs} \frac{d\overline{\gamma}}{dt} + \left(\rho_g - \rho_l + \left(\rho_l - \rho_g\right) \overline{\gamma}\right) A_{cs} \frac{dL_1}{dt} + \dot{m}_o \tag{A.203}$$

By using Equation (A.202) to rewrite Equation (A.173), it becomes:

$$\begin{aligned} &\left(\left.\frac{\partial \rho_1}{\partial h_1}\right|_p \left(h_1 - h_g\right) + \rho_1\right) L_1 A_{cs} \frac{1}{2} \frac{dh_{in}}{dt} + \left(\frac{1}{2} \left(\left.\frac{\partial \rho_1}{\partial h_1}\right|_p \frac{\partial h_g}{\partial p} \left(h_1 - h_g\right) + \rho_1 \frac{\partial h_g}{\partial p}\right) + \left.\frac{\partial \rho_1}{\partial p}\right|_{h_1} \left(h_1 - h_g\right) - 1\right) L_1 A_{cs} \frac{dp}{dt} \\ &+ \left(\rho_1 \left(h_1 - h_g\right)\right) A_{cs} \frac{dL_1}{dt} + \dot{m}_{in} \left(h_g - h_{in}\right) = \alpha_{1wf} A_{wf} \frac{L_1}{L} \left(T_{1w} - T_{1wf}\right) \end{aligned} \tag{A.204}$$

By using Equation (A.203) to rewrite Equation (A.189), it becomes:

$$\left(\frac{\partial h_l}{\partial p}\rho_l(1-\overline{\gamma})+\left(\frac{\partial\left(\rho_g h_g\right)}{\partial p}-\frac{\partial \rho_g}{\partial p}h_l\right)\overline{\gamma}-1\right)A_{cs}L_2\frac{dp}{dt}+\rho_l\left(h_g-h_l\right)\overline{\gamma}A_{cs}\frac{dL_1}{dt}+\rho_l\left(h_g-h_l\right)A_{cs}L_2\frac{d\overline{\gamma}}{dt} + \dot{m}_o\left(h_o-h_l\right)=\alpha_{2wf}A_{wf}\frac{L_2}{L}\left(T_{2w}-T_{2wf}\right) \tag{A.205}$$

Combining Equations (A.202) and (A.203), it becomes:

$$\begin{aligned} m_{in}-m_{out}=&\left[\left(\left.\frac{\partial\rho_1}{\partial p}\right|_{h_1}+\frac{1}{2}\frac{\partial\rho_1}{\partial h_1}\right|_p\frac{\partial h_g}{\partial p}\right)L_1A_{cs}+\left(\frac{\partial\rho_l}{\partial p}(1-\overline{\gamma})+\frac{\partial\rho_g}{\partial p}\overline{\gamma}\right)L_2A_{cs}\right]\frac{dp}{dt}\\ &+\left(\left(\rho_l-\rho_g\right)\overline{\gamma}+\left(\rho_1-\rho_l\right)\right)A_{cs}\frac{dL_1}{dt}+\left(\rho_g-\rho_l\right)L_2A_{cs}\frac{d\overline{\gamma}}{dt}+\frac{1}{2}\left.\frac{\partial\rho_1}{\partial h_1}\right|_pL_1A_{cs}\frac{dh_{in}}{dt}\end{aligned} \tag{A.206}$$

A.4.8. Buffer Tank

By combining the buffer tank and the condenser, Equations (A.206) and (A.205) have to be rewritten and an energy conservation of the buffer tank has to be given. The mass conservation of the buffer tank is given by:

$$\frac{dm_{bt}}{dt}=\dot{m}_{in}-\dot{m}_{out} \tag{A.207}$$

As $\dot{m}_{in}$ of the bufer tank is $\dot{m}_{out}$ of the condenser, Equation (A.206) becomes:

$$\begin{aligned} m_{in}-\frac{dm_{bt}}{dt}-\dot{m}_{bt,o}=&\left[\left(\left.\frac{\partial\rho_1}{\partial p}\right|_{h_1}+\frac{1}{2}\frac{\partial\rho_1}{\partial h_1}\right|_p\frac{\partial h_g}{\partial p}\right)L_1A_{cs}+\left(\frac{\partial\rho_l}{\partial p}(1-\overline{\gamma})+\frac{\partial\rho_g}{\partial p}\overline{\gamma}\right)L_2A_{cs}\right]\frac{dp}{dt}\\ &+\left(\left(\rho_l-\rho_g\right)\overline{\gamma}+\left(\rho_1-\rho_l\right)\right)A_{cs}\frac{dL_1}{dt}+\left(\rho_g-\rho_l\right)L_2A_{cs}\frac{d\overline{\gamma}}{dt}+\frac{1}{2}\left.\frac{\partial\rho_1}{\partial h_1}\right|_pL_1A_{cs}\frac{dh_{in}}{dt}\end{aligned} \tag{A.208}$$

Using Equation (A.207), Equation (A.205) becomes:

$$\left(\frac{\partial h_l}{\partial p}\rho_l(1-\overline{\gamma})+\left(\frac{\partial\left(\rho_g h_g\right)}{\partial p}-\frac{\partial \rho_g}{\partial p}h_l\right)\overline{\gamma}-1\right)A_{cs}L_2\frac{dp}{dt}+\rho_l\left(h_g-h_l\right)\overline{\gamma}A_{cs}\frac{dL_1}{dt}+\rho_l\left(h_g-h_l\right)A_{cs}L_2\frac{d\overline{\gamma}}{dt} + \left(\frac{dm_{bt}}{dt}+\dot{m}_{bt,o}\right)\left(h_o-h_l\right)=\alpha_{2wf}A_{wf}\frac{L_2}{L}\left(T_{2w}-T_{2wf}\right) \tag{A.209}$$

The energy conservation of the buffer tank is:

$$\frac{d\left(m_{bt}u_{bt}\right)}{dt}=\dot{m}_{cond,out}h_{cond,out}-\dot{m}_{bt,o}h_l \tag{A.210}$$

The left hand side of Equation (A.210) becomes:

$$\frac{d\left(m_{bt}u_{bt}\right)}{dt}=\frac{d\left(m_gu_g+m_lu_l\right)}{dt} \tag{A.211}$$

As $m=\rho V$, it becomes:

$$\frac{d\left(m_{bt}u_{bt}\right)}{dt}=\frac{d\left(\rho_gV_gu_g+\rho_lV_lu_l\right)}{dt} \tag{A.212}$$

By taking the derivative, it becomes:

$$\frac{d\left(m_{bt}u_{bt}\right)}{dt}=\dot{\rho}_gV_gu_g+\rho_g\dot{V}_gu_g+\rho_gV_g\dot{u}_g+\dot{\rho}_lV_lu_l+\rho_l\dot{V}_lu_l+\rho_lV_l\dot{u}_l \tag{A.213}$$

To solve this, we first need to find $\dot{V}_g$. This can be done in the following steps:

$$\frac{dm_{bt}}{dt}=\dot{\rho}_gV_g+\rho_g\dot{V}_g+\dot{\rho}_lV_l+\rho_l\dot{V}_l \tag{A.214}$$

As the total volume of the separator cannot change, $\dot{V}_l + \dot{V}_g = 0$, or $\dot{V}_l = -\dot{V}_g$. Using this, it becomes:

$$\frac{dm_{bt}}{dt} = \left(\dot{\rho}_g V_g + \dot{\rho}_l V_l\right) + \left(\rho_g - \rho_l\right)\dot{V}_g \tag{A.215}$$

By rewriting Equation (A.208) and stating that saturated density is a function of pressure, it becomes:

$$\dot{V}_g = \frac{\frac{dm_{bt}}{dt} - \left(\frac{\partial \rho_g}{\partial p} V_g + \frac{\partial \rho_l}{\partial p} V_l\right)\dot{p}}{\left(\rho_g - \rho_l\right)} \tag{A.216}$$

By implementing Equation (A.216), using $\dot{V}_g = \dot{V}_l$ and stating that saturated density is only dependent on pressure, Equation (A.213) becomes:

$$\frac{d\left(m_{bt} u_{bt}\right)}{dt} = \left(\frac{\partial \rho_g}{\partial p} V_g u_g + \rho_g V_g \frac{\partial u_g}{\partial p} + \frac{\partial \rho_l}{\partial p} V_l u_l + \rho_l V_l \frac{\partial u_l}{\partial p}\right) + \left(\rho_g u_g - \rho_l u_l\right)\left(\frac{\frac{dm_{bt}}{dt} - \left(\frac{\partial \rho_g}{\partial p} V_g + \frac{\partial \rho_l}{\partial p} V_l\right)\dot{p}}{\left(\rho_g - \rho_l\right)}\right) \tag{A.217}$$

The right hand side of Equation (A.210), using Equation (A.207), becomes:

$$\left(\frac{dm_{bt}}{dt} + m_{bt,o}\right) h_{cond,o} - m_{bt,o} h_l \tag{A.218}$$

Combining Equations (A.217) and (A.218), it becomes:

$$\begin{aligned} \frac{d\left(m_{bt} u_{bt}\right)}{dt} &= \left(\frac{\partial \rho_g}{\partial p} V_g u_g + \rho_g V_g \frac{\partial u_g}{\partial p} + \frac{\partial \rho_l}{\partial p} V_l u_l + \rho_l V_l \frac{\partial u_l}{\partial p}\right) \\ &+ \left(\rho_g u_g - \rho_l u_l\right)\left(\frac{\frac{dm_{bt}}{dt} - \left(\frac{\partial \rho_g}{\partial p} V_g + \frac{\partial \rho_l}{\partial p} V_l\right)\dot{p}}{\left(\rho_g - \rho_l\right)}\right) = \frac{dm_{bt}}{dt} h_{cond,o} + \dot{m}_{bt,o}\left(h_{cond,o} - h_l\right) \end{aligned} \tag{A.219}$$

B

Dimensionless Numbers

There are two dimensionless numbers in the single phase correlations: the Reynolds number and the Prandtl number. The Reynolds number (Re) is the ratio between the inertial forces and the viscous forces. It is given by Equation (B.1).

$$Re = \frac{Gd_e}{\mu} \tag{B.1}$$

The Prandtl number (Pr) relates the momentum diffusivity to the thermal diffusivity. It is given by Equation (B.2).

$$Pr = \frac{c_p \mu}{\lambda} \tag{B.2}$$

In the two-phase region, there are several dimensionless numbers: Boiling number, Nusselt number , Convection number, Froude number and the equivalent Reynolds number. The Boiling number (Bo) is the ratio between the mass of vapor created and the mass flow. It is given by Equation (B.3).

$$Bo = \frac{q}{Gh_{vap}} \tag{B.3}$$

The Nusselt number (Nu) relates the convective heat transfer to the conductive heat transfer. It is given by Equation (B.4).

$$Nu = \frac{\alpha d_h}{\lambda} \tag{B.4}$$

The Convection number (Co) is given by Equation (B.5).

$$Co = \left(\frac{\rho_g}{\rho_l}\right)\left(\frac{1-\overline{x}}{\overline{x}}\right)^{0.8} \tag{B.5}$$

The Froude number (Fr) relates the inertia flow to the gravity. It is given by Equation (B.6).

$$Fr = \frac{G^2}{\rho^2 g d_h} \tag{B.6}$$

The equivalent Reynolds number (Re_e) relates the two-phase region as a single-phase region, by using an equivalent mass fluw G_e. It is given by Equation (B.7).

$$Re_e = \frac{G_e d_e}{\mu} \tag{B.7}$$

where G_e is given by Equation (B.8).

$$G_e = G\left((1-\overline{x}) + \overline{x}\left(\frac{\rho_l}{\rho_g}\right)^{\frac{1}{2}}\right) \tag{B.8}$$

The Biot number (Bi) relates the convective heat transfer with the conductive heat transfer. When this value is smaller than 0.1, the lumped thermal capacity can be taken. It is given by Equation (B.9).

$$Bi = \frac{\alpha L}{k} \tag{B.9}$$

The Weber number (We) relates the fluid inertia with the surface tension. It is given by Equation (B.10).

$$We = \frac{G^2 d_h}{\rho \sigma} \tag{B.10}$$

C

P&ID & PFD

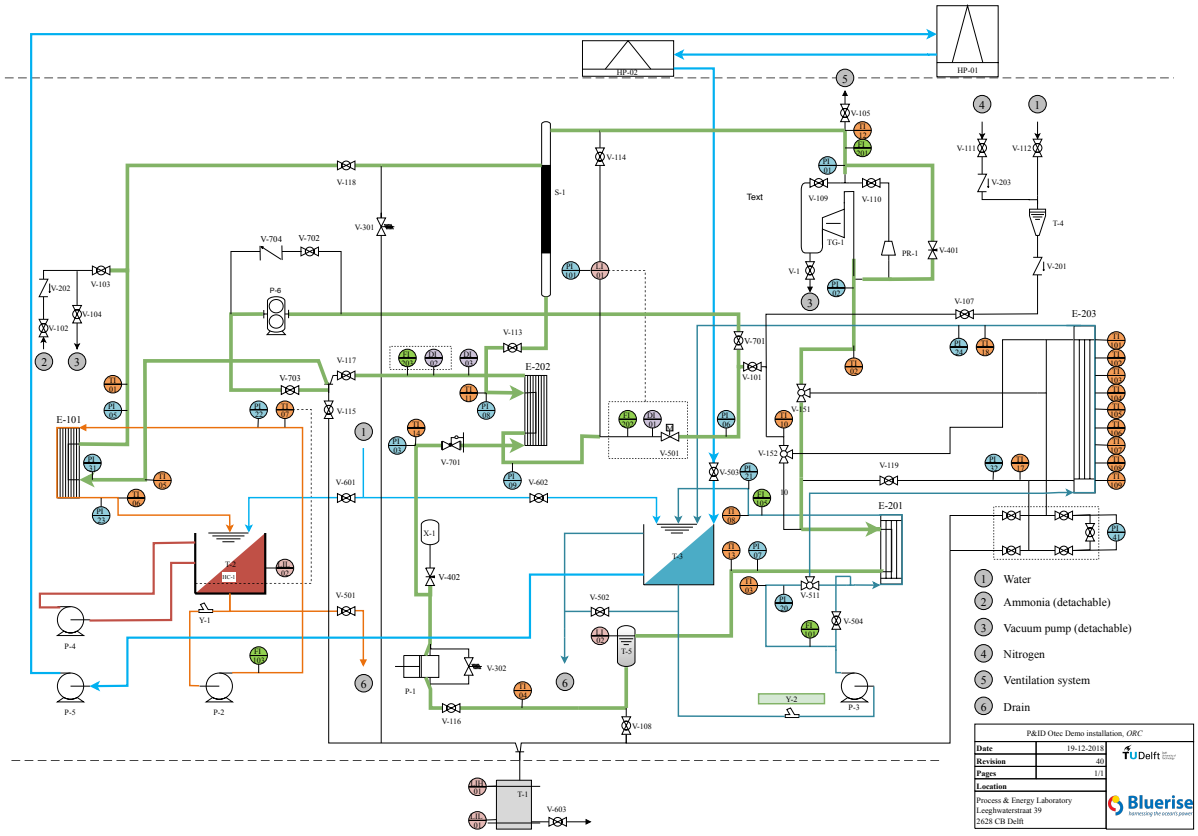

Figure C.1: P&ID of the OTEC demo, with the ORC configuration highlighted in green

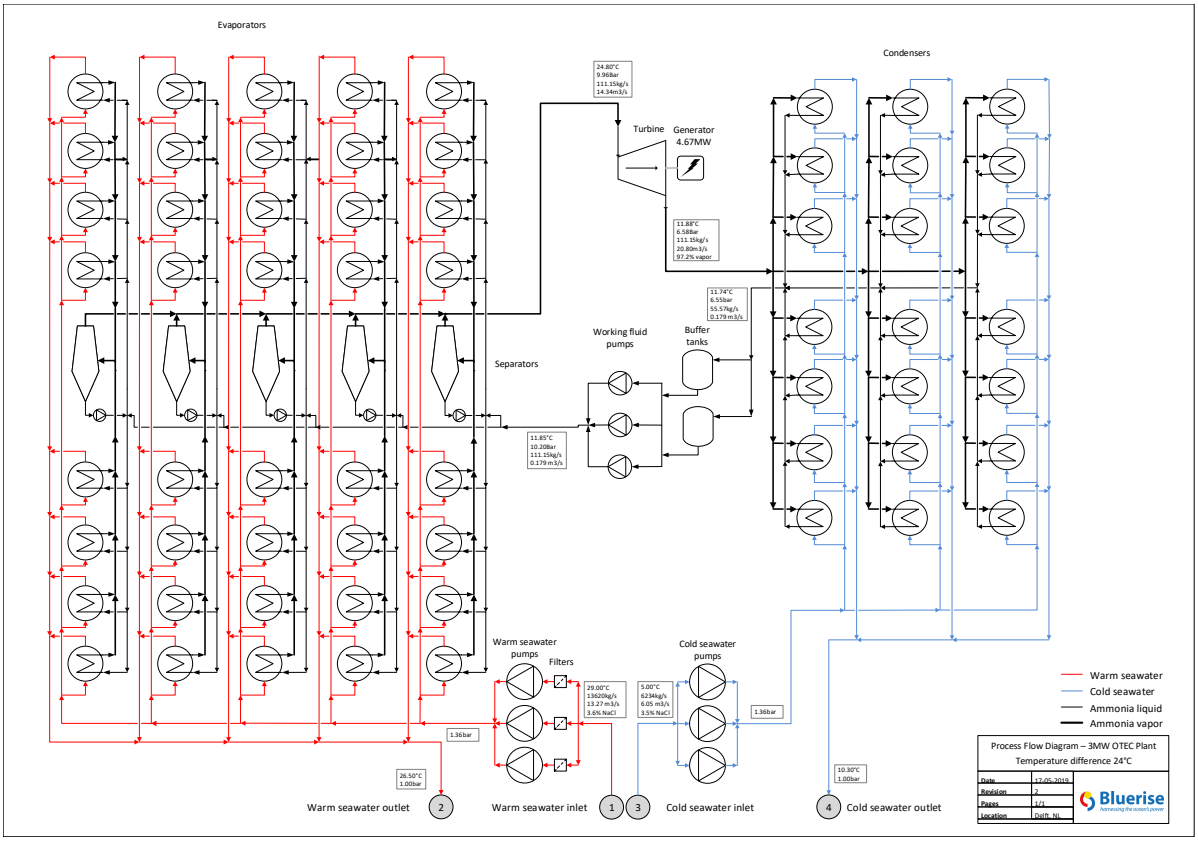

Figure C.2: PFD of the 3MW OTEC cycle, with a seawater temperature difference of 24 degrees

D

Steady-state validation

Table D.1: Steady-state validation with a pressure drop over the orifice of 3.32 bar

			Experiment	**Model**	
Component	Variable	Unit	Value	Value	Deviation [%]
Evaporator	$\dot{m}_i$	$\left[\frac{kg}{s}\right]$	0.00378	0.00378	0.00
	P_i	[bar]	9.25	9.35	1.10
	P_o	[bar]	9.23	9.34	1.23
	T_i	[°C]	19.16	14.53	-24.18
	T_o	[°C]	22.39	22.71	1.43
	$T_{sw,o}$	[°C]	25.05	24.74	-1.25
	x_o	[-]	0.57	0.61	6.26
	$\dot{Q}$	[W]	2448.83	2837.14	15.86
Orifice	P_i	[bar]	9.17	9.24	0.80
	P_o	[bar]	5.87	5.92	0.99
	T_o	[°C]	13.26	12.61	-4.92
Condenser	P_o	[bar]	5.85	5.88	0.65
	T_o	[°C]	8.52	8.72	2.41
	$T_{sw,o}$	[°C]	7.77	8.00	3.00
	$\dot{Q}$	[W]	2619.91	2841.62	8.46

Table D.2: Steady-state validation with a pressure drop over the orifice of 3.11 bar

			Experiment	**Model**	
Component	Variable	Unit	Value	Value	Deviation [%]
Evaporator	$\dot{m}_i$	$\left[\frac{kg}{s}\right]$	0.00394	0.00394	0.00
	P_i	[bar]	9.20	9.23	0.41
	P_o	[bar]	9.18	9.22	0.53
	T_i	[°C]	14.02	17.61	-20.36
	T_o	[°C]	22.16	22.30	0.64
	$T_{sw,o}$	[°C]	24.68	24.48	-0.82
	x_o	[-]	0.64	0.65	1.41
	$\dot{Q}$	[W]	2903.54	3163.91	8.97
Orifice	P_i	[bar]	9.09	9.12	0.37
	P_o	[bar]	6.00	6.01	0.31
	T_o	[°C]	13.47	12.79	-5.04
Condenser	P_o	[bar]	5.97	5.97	0.15
	T_o	[°C]	9.09	9.16	0.76
	$T_{sw,o}$	[°C]	8.25	8.35	1.19
	$\dot{Q}$	[W]	3087.16	3167.93	2.62

Table D.3: Steady-state validation with a pressure drop over the orifice of 2.75 bar

			Experiment	**Model**	
Component	Variable	Unit	Value	Value	Deviation [%]
Evaporator	$\dot{m}_i$	$\left[\frac{kg}{s}\right]$	0.00507	0.00507	0.00
	P_i	[bar]	8.99	9.05	0.67
	P_o	[bar]	8.97	9.04	0.79
	T_i	[°C]	16.29	13.88	-14.78
	T_o	[°C]	21.41	21.65	1.11
	$T_{sw,o}$	[°C]	24.24	23.99	-1.03
	x_o	[-]	0.67	0.68	1.69
	$\dot{Q}$	[W]	3457.01	3663.64	9.16
Orifice	P_i	[bar]	8.88	8.94	0.63
	P_o	[bar]	6.14	6.19	0.83
	T_o	[°C]	13.65	13.16	-3.55
Condenser	P_o	[bar]	6.11	6.15	0.66
	T_o	[°C]	9.60	9.98	3.98
	$T_{sw,o}$	[°C]	8.90	8.99	1.03
	$\dot{Q}$	[W]	3669.44	3776.88	2.93

Table D.4: Steady-state validation with a pressure drop over the orifice of 2.46 bar

			Experiment	**Model**	
Component	Variable	Unit	Value	Value	Deviation [%]
Evaporator	$\dot{m}_i$	$\left[\frac{kg}{s}\right]$	0.00472	0.00472	0.00
	P_i	[bar]	8.83	8.89	0.72
	P_o	[bar]	8.81	8.88	0.84
	T_i	[°C]	15.81	13.6	-13.97
	T_o	[°C]	20.86	21.10	1.13
	$T_{sw,o}$	[°C]	23.88	23.62	-1.09
	x_o	[-]	0.72	0.73	1.36
	$\dot{Q}$	[W]	3904.43	4238.47	8.56
Orifice	P_i	[bar]	8.71	8.78	0.79
	P_o	[bar]	6.27	6.32	0.86
	T_o	[°C]	14.07	13.44	-4.47
Condenser	P_o	[bar]	6.24	6.28	0.71
	T_o	[°C]	14.07	13.44	4.47
	$T_{sw,o}$	[°C]	9.42	9.48	0.67
	$\dot{Q}$	[W]	4158.80	4241.41	1.99

Table D.5: Steady-state validation with a pressure drop over the orifice of 2.26 bar

			Experiment	**Model**	
Component	Variable	Unit	Value	Value	Deviation [%]
Evaporator	$\dot{m}_i$	$\left[\frac{kg}{s}\right]$	0.00485	0.00485	0.00
	P_i	[bar]	8.73	8.78	0.65
	P_o	[bar]	8.71	8.77	0.77
	T_i	[°C]	15.37	13.46	-12.42
	T_o	[°C]	20.51	20.71	0.98
	$T_{sw,o}$	[°C]	23.62	23.37	-1.07
	x_o	[-]	0.76	0.77	0.66
	$\dot{Q}$	[W]	4238.47	4557.22	7.52
Orifice	P_i	[bar]	8.61	8.67	0.72
	P_o	[bar]	6.37	6.41	0.73
	T_o	[°C]	14.27	13.63	-4.48
Condenser	P_o	[bar]	6.33	6.37	0.74
	T_o	[°C]	10.51	11.03	4.88
	$T_{sw,o}$	[°C]	9.78	9.82	0.41
	$\dot{Q}$	[W]	4503.07	4560.07	1.27

Table D.6: Steady-state validation with a pressure drop over the orifice of 2.00 bar

			Experiment	**Model**	
Component	Variable	Unit	Value	Value	Deviation [%]
Evaporator	$\dot{m}_i$	$\left[\frac{kg}{s}\right]$	0.00491	0.00491	0.00
	P_i	[bar]	8.61	8.64	0.39
	P_o	[bar]	8.59	8.63	0.51
	T_i	[°C]	15.05	13.25	-11.98
	T_o	[°C]	20.09	20.20	0.54
	$T_{sw,o}$	[°C]	23.25	23.05	-0.87
	x_o	[-]	0.83	0.82	-0.83
	$\dot{Q}$	[W]	4697.49	4956.88	5.52
Orifice	P_i	[bar]	8.47	8.53	0.70
	P_o	[bar]	6.50	6.53	0.52
	T_o	[°C]	14.56	13.86	-4.80
Condenser	P_o	[bar]	6.46	6.49	0.53
	T_o	[°C]	11.08	11.56	4.39
	$T_{sw,o}$	[°C]	10.28	10.24	-0.37
	$\dot{Q}$	[W]	4989.81	4959.92	-0.60

Table D.7: Steady-state validation with a pressure drop over the orifice of 1.48 bar

			Experiment	**Model**	
Component	Variable	Unit	Value	Value	Deviation [%]
Evaporator	$\dot{m}_i$	$\left[\frac{kg}{s}\right]$	0.00512	0.00512	0.00
	P_i	[bar]	8.42	8.36	-0.61
	P_o	[bar]	8.40	8.35	-0.49
	T_i	[°C]	14.77	13.40	-9.31
	T_o	[°C]	19.39	19.19	-1.05
	$T_{sw,o}$	[°C]	22.63	22.39	-1.04
	x_o	[-]	0.93	0.93	-0.49
	$\dot{Q}$	[W]	5488.16	5776.58	5.26
Orifice	P_i	[bar]	8.28	8.25	-0.31
	P_o	[bar]	6.82	6.77	-0.60
	T_o	[°C]	15.33	14.35	-9.31
Condenser	P_o	[bar]	6.77	6.73	-0.46
	T_o	[°C]	12.41	12.61	1.93
	$T_{sw,o}$	[°C]	11.52	11.11	-3.55
	$\dot{Q}$	[W]	5793.71	5781.80	-0.21

E

Sensitivity Analysis

Here, the full sensitivity analysis is shown. On the left are all the output parameters, on the top are the input parameters. With a change of 1% of the input parameter, the output parameter changes with a percentage that corresponds with the table. For example, if the pressure of the condenser has a value of 0.4 with the working fluid pump rotation, this means that 1% change of rotational speed results in a change of 0.4% in the same direction for the pressure. If the value is negative, the change is in the other direction.

	f_{VTG}	n_{pump}	n_{gear}	$n_{swpump\ hot}$	$n_{swpump\ cold}$
H_{bt}	10.92	-2.62	-2.70	5.87	9.09
$\dot{m}_{inwf\ evap}$	0.08	1.20	0.18	-0.03	-0.06
W_{gear}	0.00	0.00	-0.38	0.00	0.00
$W_{sw\ cold}$	0.00	0.00	0.00	0.00	3.02
$W_{sw\ hot}$	0.00	0.00	0.00	3.01	0.00
W_{pump}	-0.35	1.75	0.01	0.11	0.24
w_{turb}	0.16	0.06	0.01	0.21	0.53
$\dot{m}_{turb}$	0.75	0.03	0.01	0.11	0.13
$\dot{m}_{gear}$	-0.01	-0.01	1.00	0.00	0.00
$\dot{m}_{pump}$	0.10	1.47	0.00	-0.04	-0.07
$\dot{m}_{sw\ hot}$	0.00	0.00	0.00	1.00	0.00
$\dot{m}_{sw\ cold}$	0.00	0.00	0.00	0.00	1.20
W_{net}	0.26	0.04	0.02	-0.72	0.29
$\frac{d\dot{m}_{bt}}{dt}$	-150.56	334.01	-2.30	-22.53	-28.73
p_{cond}	0.14	0.00	0.00	0.02	-0.19
γ_{cond}	-0.01	0.01	0.00	0.00	0.01
$\alpha_{sw\ cold}$	0.04	0.00	0.00	0.01	0.80
$T_{swout\ cold}$	0.38	0.01	0.00	0.05	-0.56
$\dot{Q}_{cond}$	0.76	0.01	0.01	0.10	0.14
$T_{wf\ cond}$	0.40	0.01	0.00	0.05	-0.54
$\alpha_{wf\ cond}$	-0.31	-0.03	0.00	-0.04	0.01
$\frac{\dot{m}_{sep}}{dt}$	-150.15	333.71	-2.36	-22.27	-28.55
$\alpha_{sw\ evap}$	-0.02	0.00	0.00	0.74	0.00
H_{sep}	-1.99	0.07	0.49	-1.51	-2.23
p_{evap}	-0.08	0.02	0.00	0.07	-0.01
γ_{evap}	0.11	-0.18	-0.03	0.02	0.03
$x_{out\ evap}$	0.68	-1.20	-0.17	0.14	0.19
$T_{sw,out\ evap}$	-0.07	-0.01	0.00	0.10	-0.01
$T_{wf\ evap}$	-0.11	0.02	0.01	0.09	-0.02
$\dot{Q}_{evap}$	0.77	0.01	0.01	0.10	0.13
$\alpha\_wf\ evap$	0.33	0.39	0.12	0.03	0.03
$dp_{sw\ cold}$	0.00	0.00	0.00	0.00	2.03
$dp_{sw\ hot}$	0.00	0.00	0.00	1.99	0.00
dp	-0.51	0.04	0.01	0.16	0.34

Bibliography

[1] Bamgbopa, M. O. and Uzgoren, E. Quasi-dynamic model for an organic rankine cycle. *Energy Conversion and Management*, 72:117–124, 2013.

[2] Bell, I. H., Wronski, J., Quoilin, S., and Lemort, V. Pure and pseudo-pure fluid thermophysical property evaluation and the open-source thermophysical property library coolprop. *Industrial & Engineering Chemistry Research*, 53(6):2498–2508, 2014. doi: 10.1021/ie4033999. URL `http://pubs.acs.org/doi/abs/10.1021/ie4033999`.

[3] Bendapudi, S., Braun, J. E., and Groll, E. A. A comparison of moving-boundary and finite-volume formulations for transients in centrifugal chillers. *International journal of refrigeration*, 31(8):1437–1452, 2008.

[4] Colebrook, C. F., Blench, T., Chatley, H., Essex, E., Finniecome, J., Lacey, G., Williamson, J., and Macdonald, G. Correspondence. turbulent flow in pipes, with particular reference to the transition region between the smooth and rough pipe laws.(includes plates). *Journal of the Institution of Civil engineers*, 12(8):393–422, 1939.

[5] Colonna, P. and van der Stelt, T. P. FluidProp: A Program for the Estimation of Thermophysical Properties of Fluids, 2005. URL `www.fluidprop.com`.

[6] Colonna, P. and Van Putten, H. Dynamic modeling of steam power cycles.: Part i—modeling paradigm and validation. *Applied Thermal Engineering*, 27(2-3):467–480, 2007.

[7] Colonna, P. and Van Putten, H. Dynamic modeling of steam power cycles: Part ii–simulation of a small simple rankine cycle system. *Applied Thermal Engineering*, 27(14-15):2566–2582, 2007.

[8] Dankerlui, P. Ammonia Turbine Design for Ocean Thermal Energy Conversion. MSc thesis, TU Delft, 2016.

[9] Darcy, H. *Recherches expérimentales relatives au mouvement de l'eau dans les tuyaux*, volume 1. Impr. Impériale, 1857.

[10] Desideri, A., Dechesne, B., Wronski, J., Van den Broek, M., Gusev, S., Lemort, V., and Quoilin, S. Comparison of moving boundary and finite-volume heat exchanger models in the modelica language. *Energies*, 9(5):339, 2016.

[11] Dijoux, A., Sinama, F., Marc, O., and Castaing-Lasvignottes, J. Modelling and experimentation of heat exchangers for ocean thermal energy conversion during transient operation. *Procedia Manufacturing*, 35:298–303, 2019.

[12] Djordjevic, E. and Kabelac, S. Flow boiling of r134a and ammonia in a plate heat exchanger. *International Journal of Heat and Mass Transfer*, 51(25-26):6235–6242, 2008.

[13] Donowski, V. D. and Kandlikar, S. G. Correlating evaporation heat transfer coefficient of refrigerant r-134a in a plate heat exchanger. In *Engineering Foundation Conference on Pool and Flow Boiling, Anchorage, AK, Apr*, pages 1–18, 2000.

[14] Dorfman, A. and Fridman, E. Vapor quality measurement by a discharging calorimeter. *Fluid phase equilibria*, 244(1):46–51, 2006.

[15] Eldredge, B. D., Rasmussen, B. P., and Alleyne, A. G. Moving-boundary heat exchanger models with variable outlet phase. *Journal of dynamic systems, measurement, and control*, 130(6):061003, 2008.

[16] Fasl, J. Modeling and control of hybrid vapor compression cycles. Master's thesis, University of Illinois, 2013.

[17] Ganic, E. and Wu, J. Comparative study of working fluids for otec power plants. Technical report, Illinois Univ., Chicago (USA). Dept. of Energy Engineering, 1979.

[18] Glenn, J. C., Gordon, T. J., and Florescu, E. State of the future. *Washington, DC: The Millennium Project*, 2014.

[19] Goudriaan, R. Performance analysis of ammonia and ammonia-water as working lfuids for Ocean Thermal Energy Conversion power plants. MSc thesis, TU Delft, 2016.

[20] Haaland, S. E. Simple and explicit formulas for the friction factor in turbulent pipe flow. *Journal of Fluids Engineering*, 105(1):89–90, 1983.

[21] Haglind, F. Variable geometry gas turbines for improving the part-load performance of marine combined cycles–gas turbine performance. *Energy*, 35(2):562–570, 2010.

[22] He, X.-D., Liu, S., and Asada, H. H. Modeling of Vapor Compression Cycles for Multivariable Feedback Control of HVAC Systems. *Journal of Dynamic Systems, Measurement, and Control*, 119(2):183–191, 06 1997. ISSN 0022-0434. doi: 10.1115/1.2801231. URL https://doi.org/10.1115/1.2801231.

[23] Horst, T. A., Rottengruber, H.-S., Seifert, M., and Ringler, J. Dynamic heat exchanger model for performance prediction and control system design of automotive waste heat recovery systems. *Applied Energy*, 105:293–303, 2013.

[24] Huster, W. R., Vaupel, Y., Mhamdi, A., and Mitsos, A. Validated dynamic model of an organic rankine cycle (orc) for waste heat recovery in a diesel truck. *Energy*, 151:647–661, 2018.

[25] Idel'chik, I. *Handbook of Hydraulic Resistance*. CRC Press, 1960. ISBN 9780849399084. URL https://books.google.nl/books?id=EpcQAQAAMAAJ.

[26] Jorgensen, S. E. and Johnsen, I. *Principles of environmental science and technology*. Elsevier, 2011.

[27] Judes, M. and Tsatsaronis, G. Design optimization of power plants by considering multiple partial load operation points. In *ASME 2007 International Mechanical Engineering Congress and Exposition*, pages 217–225. American Society of Mechanical Engineers, 2007.

[28] Keeley, K. A theoretical investigation of the part-load characteristics of lp steam turbine stages. *CEGB memorandum RD/L/ES0817 M*, 88, 1988.

[29] Khan, M. S., Khan, T. S., Chyu, M.-C., and Ayub, Z. H. Evaporation heat transfer and pressure drop of ammonia in a mixed configuration chevron plate heat exchanger. *International Journal of Refrigeration*, 41:92–102, 2014.

[30] Kirkenier, J. Techno-economic optimization of Organic Rankine Cycles using working fluid mixtures for 10 to 25 MW OTEC power plants. MSc thesis, TU Delft, 2014.

[31] Kuo, W., Lie, Y., Hsieh, Y., and Lin, T. Condensation heat transfer and pressure drop of refrigerant r-410a flow in a vertical plate heat exchanger. *International Journal of Heat and Mass Transfer*, 48(25-26): 5205–5220, 2005.

[32] Lemmon, E. W., , Bell, I. H., Huber, M. L., and McLinden, M. O. NIST Standard Reference Database 23: Reference Fluid Thermodynamic and Transport Properties-REFPROP, Version 10.0, National Institute of Standards and Technology, 2018. URL https://www.nist.gov/srd/refprop.

[33] Li, B. and Alleyne, A. G. A dynamic model of a vapor compression cycle with shut-down and start-up operations. *International Journal of refrigeration*, 33(3):538–552, 2010.

[34] Lockhart, R. and Martinelli, R. Proposed correlation of data for isothermal two-phase, two-component flow in pipes. *Chem. Eng. Prog*, 45(1):39–48, 1949.

[35] MacArthur, J. W. and Grald, E. W. Unsteady compressible two-phase flow model for predicting cyclic heat pump performance and a comparison with experimental data. *International Journal of refrigeration*, 12 (1):29–41, 1989.

[36] Marchionni, M., Bianchi, G., Karvountzis-Kontakiotis, A., Pesiridis, A., and Tassou, S. A. Dynamic modeling and optimization of an orc unit equipped with plate heat exchangers and turbomachines. *Energy Procedia*, 129:224–231, 2017.

[37] Martin, H. A theoretical approach to predict the performance of chevron-type plate heat exchangers. *Chemical Engineering and Processing: Process Intensification*, 35(4):301–310, 1996.

[38] MATLAB. *version 9.7 (R2019b)*. The MathWorks Inc., Natick, Massachusetts, 2019.

[39] Miller, D. S. *Internal Flow Systems*. BHRA Fluid Engineering, 1978. ISBN 0900983787.

[40] Moody, L. F. Friction factors for pipe flow. *Trans. Asme*, 66:671–684, 1944.

[41] Nusselt, W. Die oberflachenkondensation des wasserdamphes. *VDI-Zs*, 60:541, 1916.

[42] Pangborn, H., Alleyne, A. G., and Wu, N. A comparison between finite volume and switched moving boundary approaches for dynamic vapor compression system modeling. *International Journal of Refrigeration*, 53:101–114, 2015.

[43] Poiseuille, J. L. *Recherches expérimentales sur le mouvement des liquides dans les tubes de très-petits diamètres*. Imprimerie Royale, 1844.

[44] Qiao, H. and Laughman, C. R. Comparison of approximate momentum equations in dynamic models of vapor compression systems. In *Proceedings of the 16th International Heat Transfer Conference*, 2018.

[45] Qiao, H., Aute, V., and Radermacher, R. An improved moving boundary heat exchanger model with pressure drop. *International Refrigeration and Air Conditioning Conference*, 2014.

[46] Qiao, H., Aute, V., and Radermacher, R. Transient modeling of a flash tank vapor injection heat pump system–part i: model development. *International journal of refrigeration*, 49:169–182, 2015.

[47] Quoilin, S., Aumann, R., Grill, A., Schuster, A., Lemort, V., and Spliethoff, H. Dynamic modeling and optimal control strategy of waste heat recovery organic rankine cycles. *Applied energy*, 88(6):2183–2190, 2011.

[48] Rasmussen, B. P. and Alleyne, A. G. Dynamic modeling and advanced control of air conditioning and refrigeration systems. Technical report, Air Conditioning and Refrigeration Center. College of Engineering . . . , 2006.

[49] Rasmussen, B. P. and Shenoy, B. Dynamic modeling for vapor compression systems—part ii: Simulation tutorial. *HVAC&R Research*, 18(5):956–973, 2012.

[50] Shah, R., Alleyne, A. G., Bullard, C. W., Rasmussen, B. P., and Hrnjak, P. Dynamic modeling and control of single and multi-evaporator subcritical vapor compression systems. Technical report, Air Conditioning and Refrigeration Center. College of Engineering . . . , 2003.

[51] Sohel, M. I., Krumdieck, S., Sellier, M., and Brackney, L. J. Dynamic modelling and simulation of an organic rankine cycle unit of a geothermal power plant. In *Proceedings World Geothermal Congress*, pages 25–29, 2010.

[52] Stelwagen, J. A study on the ORC for OTEC applications: Performance analysis for a changed configuration. MSc thesis, TU Delft, 2019.

[53] Stodola, A. and Loewenstein, L. C. *Steam Turbines: With an Appendix on Gas Turbines and the Future of Head Engines*. D. Van Nostrand Company, 1905.

[54] Taboas, F., Valles, M., Bourouis, M., and Coronas, A. Assessment of boiling heat transfer and pressure drop correlations of ammonia/water mixture in a plate heat exchanger. *international journal of refrigeration*, 35(3):633–644, 2012.

[55] Tao, X. and Infante Ferreira, C. Nh3 condensation in a plate heat exchangers - part 2: Mechanistic models of heat transfer and frictional pressure drop. *International Journal of Heat and Mass Transfer*, 2020.

[56] Tao, X., Kirkenier, J., and Infante Ferreira, C. A. Condensation of nh3 within a plate heat exchanger of small diameter channel. In *Proceedings of the 6th ASME International Conference on Micro/Nanoscale Heat and Mass Transfer 2019*. American Society of Mechanical Engineers, 2007.

[57] Tummescheit, H. *Design and implementation of object-oriented model libraries using modelica*. PhD thesis, Lund University, 2002.

[58] Vaja, I. *Definition of an object oriented library for the dynamic simulation of advanced energy systems: methodologies, tools and application to combined ICE-ORC power plants*. PhD thesis, Università di Parma, Dipartimento di Ingegneria Industriale, 2009.

[59] van Strijp, P. Impact of turbine performance on the operating conditions of a 10 MW OTEC plant. MSc thesis, TU Delft, 2018.

[60] Walsh, P. P. and Fletcher, P. *Gas turbine performance*. John Wiley & Sons, 2004.

[61] Wedekind, G., Bhatt, B., and Beck, B. A system mean void fraction model for predicting various transient phenomena associated with two-phase evaporating and condensing flows. *International Journal of Multiphase Flow*, 4(1):97–114, 1978.

[62] Weerstra, J. Dynamic behavior of CO_2 refrigeration system with integrated ejector. MSc thesis, TU Delft, 2014.

[63] Wei, D., Lu, X., Lu, Z., and Gu, J. Dynamic modeling and simulation of an organic rankine cycle (orc) system for waste heat recovery. *Applied Thermal Engineering*, 28(10):1216–1224, 2008.

[64] Weisbach, J. Lehrbuch der ingenieur und maschinen mechanik, vol. 1. *Theoretische Mechanik, Vieweg und Sohn, Braunschweig*, 535, 1845.

[65] Willatzen, M., Pettit, N., and Ploug-Sørensen, L. A general dynamic simulation model for evaporators and condensers in refrigeration. part i: moving-boundary formulation of two-phase flows with heat exchange. *International Journal of refrigeration*, 21(5):398–403, 1998.

[66] Wilson, M. J. Experimental investigation of void fraction during horizontal flow in larger diameter refrigeration applications. Technical report, Air Conditioning and Refrigeration Center. College of Engineering . . . , 1998.

[67] Yan, Y. Y. and Lin, T. F. Evaporation heat transfer and pressure drop of refrigerant r-134a in a plate heat exchanger. *Journal of Heat Transfer*, 121(1):118–127, 1999.

[68] Zhang, J., Zhang, W., Hou, G., and Fang, F. Dynamic modeling and multivariable control of organic rankine cycles in waste heat utilizing processes. *Computers & Mathematics with Applications*, 64(5): 908–921, 2012.

[69] Zhang, W. J., Zhang, C., and Ding, G. On three forms of momentum equation in transient modeling of residential refrigeration systems. *International Journal of Refrigeration*, 32(5):938–944, 2009.

[70] Zivi, S. Estimation of steady-state steam void-fraction by means of the principle of minimum entropy production. *Journal of heat transfer*, 86(2):247–251, 1964.

[71] Ziviani, D., Woodland, B., Georges, E., Groll, E., Braun, J., Horton, W., Van den Broek, M., and De Paepe, M. Development and a validation of a charge sensitive organic rankine cycle (orc) simulation tool. *Energies*, 9(6):389, 2016.